The Use of Sun-Induced Fluorescence to Remotely Characterise Phytoplankton Dynamics

A thesis presented to the

Department of Oceanography

University of Cape Town

In fulfilment of the requirements for the degree

Masters of Science

by

Christelle Balt

July 2006

Acknowledgements

I am grateful to Dr Stewart Bernard for much guidance. Thank you to my supervisor, Professor F.A. Shillington, for valuable advice.

I would like to express appreciation to the following people for their contributions to this study:

Dr R. Barlow

Ms D. Calder

Mr A. du Randt

Ms A. Fawcett

Dr G. Pitcher

Dr T. Probyn

Ms H. Sessions

Funding was received from:

National Research Foundation

Benguela Current Large Marine Ecosystem Programme

University of Cape Town

A special thank you to Mara, Selma, Jan, Pannies, Tinus, and Stuart

Table of Contents

Abstract 1

1 Introduction 3

2 Literature Review 7

2.1 Fluorescence Theory....7

2.1.1 Molecular Fluorescence....7

2.1.2 Cellular Mechanisms....8

2.1.3 Cellular Fluorescence Controls....9

2.1.4 Summary....11

2.2 Fluorescence Measurement Techniques....11

2.2.1 Simple Active Fluorometry....11

2.2.2 Variable Active Fluorometry....12

2.2.3 Spectral Active Fluorometry....13

2.2.4 Passive Fluorometry Methods....14

2.2.5 Summary....15

2.3 Fluorescence Variability....16

2.3.1 Spatial Distribution of Fluorescence....17

2.3.2 Nutrient and Temperature Related Fluorescence Response....18

2.3.3 Fluorescence-Light Dependence....20

2.3.4 Fluorescence Variability Summary....24

2.3.5 Mechanisms of Fluorescence Change....26

2.3.6 Summary....28

2.4 Fluorescence Application....29

3 Field Study 33

3.1 Field Methods....34

3.1.1 Fluorescence Measurement and ϕ_f Derivation....34

3.1.2 Absorption Measurement....36

3.1.3 Photosynthesis Measurement and ϕ_c Derivation....36

3.1.4 Pigment Concentration Measurements....40

3.1.5 Effective Diameter Measurement....41

3.1.6 Nitrate Measurement....41

3.2 Error Analysis....41
3.2.1 Error Estimates of F and ϕ_f....42
3.2.2 Error Estimate of $a_\phi(\lambda)$....42
3.2.3 Error Estimations for P/E Parameters....42
3.2.4 Additional Sources of Error....43
3.3 Statistical Analysis....43
3.4 Field Results....44
3.5 Field Discussion....54
3.6 Field Conclusion....56
4 Fluorescence Algorithm 59
4.1 Model Theory....59
4.2 *In Situ* Model Development....62
4.2.1 Parameter Computation....62
4.2.2 Assessment of Assumptions....67
4.3 Satellite Model Development....69
4.3.1 Parameter Computation....69
4.3.2 Assessment of Assumptions....73
4.4 Algorithm Nesting....74
4.5 Model Validation and Testing....75
4.5.1 Restrictions of the FLH Method....78
4.5.2 Algorithm Validation....79
4.5.3 Comparison of Algorithm Methods....81
4.5.4 Fluorescence as a Tool: Potential Application....84
4.6 Summary....87
5 Application 89
5.1 Primary Production....90
5.1.1 Model Theory and Implementation....90
5.1.2 Assessment of Assumptions....93
5.1.3 Parameterisation of ϕ_c / ϕ_f....95
5.1.4 Initial Comparison of Production Methods....99
5.2 Fluorescence Algorithm with Bio-Optical Moorings....101
5.3 Satellite Application....108
5.4 Summary....113

6 Conclusion 115
References 119
Appendix A. Glossary of Symbols 131
Appendix B. Acronyms 137

Abstract

Sun-induced fluorescence of phytoplankton chlorophyll-a can be used for the study of phytoplankton assemblage physiology. Fluorescence is related to cellular growth mechanisms, which are affected by environmental conditions. Since fluorescence depends on absorption efficiency of cells, it varies with phytoplankton species. The fluorescence quantum yield is defined as the ratio of photons emitted as fluorescence to photons absorbed by phytoplankton cells. This parameter signifies physiological change that affects fluorescence and photosynthetic efficiencies of cells. Fluorescence is therefore also related to photosynthesis, and might be employed for primary production estimation.

This study exploits the remotely sensed sun-induced fluorescence signal to infer phytoplankton assemblage dynamics in the southern Benguela via *in situ* bio-optical moorings, and through the use of satellite sensors. An algorithm is developed to facilitate the extraction of the fluorescence signal from hyperspectral *in situ* upward radiance data, and multi-spectral water-leaving reflectance imagery. Derivation of the fluorescence quantum yield is also achieved. *In situ* fluorescence parameter derivations allow the near real-time assessment of assemblages, whilst derivations from satellite imagery provide the means to assess phytoplankton dynamics synoptically, and over large spatial scales.

The algorithm produces viable estimations of the fluorescence parameters. Derived parameters are regarded very useful in the general assessment of phytoplankton dynamics, and the formative stages of HAB events. The functioning of the algorithm requires that fluorescence parameters not be calculated for very high biomass waters. Harmful algal bloom (HAB) dynamics of the southern Benguela can thus not directly be assessed. A preliminary assessment of instantaneous primary production is found to be useful in a qualitative sense.

The study found that the interpretation of fluorescence parameter variability for natural marine phytoplankton assemblages is complicated, especially for parameters derived from Eulerian bio-optical data. However, derived satellite imagery can be assessed in terms of effective diameter descriptions, and physiology, which provides a powerful tool for the study of natural assemblage dynamics, and potentially for operational monitoring.

Chapter 1

Introduction

Cellular fluorescence of phytoplankton chlorophyll-a occurs as one branch of the trifurcation of absorbed light energy within phytoplankton cells. Absorbed light energy can be utilised for fluorescence, photosynthesis, and heat dissipation (Falkowski and Kiefer, 1985). Fluorescence thus varies generally according to the following: the availability, intensity, and spectral signature of ambient light (Kiefer, 1973a); the efficiency of light absorption by a phytoplankton cell (*ibid.*); the efficiency with which the energy is transferred within the cell (Falkowski and Kolber, 1995); the level of reabsorption of emitted fluorescence by the cell (Collins *et al.*, 1985); and the variability of photosynthesis (Falkowski and Kolber, 1995) and heat dissipation (Clayton, 1980 as cited in Babin *et al.*, 1996). Cellular light absorption depends on the composition and abundance of light harvesting pigments within cells (Bricaud *et al.* 1995), which vary between phytoplankton groups (Yentsch and Phinney, 1985), but also as a result of photoadaptation amongst cells of the same phytoplankton group (Falkowski and Kiefer, 1985). Absorption of cells also varies between phytoplankton species as a result of changes in cell sizes, cell shapes, and pigment packaging (Morel, 1990 as cited in Cullen and Lewis, 1995). Absorbed energy transfer efficiency depends on the level of environmental strain that cells experience subject to, for example, nutrient availability (Kolber *et al.*, 1988; Falkowski *et al.*, 1992). Variability of photosynthesis is linked to the same mechanisms of light absorption by photosynthetic pigments and energy transportation that affect fluorescence variability. However, the process of photosynthesis varies distinctly with available excitation energy (Falkowski and Kiefer, 1985). Damage to the photosynthetic apparatus causes variability that is separate from change induced via the mechanisms of energy absorption and transfer. Heat dissipation is related to the production of photoprotectant cellular accessory pigments (Müller *et al.*, 2001). Light absorbed by the photoprotectant pigments is not used for either fluorescence or photosynthesis (*ibid.*). A large portion of the fluorescence variability discussed above is represented by the fluorescence quantum yield parameter, which describes the amount of energy that is fluoresced per total energy absorbed (Babin *et al.*, 1996).

Cellular fluorescence of phytoplankton chlorophyll-a is thus closely linked to the mechanisms of light absorption, energy transfer, photosynthesis, and heat dissipation, which all depend on the

physiological state of the phytoplankton cells, and a particular phytoplankton species. A thorough understanding of fluorescence variability in terms of these cellular mechanisms, and the effect of environmental change on phytoplankton cells, could allow the use of fluorescence as a physiological proxy, or a tool for phytoplankton group distinction in ocean phytoplankton assemblages, especially through the fluorescence quantum yield parameter.

Sun-induced chlorophyll-a fluorescence of ocean phytoplankton assemblages can be detected in the upward radiance signal measured by bio-optical instruments *in situ* (Morel and Prieur, 1977; Kiefer *et al.*, 1989), as well as in the water-leaving reflectance signal as measured by satellite optical sensors (Neville and Gower, 1977; Gower *et al.*, 1999). The fluorescence signal can be identified from upward radiance or water-leaving reflectance spectra as a peak in the red portion of the electromagnetic spectrum. Near-surface passive autonomous hyperspectral radiometric buoy systems provide high-frequency, and high-resolution, upward radiance and downward irradiance data (Kiefer *et al.*, 1989). Satellite spectroradiometers provide water-leaving reflectance imagery that are synoptic and are obtained for spatially extensive ocean regions (Neville and Gower, 1977). The extraction of the fluorescence signal and the derivation of the fluorescence quantum yield via these instruments, provide real-time phytoplankton assemblage fluorescence characteristics in the case of *in situ* moorings, as well as instantaneous, spatially large-scale fluorescence characteristics remotely from space.

A primary objective of this study is to develop a fluorescence algorithm that enables the extraction of the fluorescence peak from hyperspectral *in situ* buoy data acquired real-time via cellular phone telemetry, and from multi-spectral satellite data provided by satellite databases. The algorithm also calculates the fluorescence quantum yield through nesting of the fluorescence algorithm within a hyperspectral inverse reflectance algorithm (Bernard, 2005). These fluorescence parameters are assessed in terms of their use as indicators of phytoplankton assemblage physiological state, and possible group or species identifiers, potentially contributing to an operational harmful algal bloom (HAB) detection and forecasting system.

HAB events in the Benguela are associated with toxic or otherwise harmful phytoplankton species that are dominating and flourishing (Pitcher and Calder, 2000). HABs can negatively influence commercial and recreational fisheries (*ibid.*). Human illness can be associated with these blooms through the consumption of contaminated seafood (*ibid.*). The HAB monitoring programme of the southern Benguela upwelling system aims to enable the detection and

characterisation of blooms in this region. This programme also aspires towards effective forecasting of HABs. The southern Benguela, considered throughout this study, is highly productive and it experiences frequent occurrences of HABs (*ibid.*).

There are two primary bio-optical instruments available to the southern Benguela HAB monitoring programme. These instruments provide data appropriate to the development of the algorithm. The multi-sensor bio-optical mooring, namely the Benguela Optical Buoy (BOB) (Fawcett *et al.*, 2006), is moored off Lamberts Bay on the western coast of South Africa and offers *in situ* radiometric data. BOB is a pencil buoy fitted with a hyperspectral irradiance sensor located above the surface of the water, and a vertically orientated hyperspectral radiance sensor below the surface, free from shading by the buoy (*ibid.*). BOB data is accessible via cellular phone telemetry (*ibid.*). The Medium Resolution Imaging Spectrometer (MERIS) aboard the polar-orbiting Envisat satellite of the European Space Agency (ESA) provides multi-spectral reflectance imagery. MERIS is a 68.5° field-of-view push-broom imaging spectrometer (MERIS Product Handbook, ESA, Paris). It obtains reflectance from the earth via 15 spectral bands in the visible and the near-infrared. A pixel in a Full-Resolution (FR) MERIS image represents an area of 260m by 290m on the earth's surface. Global coverage of Envisat is achieved in three days and data is available from the ACRI database following acquisition.

A field survey was conducted off the coast of Lamberts Bay as part of this study to ensure that the algorithm estimations are acceptable for this region, and to assist in the appropriate interpretation of calculated fluorescence parameters. To assess the use of sun-induced fluorescence of natural phytoplankton assemblages as a physiological proxy, or as an indicator of phytoplankton groups, the field-measured data were studied to examine both causal factors of fluorescence variability, and whether operationally useful empirical relationships could be established.

As fluorescence is closely linked to photosynthesis, fluorescence might be used to estimate primary production of natural phytoplankton assemblages (Kiefer *et al.* 1989). As a first assessment, fluorescence acquired through the algorithm is used to derive experimental estimations of instantaneous primary production. Empirical parameterisations assist in the derivation of real-time *in situ* instantaneous primary production, as well as synoptic large-scale instantaneous primary production.

The study is presented in the following way. A thorough account of published studies regarding the phytoplankton fluorescence mechanism, fluorescence measurement techniques, fluorescence variability, and fluorescence applications is given in the literature review in Chapter 2. Although a variety of fluorescence measurement techniques are discussed to ensure a comprehensive review, it should be born in mind that the present study primarily concerns the remote optical detection and interpretation of sun-induced *in vivo* chlorophyll-a fluorescence of natural marine phytoplankton assemblages. The field study is described in Chapter 3. Laboratory measurements of fluorescence and photosynthesis parameters afford comparison with algorithm-derived parameters, while possible environmental controls of these parameters can also be assessed through comparison with measured environmental variables. The development, performance, and utility of the algorithm are discussed in Chapter 4. Chapter 5 demonstrates the application of the developed algorithm. Preliminary estimates and methods for the remote derivation of instantaneous primary production are described. Algorithm products are exhibited as time series that are derived from BOB radiometric data, in addition to derived satellite imagery from MERIS spectroradiometer data. Concluding remarks are given in Chapter 6.

Chapter 2

Literature Review

Previous research on fluorescence theory, measurement techniques, fluorescence variability, and useful application of fluorescence are discussed in this chapter. Fluorescence theory encompasses the fundamental mechanism of fluorescence at the molecular level, the mechanisms of phytoplankton cellular fluorescence, and the factors that enhance or inhibit this fluorescence. Various fluorescence measurement techniques employing different instruments and approaches are discussed. The different measured and derived parameters are explained. Factors that control fluorescence variability are examined. Finally, the various applications of fluorescence parameters in bio-optical ocean studies are discussed.

2.1 Fluorescence Theory

2.1.1 Molecular Fluorescence

At any given moment a molecule can experience only one discreet rotational, vibrational, and electronic state. When a transfer of energy occurs due to the absorption of a photon, energy level transitions can occur within a molecule. The capture of a photon by a molecule will therefore lead to a transition of an electron from the ground state to an excited state corresponding to the photon energy. (Kirk, 1996)

Chlorophyll-a, the major photosynthetic pigment of phytoplankton is a complex molecule, which allows a number of transitions to take place each time a photon is absorbed. Although chlorophyll-a possesses two main absorption bands, which lead to dissimilar energy transitions, all the absorbed visible quanta produce identical photosynthesis due to an overlap of the two electronic states. Fluorescence of chlorophyll-a occurs when excitation energy undergoes a transition to below the state where it is utilised for photosynthesis, with a subsequent emission of a photon. The emitted photon is necessarily of a greater wavelength than the photon of excitation. In photosynthesising phytoplankton cells typically only a small fraction of absorbed light is fluoresced. (*ibid.*)

The fluorescence emission spectrum of fluorophores is independent of the excitation spectrum. Therefore, excitation light of any colour produces fluorescence along the same spectral range. Chlorophyll-a is a fluorophore that emits fluorescence in a spectral band centred at 685nm. The intensity of this emitted fluorescence however does vary with the excitation spectrum, since absorption of light by chlorophyll-a is wavelength dependent. Excitation light in the blue or red that corresponds to wavebands where chlorophyll-a absorbs optimally produces fluorescence of highest intensities. (Mobley, 1994)

2.1.2 Cellular Mechanisms

Various processes within phytoplankton cells compete for the use of absorbed photons. Biophysical models are useful to describe the cellular mechanisms that determine the fate of absorbed light energy, and they provide a description of the link that exists between fluorescence and competing cellular processes. One such model is described below (Kolber and Falkowski, 1993).

Inside a cell, fluorescence is associated with the light reactions of photosynthesis, which occur inside a photosynthetic unit (PSU). The PSU consists of two photosystems that each contains a reaction centre and light harvesting antennae, composed of chlorophyll-a and accessory pigments. The composition of pigments in the antennae depends on whether they belong to photosystem I (PSI) or photosystem II (PSII), but it also varies with regard to the phytoplankton species and the physiological status of the cell.

PSII reaction centres are composed of specialised protein-complexed chlorophyll-a molecules denoted P_{680}. P_{680} is the primary electron donor and is accompanied by a quinone called Q_a, the primary electron acceptor. Photons that are absorbed by photosynthetic pigments function as excitation energy that triggers charge separation within the reaction centre. Charge separation involves the oxidation of P_{680} to P_{680}^+ and the consequent reduction of Q_a to Q_a^-. This process causes the reaction centre to close, rendering absorbed photons photochemically ineffective until P_{680}^+ is re-reduced and Q_a^- is re-oxidised. A plastoquinone (PQ) denoted Q_b acts as secondary acceptor that oxidises Q_a^-, and subsequently becomes removed from the reaction centre into the PQ pool where electrons are stored temporarily between PSII and PSI. Each dissociated PQ is replaced by another to ensure continual electron transport from Q_a. A Q_b accepts two electrons to

form a plastoquinol (PQH_2); its oxidation is controlled by the dark reactions of photosynthesis on the acceptor side of PSI. With increasing light imposed upon the PSU the PQ pool is progressively reduced. Continual reduction of the PQ pool impedes re-oxidation of Q_a^- due to the scarcity of PQ replacements. As a consequence, the fraction of closed reaction centres increases and there is a reduction in the quantum efficiency of photosynthesis compared to the relatively high efficiency of electron transport at low photon fluxes. Conversely, in the total absence of ambient photons the reaction centres are open, since P_{680} is reduced and Q_a is oxidised.

Excitation energy received by PSII can be used for photosynthesis when the light energy is converted to chemical energy via photochemical charge separation. There are two additional pathways for the excitation energy. Fluorescence is emitted almost solely from PSII. In addition, light energy can be dissipated as heat. In PSII, the probability that fluorescence will occur is variable, but occurrence is more probable when the reaction centre is closed. So, fluorescence of cells is minimal in the dark and maximal when all reaction centres are closed.

2.1.3 Cellular Fluorescence Controls

Fluorescence emission at the phytoplankton cellular level is regulated by competing pathways of absorbed light energy in PSII, and by cellular structural factors that influence the mode of light absorption. The efficiency with which absorbed energy is converted into carbohydrates via photosynthesis, or emitted as fluorescence, is expressed through the quantum yields of these properties. The fluorescence quantum yield is defined as the ratio of energy emitted as fluorescence to energy absorbed.

The fluorescence quantum yield is the primary indicator of variation in fluorescence output from PSII relative to photochemistry (Falkowski and Kiefer, 1985). Another source of fluorescence variability is the rate of light absorption by the cells, which is largely determined by the mean incident light, but also by the PSII concentration in the cell suspension, and the functional absorption cross-section of PSII (*ibid.*) depending on the environment, species, and photoadaptation. Intracellular reabsorption of fluorescence due to pigment packaging also causes variation in fluorescence (Kiefer, 1973a). As one of the major absorption bands of chlorophyll-a occurs in the red part of the electromagnetic spectrum, typically centred at 674nm, it partially overlaps the fluorescence band centred at 685nm. The cell can thus reabsorb some of the PSII-emitted fluorescence (Collins *et al.*, 1985).

form a plastoquinol (PQH_2); its oxidation is controlled by the dark reactions of photosynthesis on the acceptor side of PSI. With increasing light imposed upon the PSU the PQ pool is progressively reduced. Continual reduction of the PQ pool impedes re-oxidation of Q_a^- due to the scarcity of PQ replacements. As a consequence, the fraction of closed reaction centres increases and there is a reduction in the quantum efficiency of photosynthesis compared to the relatively high efficiency of electron transport at low photon fluxes. Conversely, in the total absence of ambient photons the reaction centres are open, since P_{680} is reduced and Q_a is oxidised.

Excitation energy received by PSII can be used for photosynthesis when the light energy is converted to chemical energy via photochemical charge separation. There are two additional pathways for the excitation energy. Fluorescence is emitted almost solely from PSII. In addition, light energy can be dissipated as heat. In PSII, the probability that fluorescence will occur is variable, but occurrence is more probable when the reaction centre is closed. So, fluorescence of cells is minimal in the dark and maximal when all reaction centres are closed.

2.1.3 Cellular Fluorescence Controls

Fluorescence emission at the phytoplankton cellular level is regulated by competing pathways of absorbed light energy in PSII, and by cellular structural factors that influence the mode of light absorption. The efficiency with which absorbed energy is converted into carbohydrates via photosynthesis, or emitted as fluorescence, is expressed through the quantum yields of these properties. The fluorescence quantum yield is defined as the ratio of energy emitted as fluorescence to energy absorbed.

The fluorescence quantum yield is the primary indicator of variation in fluorescence output from PSII relative to photochemistry (Falkowski and Kiefer, 1985). Another source of fluorescence variability is the rate of light absorption by the cells, which is largely determined by the mean incident light, but also by the PSII concentration in the cell suspension, and the functional absorption cross-section of PSII (*ibid.*) depending on the environment, species, and photoadaptation. Intracellular reabsorption of fluorescence due to pigment packaging also causes variation in fluorescence (Kiefer, 1973a). As one of the major absorption bands of chlorophyll-a occurs in the red part of the electromagnetic spectrum, typically centred at 674nm, it partially overlaps the fluorescence band centred at 685nm. The cell can thus reabsorb some of the PSII-emitted fluorescence (Collins *et al.*, 1985).

One of the key determinants of fluorescence quantum yield variability is fluorescence quenching, which can be expressed in terms of photochemical- and nonphotochemical quenching of fluorescence (Babin *et al.*, 1996).

Photochemical quenching of fluorescence is defined as a diminishing of fluorescence emission owing to photochemical activity. It can be related to the fraction of open reaction centres within a cell, which is influenced by the availability of light energy and the functional absorption cross-section of PSII. The functional absorption cross-section of PSII is a product of the light-harvesting potential of pigments and the efficiency of excitation transfer to the reaction centre. (*ibid.*)

Nonphotochemical quenching of fluorescence causes fluorescence emission to be sub-optimal as a result of factors unrelated to photochemistry (*ibid.*). Chlorophylls, phycobilins, and some carotenoid pigments are able to transfer absorbed photons with great efficiency (*ibid.*). However, various carotenoids perform a photoprotective role by dissipating excess photons as heat (*ibid.*). Relative increases in intracellular photoprotectant pigments in association with intense light exposure can bring about increased heat dissipation of excitation energy, thus reducing the amount of excitation energy in PSII that can de-excite to fluorescence (Müller *et al.*, 2001). Furthermore, excessive radiation might cause reaction centres to become inactivated. The primary site of photodamage of PSII, also known as photoinhibition, is the reaction centre chlorophyll-a, P_{680} (Critchley, 1988). Photoinhibition results in an increase of thermal quenching of fluorescence (Müller *et al.*, 2001). Nutrient limitation in phytoplankton is known to have a similar effect to photodamage on PSII, also causing reductions in fluorescence emission (Babin *et al.*, 1995).

Species-dependent fluorescence variability results from the effect of phytoplankton cell size, cell shape, and pigment structure (Falkowski and Kiefer, 1985). Different pigments are known to have dissimilar absorption spectra, such that phytoplankton species with particular pigment compositions absorb light energy in a different way (Yentsch and Yentsch, 1979). Cell size and shape affect absorption and scattering dynamics, but these properties also relate to the packaging of pigments within the cell, and the incidence of fluorescence reabsorption within cells. Photoadaptation refers to the ability of phytoplankton cells to adapt to changing environmental conditions by altering their cellular pigment compositions, consequently changing the functional absorption cross-section of PSII (Neori *et al.*, 1984).

2.1.4 Summary

Fluorescence variability that is caused by changes in light absorption is species dependent and relates to photoadaptational state. Fluorescence quantum yield variability indicates the physiological state of phytoplankton cells, as well as the correlation that exists between fluorescence and photosynthesis in PSII. Successful identification of these features intrinsic in the remote sensing fluorescence signal could provide a tool for phytoplankton group distinction, and the prospect exists that fluorescence variability can be used as a phytoplankton physiological proxy. If the link between fluorescence and photosynthesis can be adequately described at a fundamental level, or empirically, it would allow estimation of primary production from the fluorescence signal.

2.2 Fluorescence Measurement Techniques

Various procedures that employ a range of instruments have been developed to allow the study of chlorophyll-a fluorescence in phytoplankton cells. Studies of fluorescence rely on two general approaches. Active fluorescence methods use artificial illumination to induce chlorophyll-a fluorescence, whilst passive fluorescence methods rely on solar excitation energy for fluorescence stimulation.

2.2.1 Simple Active Fluorometry

Single waveband fluorometers, such as the Turner 10-AU fluorometer, detect chlorophyll-a fluorescence by transmitting a beam of blue excitation light through a sample, and measuring the magnitude of the red portion of the emitted spectrum. For *in vivo* fluorescence analysis the excitation beam is typically at 460nm, while the measured emitted beam is at 685nm. Fluorescence emission is acquired in relative units; actual chlorophyll-a concentrations ($[chla]$) are typically calculated by calibration with extracted chlorophyll-a samples. (Turner 10-AU Manual, Turner Designs, Sunnyvale)

These fluorometers can be deployed in a number of ways. Bench top fluorometers are equipped with cuvette holders that allow fluorescence measurements of discrete field collected samples or

laboratory cultures. Flowthrough fluorometers are bench top instruments that contain flowcells, which allow continuous measurement of phytoplankton fluorescence, e.g. along a ship's track. Submersible fluorometers permit *in situ* measurements of fluorescence in the water column and they can be mounted on moorings or profiling packages for real-time, continuous data acquisition. (*ibid.*)

A parameter derived from fluorometer measurements is the fluorescence number. A sample is analysed by recording its fluorescence and, in addition, chlorophyll-a of the sample is extracted in 90% acetone and analysed with the same fluorometer. The fluorescence number is then the ratio of chlorophyll-a fluorescence *in vivo* to chlorophyll-a fluorescence in a 90% acetone extract (Kiefer, 1973b). Fluorescence number is a function of the chlorophyll-a specific absorption rate and the fluorescence quantum yield.

2.2.2 Variable Active Fluorometry

Variable fluorometry, designed to examine the physiology of phytoplankton, was motivated by the knowledge that the fluorescence quantum yield of phytoplankton indicates physiological state as influenced by environmental conditions (Cullen *et al.*, 1997).

An early method of exploiting variable fluorescence involved the measurement of *in vivo* fluorescence via a fluorometer in the presence and absence of DCMU (3-(3,4-dichlorophenyl)-1,1-dimethylurea), a photosynthesis inhibitor, after dark-adaptation of cells (Prézelin and Ley, 1980). Dark adaptation ensures that PSII cellular reaction centres are all open, i.e. that photochemical fluorescence quenching is maximal, and that nonphotochemical quenching of fluorescence by photoprotectant pigments is eliminated (Kolber *et al.*, 1988). DCMU treatment is assumed to completely obstruct energy transport between PSII and PSI (Droop, 1985), thus abolishing the effects of photochemistry. So, fluorescence in DCMU-treated, dark-adapted cells is saturated and maximal (Prézelin and Ley, 1980). The ratio of the difference between the DCMU fluorescence and *in vivo* chlorophyll-a fluorescence to DCMU fluorescence is the dimensionless fluorescence index. Fluorescence index is an indicator of photochemical efficiency of PSII (*ibid.*).

The principle of variable fluorescence can be extended to *in situ*, non-invasive measurements through more recent fluorometry techniques (Cullen *et al.*, 1997). These include the pulse amplitude modulation (PAM) technique, the pump and probe technique (P&P), and fast repetition

rate fluorometry (FRRF). Techniques are based on the progressive closure of PSII reaction centres by a brief succession of strong (pump) and weak (probe) excitation light flashes, which cause a subsequent increase in fluorescence (Sakshaug *et al.*, 1998).

After dark-adaptation of a sample an applied low intensity light pulse measures the minimum fluorescence yield (F_o) when photochemical fluorescence quenching is at a maximum. A subsequent strong pulse of incident irradiance causes PSII reaction centres to close, reducing or eliminating photochemical quenching. After a short delay, another low intensity pulse enables the measurement of the maximal fluorescence yield (F_m) (Aiken, 2001). The maximum change in the quantum yield of fluorescence is calculated as $F_v / F_m = (F_m - F_o)/ F_m$, where the variable fluorescence (F_v) is a measure of the maximum photochemical quenching (Kolber and Falkowski, 1993). F_v / F_m is a quantitative assessment of the fraction of functional PSII reaction centres, i.e. it is a measure of photosynthetic energy conversion efficiency (Kolber *et al.*, 1990). If the pump flash is saturating, the quantum efficiency of photochemistry for PSII becomes $\Delta\phi_{sat}$, where $F_v / F_m = \Delta\phi_{sat} /(\Delta\phi_{sat} - 1)$ (Falkowski and Kolber, 1995).

By varying pump flash intensity at constant time intervals it is possible to derive the relative functional absorption cross-section for PSII (σ_{PSII}), representing the rate of light absorption in PSII, from the slope of a flash-intensity saturation curve (Kolber *et al.*, 1990). Applying different time intervals between pump and probe flashes allows the deduction of the kinetics of electron transport on the acceptor side of PSII (Kolber *et al.*, 1998).

The PAM technique employs a multiple-turnover pump flash, whilst the P&P method uses a single-turnover light pulse. However, the FRRF instrument is more flexible and permits both single-turnover and multiple-turnover flashes to be generated (Kolber *et al.*, 1998). As different excitation protocols are used, the measured variable fluorescence parameters from different methods are not equivalent (*ibid.*).

2.2.3 Spectral Active Fluorometry

Spectral fluorometry allows the assessment of fluorescence through well-defined spectral ranges, as opposed to using broadband excitation and detection. A spectrofluorometer typically consists

of a light emitting lamp, an excitation monochromator, a beam splitter, a monitor detector, an emission monochromator, a photomultiplier, and a variety of mirrors and lenses (Hitachi F-4000 manual, Hitachi Ltd., Tokyo). It can be configured to excite a filter pad or cuvette sample at one wavelength or through a range of wavelengths at specified wavelength intervals. The emission monochromator permits either monochromatic or spectral measurements of emitted light.

The instrument thus permits excitation scans and emission scans at specified wavelengths, as well as 'both scans' that are performed on both excitation and emission sides simultaneously (*ibid.*). In order to measure fluorescence emission of a phytoplankton sample the excitation wavelength can be specified in the blue region of the spectrum and an emission scan performed. The fluorescence emission peak can then be integrated to obtain total emitted fluorescence.

Spectral fluorometry is fundamental to the application of automatic flow cytometry. A flow cytometer enables rapid optical measurements of individual cells by directing suspended particles into a narrow stream and illuminating them with an intense light source. The instrument typically detects side scattering and fluorescence emission; it is possible to adjust excitation wavelengths to ensure that individual particle fluorescence emission is maximised (Yentsch *et al.*, 1983).

Airborne laser systems also employ spectral excitation to induce fluorescence of phytoplankton; these systems are able to detect the resulting artificially stimulated fluorescence (Hoge and Swift, 1983).

2.2.4 Passive Fluorometry Methods

Reflectance ratios calculated from upward and downward spectral irradiance measurements below the ocean surface reveal peaks in the range 683nm – 685nm as a result of the sun-induced *in vivo* fluorescence of chlorophyll-a (Morel and Prieur, 1977). Fluorescence emission causes a signal in the upper, illuminated portion of the water column, which is weak, as the water has a very high absorption coefficient at the wavelengths 683nm – 685nm. However, the signal is also perceptible in the water-leaving reflectance spectra above the ocean surface (Neville and Gower, 1977).

A variety of instruments may be used to study the *in situ* fluorescence signal. An *in situ* spectroradiometer can be employed to measure the upward radiance at 683nm at a given depth

attributable to the contribution of attenuated fluorescence from cells below the sensor (Kiefer *et al.*, 1989). Some instruments incorporate multispectral upward radiance sensors (Cullen *et al.*, 1997), and spectroradiometers can be configured to make hyperspectral radiance and irradiance measurements (Maritorena *et al.*, 2000).A single underwater package incorporating sensors necessary for sun-induced fluorescence derivation is the Profiling Natural Fluorometer (PNF) (Chamberlin *et al.*, 1990). Furthermore, the fluorescence emission signal can be studied from space through satellite spectroradiometers (Neville and Gower, 1977).

Measurements of sun-induced fluorescence allow the estimation of the fluorescence quantum yield (ϕ_f) provided that $[chla]$ was measured concurrent with the fluorescence measurements, and that a reasonable estimation of the phytoplankton absorption coefficient can be made (Chamberlin *et al.*, 1990) or that it can be calculated (Maritorena *et al.*, 2000), or measured (Babin *et al.*, 1995). ϕ_f is defined as the ratio of the number of photons emitted as fluorescence to the number of photons absorbed by the cell.

The ϕ_f parameter can be derived from field measurements as discussed above. The photosynthetic quantum yield ϕ_c, defined as the ratio of the number of carbon atoms fixed in photosynthesis to the number of photons absorbed by the cell, is calculated following carbon assimilation experiments. It is thus not possible to measure ϕ_c on the same space and time scales as is possible for ϕ_f. However, the quantum yield ratio ϕ_c / ϕ_f is a fundamental parameter in the assessment of the relationship between fluorescence and photosynthesis. This fact prompted several investigators to predict quantum yield relationships through the simultaneous analysis of carbon assimilation and fluorescence emission, especially towards the subsequent remote sensing estimation of primary production in the ocean (Chamberlin *et al.*, 1990; Garcia-Mendoza and Maske, 1996). An understanding of the variability of ϕ_c / ϕ_f is principal to the successful prediction of photosynthesis from solar-induced fluorescence through remote sensing techniques (Stegmann and Lewis, 1997).

2.2.5 Summary

Active fluorometry has potential for non-invasive estimation of photosynthetic rate and for inferring the physiological state of natural phytoplankton (Kolber and Falkowski, 1993). More

specifically, measurements of variable fluorescence and σ_{PSII} are essential to improve understanding of photosynthetic electron transport through PSII in ambient light, and of the biophysical origin of quenching processes (Falkowski and Kolber, 1995). It thus provides coherent information at the level of cellular processes of photosynthesis and fluorescence. Although active fluorescence techniques offer much control and insight into cellular mechanisms that are useful also to the understanding of the sun-induced fluorescence signal (Cullen et al., 1997), active systems cannot be used for remote sensing (Maritorena *et al.*, 2000). In contrast, sun-induced fluorescence measured via passive systems has been proposed as a rapid remote sensing method for estimation of phytoplankton biomass and primary production on large spatial and temporal scales (Kiefer *et al.*, 1989; Chamberlin *et al.*, 1990); it might also be possible to deduce phytoplankton physiology and assemblage composition from these measurements.

2.3 Fluorescence Variability

Mechanisms underlying fluorescence variability must be considered with regard to phytoplankton physiology, as fluorescence represents only one of the three ways that absorbed excitation energy can be channelled within a cell. The amount of absorbed energy trifurcated to fluorescence, photochemistry, and heat dissipation is variable, and it is dependent on the physiological status of the cells. Furthermore, fluorescence varies due to phytoplankton absorption variability. Absorption of light is dependent on cell structure, which can be species inter- and intra-specific (Bricaud *et al.*, 1995). Environmental factors are known to influence both cellular absorption, and the efficiency of intracellular energy transport, and thus contribute to the fluorescence variability of cells. This cellular fluorescence variability in the ocean reflects changes in natural assemblage physiological state or species composition (Kiefer, 1973a). So, for a natural population the intensity of fluorescence is a function of assemblage size, the species composition, and the assemblage physiological state.

Studies of both *in situ* and cultured phytoplankton populations have revealed large variability in fluorescence (Kiefer, 1973a), and have aimed to assess the sources of this variability for the purpose of using fluorescence as an ecological or physiological tool (*ibid.*). Laboratory culture experiments are fundamental to an understanding of the physical and chemical influences on natural phytoplankton fluorescence, allowing controlling mechanisms to be studied independently

and under controlled conditions (Laney *et al.*, 2001). Environmental forcing factors found to be relevant to fluorescence variability include the spectral irradiance field and rate of nutrient supply (Kiefer, 1973b). The effect of water temperature on phytoplankton physiology has also been studied through fluorescence variability (Chamberlin and Marra, 1992). These factors vary temporally and spatially in the ocean, and with vertical mixing within the water column. A synopsis of previous research into fluorescence variability follows in this section.

Laboratory culture experiments and *in situ* field observations have employed passive and active fluorescence measurement techniques to study *in vivo* fluorescence and related physiological parameters in terms of the changing ambient conditions of phytoplankton experiencing steady-state growth. Since rates of fluorescence and photosynthesis are complementing functions (Slovacek and Hannan, 1977) – both depend on the absorption of incident light by the photochemical apparatus (Stegmann *et al.*, 1992) – the discussion that follows considers the interrelated processes of fluorescence, absorption, and photosynthesis.

2.3.1 Spatial Distribution of Fluorescence

Field studies focused on gaining insight into fluorescence of phytoplankton in their natural environment consistently found it to vary extensively spatially between stations of specific study areas, and also for different geographical regions.

Passive instruments were employed in various field studies to make fluorescence measurements encompassing a wide range of marine ecosystems. Data of measured fluorescence rate, F, and photosynthetic rate, P, of phytoplankton examined in the South Pacific, the Sargasso Sea, the Weddell-Scotia Seas, the North Atlantic, and Puget Sound ranged over five orders of magnitude (Chamberlin and Marra, 1992). Research in the equatorial Pacific along 150°W found that spatial changes in fluorescence and photosynthesis caused variability also of the fluorescence-photosynthesis relationship (Stegmann *et al.*, 1992). Maximum ϕ_C measured along a path of drifting buoys in the Gulf of St. Lawrence varied by a factor of 20 (Babin *et al.*, 1995).

Active fluorescence methods were also used to assess the spatial variability of fluorescence parameters in the ocean. A study comprising five cruises that sampled San Diego coastal waters, the Gulf of California, Lake Tahoe, and the north central Pacific gyre aimed to derive the

Dunaliella tertiolecta was cultured in four different nitrogen limitation environments (Sosik and Mitchell, 1991). Cellular growth rate roughly increased with an increase in nitrogen concentration. Fluorescence measurements were made with a Sea Tech *in situ* fluorometer. F^* was relatively low at higher growth rates. Values of c_i were seen to increase with growth rate, whilst a_ϕ^* decreased. Maximum ϕ_c values were measured for cells with highest growth rates.

Nitrogen was limited in cultures of *Dunaliella tertiolecta*, *Thalassiosira weissflogii*, the diatoms *Thalassiosira pseudonana* and *Skeletonema costatum*, and a haptophyte *Isochrysis* species (Kolber *et al.*, 1988). With a lowering of nitrogen, total c_i declined and σ_{PSII}, derived from P&P measurements, increased for each culture; values of $\Delta\phi_{sat}$ decreased.

The chlorophyte *Dunaliella salina* and *Thalassiosira weissflogii* were grown subject to fluctuating nutrient supply (Lippemeier *et al.*, 2001). PAM fluorescence of these cultures was measured. Derived F_v / F_m was found to be minimal when cells were nitrogen, phosphorus, and silicon starved. This phenomenon was linked with a corresponding decrease in active PSII centres per cell in some species.

Apart from studying cultured species, active fluorescence techniques were also employed to assess nutrient effects on ocean phytoplankton assemblages. Investigators that employed the P&P fluorescence technique found important correlations. Values of $\Delta\phi_{sat}$ for diatom-dominated samples collected in the Gulf of Maine were low in regions of plentiful nutrients and deep vertical mixing (Kolber *et al.*, 1990). Downstream of the nitrogen source it appeared that an inverse correlation existed between $\Delta\phi_{sat}$ and distance from the source of dissolved inorganic nitrogen. It was proposed that spatial variations of $\Delta\phi_{sat}$ showed that the nutrient regeneration rate in the ocean is not always high enough to optimally maintain phytoplankton photosynthesis. An inquiry into $\Delta\phi_{sat}$ in the subtropical Pacific revealed that spatial variability of $\Delta\phi_{sat}$ was related to nutrient supply (Falkowski *et al.*, 1991). With an increase in nutrient concentration the values of $\Delta\phi_{sat}$ was seen to increase. It was concluded that phytoplankton growth rate was physiologically limited by nutrient availability in this region. During four research cruises in the northwest Atlantic it was noted that F_v / F_m in nutrient limited conditions was variable but relatively low throughout the euphotic zone (Kolber and Falkowski, 1993). Data from the North Atlantic study

did not show an obvious relationship between nutrient supply and F_v / F_m, but a clear correlation was observed between nutrient supply and biomass accumulation (Olaizola *et al.*, 1996). The investigators were able to conclude that F_v / F_m variability in natural assemblages were not solely due to changes in nutrient concentrations.

A study conducted in the eastern equatorial Pacific that contained high-nutrient, low-chlorophyll (HNLC) tropical waters and oligotrophic subtropical waters revealed that FRRF-measured F_v / F_m was relatively low in the nutrient-rich equatorial region, and only slightly higher in the oligotrophic waters (Greene *et al.*, 1994). The nutrient-rich regions also displayed high values of F^* and σ_{PSII}. The results indicated phytoplankton physiological limitations in both the nutrient-rich and oligotrophic conditions, which were attributed to iron limitation across the entire study region.

Passive optical PNF field measurements from seven ocean regions provided combined evidence that light and temperature caused variability in ϕ_c / ϕ_f of natural phytoplankton assemblages (Chamberlin and Marra, 1992). More specifically, a positive linear relationship was observed between ϕ_c / ϕ_f and temperature. However, no relationship could be found between ϕ_c / ϕ_f and nutrient concentration, or ϕ_c / ϕ_f and temperature from data obtained in the California Current and the Gulf of California (Garcia-Mendoza and Maske, 1996). The investigators concluded that ϕ_c / ϕ_f was only dependent on irradiance and they cautioned against misinterpretation of nutrient and temperature effects when irradiance influences had not been eliminated. Data from a cruise to the Canadian sub-arctic and the Scotian Shelf were employed in the modeling of ϕ_c / ϕ_f, which depicted an inverse relationship with temperature (Stegmann and Lewis, 1997).

2.3.3 Fluorescence-Light Dependence

Active fluorescence techniques were used to study the fluorescence-light dependence in cultures. Continuous exposure to high light intensities was seen to cause decreases in F over relatively short, as well as longer time scales in cultures of the diatom *Lauderia borealis* (Kiefer, 1973b). A Turner fluorometer was used to measure these decreases in F, which were concurrent with P

inhibition. Maximum fluorescence numbers were measured at night, while midday values were lowest, thus revealing diel fluorescence variability. Cultures of *Thalassiosira weissflogii* survived for two weeks in a light-deprived environment and revealed very little physiological stress during that time (Berges and Falkowski, 1998). However, *Dunaliella tertiolecta* suffered considerable mortalities subject to the same conditions, which was concurrent with decreases of F_v / F_m. Kolber *et al.* (1988) studied photo-physiological response under growth environments of limited light for five cultured species. In all but one species, namely *Thalassiosira weissflogii*, did they found that with a decrease in irradiance there was a species-dependent increase in σ_{PSII}, but $\Delta\phi_{sat}$ remained unaffected.

Active fluorescence methods were also instrumental in providing an understanding of fluorescence variability with light in ocean field experiments. Kiefer (1973a) found that the change in solar irradiance throughout the day and with depth had an effect on fluorescence near the surface. However, below a specific irradiance limit the fluorescence variability due to changes in light ceased. Fluorescence numbers were maximal during the night, whereas midday values were lowest.

An investigation into the response of phytoplankton fluorescence with ambient variations of light in Lake Tahoe showed that changes in F, measured with an *in situ* fluorometer, are negatively related to changes in light at the surface (Abbott *et al.*, 1982). It was seen that the intensity of F variability with ambient light was dependent on depth, an occurrence that could not be explained by nutrients or photosynthetic rates. Also, the fluctuations of light over longer time periods caused relatively small changes in F compared to short-term light fluctuations.

Measured F_v / F_m of the northwest Atlantic study was found to exhibit a diel cycle with lower values observed during the day as compared to night time values, although reduced values could be observed at night in the deep euphotic zone (Kolber and Falkowski, 1993). A lack of F_v / F_m temporal variability was found in the North Atlantic during the day (Olaizola *et al.*, 1996). Values for F_v / F_m collected above the chlorophyll maximum suggested that it was independent of depth. Prominent diel variability was observed in F_v / F_m during the eastern equatorial Pacific study (Greene *et al.*, 1994). It showed a midday decline and a recovery during the night.

Passive fluorescence techniques were used to study fluorescence as a function of light in cultures as well as in natural assemblages. Sun-induced fluorescence of cultured *Thalassiosira weissflogii* was measured using a photomultiplier tube and filter to study photo-physiological response (Laney *et al.*, 2005). F revealed a strong dependence on irradiance intensity. Temporal variation was evident owing to the daily maximum in F at solar noon, when light was most intense. Midday depressions of ϕ_f were evident under these high light conditions. It was apparent that ϕ_f exhibited three identifiable trends under low light conditions in association with phases of positive, stable, or decreasing population growth.

Field experiments conducted with PNF and spectroradiometer instruments are discussed next. Vertical profiles of F versus irradiance from below six meters showed a resemblance in shape to $[chla]$ profiles in the temperate and tropical waters of the western South Pacific gyre (Kiefer *et al.*, 1989). Values of F and irradiance decreased more gradually with depth in oligotrophic waters compared to mesotrophic regions. Variations in profiles suggested that ϕ_f was lower at elevated light intensities. A diurnal response was observed in F, which indicated the dependence of fluorescence temporal variation on light intensity.

A study using a combined dataset from the central South Pacific, the western Sargasso Sea, and two sheltered bays (Chamberlin *et al.*, 1990) revealed that with an increase in irradiance, ϕ_C decreased at a higher rate than ϕ_f, and thus ϕ_C / ϕ_f decreased with increasing light intensity. Data suggested that neither P nor F varied linearly with irradiance at high intensities of light. It emerged that P, F, and irradiance were related in a predictable fashion.

Measurements performed during the 150°W equatorial Pacific cruise showed that the chlorophyll-a specific photosynthetic rate P^*, and F^* increased linearly with increasing low light intensities, but they exhibited a reduction in rate of increase at higher intensities. Abbott *et al.* (1995) observed similar trends in F^* against irradiance for data obtained from a drifter in the California Current. It was evident that near-surface F and P were non-linear at high irradiance levels. These parameters were higher at midday than in the morning, but lowest in the evening (Stegmann *et al.*, 1992). Modeled ϕ_C / ϕ_f was highest at morning stations and lowest for

measurements made during the evening, which led to the conclusion that ϕ_c / ϕ_f depended appreciably on diurnal variations of light.

Concerning the drifting buoy study in the Gulf of St. Lawrence, measured maximum ϕ_c revealed a diel cycle, although the minimum ϕ_f did not reveal a diel pattern (Babin *et al.*, 1995). Increases in both these properties with depth to the bottom of the euphotic zone were seen in data obtained during the day as well as at night, although the nocturnal increases were weak. In the estuary vertical covariability between maximum ϕ_c and minimum ϕ_f was driven by light and nutrient deficiency.

Results from the Stegmann and Lewis (1997) cruise showed that measured P^* decreased gradually with an increase in depth. It was affirmed that the fluorescence-light and photosynthesis-light relationships lost their linearity near the surface, especially via plots depicting profiles of P^* versus profiles of irradiance, showing a reduced rate of increase in P^* at high light levels. These plots revealed similar P^* with increasing irradiance at morning and evening stations, but midday stations had lower rates. Higher values of F^* with irradiance were confirmed for the morning and evening data in contrast with the midday measurements. F^* increases did not level off at higher intensities of light. It was found that at intermediate irradiance levels, F^* increased faster than P^*. The modeled ϕ_c / ϕ_f was very similar for morning and midday stations, while a lower ratio was achieved at the evening stations.

Phytoplankton optical properties were profiled along 150°W in the Pacific Ocean and in the Peruvian upwelling region (Maritorena *et al.*, 2000). Oligotrophic waters revealed relatively low ϕ_f values in conjunction with high a_ϕ^* values, but in eutrophic waters ϕ_f was high and a_ϕ^* was relatively low. Values of ϕ_f were depressed during maximum irradiance at noon. This effect was most pronounced at the surface. A general increase in ϕ_f was observed with depth.

2.3.4 Fluorescence Variability Summary

The various fluorescence-related studies discussed provide insight into the appropriate interpretation of phytoplankton fluorescence with regard to environmental conditions. These findings can now be summarised.

Culture studies afforded controlled ambient conditions for phytoplankton growth. Although laboratory studies of phytoplankton characteristics are not directly representative of ocean field assemblages, they reveal basic cellular mechanisms.

With regard to fluorescence parameter responses to modulating nutrients, the studies show general consensus. F, F^*, and ϕ_f were all observed to increase as a result of inorganic nitrogen reduction. Similarly, the fluorescence number decreased with increasing nitrogen concentrations, and F and F^* were minimal in conditions of sufficient nutrients. Examination of ϕ_c and $\Delta\phi_{sat}$ with decreasing nitrogen concentrations revealed reductions of these parameters, whereas F_v / F_m was minimal in phytoplankton starved of nutrients. The extent to which F_v / F_m was reduced with nitrogen starvation of phytoplankton was seen to vary with species. With decreases in nitrogen, species-dependent increases of a_ϕ^* and σ_{PSII} as a result of concurrent c_i reductions were evident. Conversely, an increase in c_i was seen when nitrogen concentration was raised, causing a_ϕ^* to decrease.

Light intensity proved fundamental to the variability of fluorescence characteristics. In continuous elevated light conditions, F was seen to decrease. Comparable conditions were also responsible for the inhibition of P. Decreasing irradiance intensities caused an increase in σ_{PSII}, whilst no effect could be detected in values of $\Delta\phi_{sat}$.

Diel variability was observable in the fluorescence number with maximal values measured at night and minimal values at midday. F had a daily maximum around solar noon when the incoming irradiance was at a maximum. Midday depressions of ϕ_f were apparent with high light conditions.

Fluorescence variability measured in natural phytoplankton communities in the ocean appeared more ambiguous compared to the laboratory studies, due to multiple effects of environment dynamics and assemblage diversity, which could not be controlled.

Lower values of a_{ϕ}^{*} in eutrophic waters coincided with relatively high ϕ_f, in comparison to values of ϕ_f in oligotrophic waters. No apparent relationship was observed between F_v / F_m and nutrient availability. Nutrient variability was also seen to be uncorrelated with changes in ϕ_c / ϕ_f. An increase in $\Delta\phi_{sat}$ was observed with increasing nutrient availability, but one study showed that it was low in conditions of high nutrients and deep vertical mixing. Values of F^* and σ_{PSII} were high in HNLC waters where a limitation in iron content caused phytoplankton physiological stress despite high nutrient concentrations. F_v / F_m was low in these regions and slightly higher in iron-limited oligotrophic waters.

There seems to be controversy regarding the effect of temperature changes on ocean phytoplankton. Three studies disagreed on whether ϕ_c / ϕ_f is positively or inversely related to temperature, or if in fact no relationship can be inferred. Findings from another study led the researchers to the conclusion that fluorescence variability that is not associated with irradiance changes could not be explained in terms of temperature variation.

As a general trend F^* was seen to increase linearly as irradiance intensified, provided that light levels remained relatively low. A reduction in the rate of increase was seen at higher ambient light conditions. Moreover, the linear relationship was seen to break down at these intensities, typically occurring near the ocean surface. A similar trend was observed for P^*. F^* and P^* thus typically decreased with depth. Increases in ϕ_f and ϕ_c were evident with depth as direct functions of decreasing *in situ* irradiance, and both parameters decreased markedly near the ocean surface as phytoplankton became subject to high irradiance. With increasing irradiance, ϕ_c decreased at a higher rate than ϕ_f, causing ϕ_c / ϕ_f to decrease. Below some light level the fluorescence-irradiance dependence ceased. Large changes in fluorescence were observed with short-term light fluctuations as opposed to longer-term fluctuations.

A diel cycle could be detected for most of the measured and derived parameters related to fluorescence. Generally, F and P were maximal at midday and minimal during the evening. These parameters were seen to increase in the morning from the low evening values to noon maxima. ϕ_f revealed a depression at noon with maximum irradiance, especially near the surface. Morning and midday values of ϕ_c / ϕ_f were typically relatively high compared to low evening values. The fluorescence number and F_v / F_m were typically relatively high at night, though somewhat reduced in the lower euphotic zone, and low during the daytime with minima occurring at midday. In one study no temporal variation of F_v / F_m could be detected during the day.

2.3.5 Mechanisms of Fluorescence Change

Spatial variations of fluorescence and photosynthesis were found to be attributable to changes in biomass, photoadaptation, species variations, and the efficacy with which phytoplankton utilised sunlight irradiance and nutrients (Stegmann *et al.*, 1992). Using appropriate measurement techniques the various investigators were able to deduce mechanisms underlying fluorescence variability.

Phytoplankton cellular protein synthesis was found to be dependent on the availability of inorganic nitrogen. A reduction in the relative abundance of cellular proteins was believed to occur when nitrogen supply was limited (Kolber *et al.*, 1988). Investigators thus deduced that with a decrease in nitrogen there was a decline in PSII activity in the form of electron transport inefficiency, or reaction centre impairment. Researchers conveyed slightly different perceptions of what this entails:

Kolber *et al.* (1988) specified that electron transport activity was modified on the acceptor side of PSII. Falkowski *et al.* (1991) mentioned the inefficiency of energy transfer from light-harvesting antennae to PSII reaction centres, which according to Kolber *et al.* (1990) was due to a reduction in the production of two specific protein complexes. Greene *et al.* (1994) indicated the inefficiency of excitation energy trapping in PSII. Nutrient limitation that led to a deficiency of some reaction centre proteins was seen to have an effect like photodamage (Babin *et al.*, 1995).

Kolber *et al.* (1988) stated that a reduction in the cellular density of PSII reaction centres occurred with nitrogen limitation. Olaizola *et al.* (1996) considered the construction of functional

PSII reaction centres to be prevented, but Lippemeier *et al.* (2001) suggested that functional PSII reaction centres were reduced, due to a decrease in a specific PSII reaction centre protein. Others mentioned a functional impairment of PSII reaction centres (Kolber and Falkowski, 1993; Greene *et al.*, 1994).

Losses of pigment-protein complexes due to nitrogen limitation caused changes in relative intracellular pigment concentrations (Cleveland and Perry, 1987). In particular, c_i was seen to decrease, which facilitated an increase in a_ϕ^* due to a reduced amount of self-shading as dictated by the package effect (Morel and Bricaud, 1981). Reduced self-shading implied that pigments were more effectively exposed to incident light. Therefore, during nitrogen deficiency the excitation energy was efficiently absorbed, but inadequately utilised (*ibid.*).

It can be deduced that increases in F^* and ϕ_f of phytoplankton in nitrogen-limited conditions were due to increased a_ϕ^*, and the reduced photochemical efficiency of PSII. The latter provides an explanation for observed decreases in P^* and ϕ_C.

Excess irradiance caused photoinhibition of photosynthesis by inactivating a fraction of reaction centres, i.e. causing photodamage to a PSII reaction centre protein (Marshall *et al.*, 2000), and by dissipating excitation energy into the photoprotectant pigments as heat (Babin *et al.*, 1995; Marra, 1997). An increase in the relative proportion of photoprotectant pigments when irradiance was maximal implied that the fraction of excitation energy arriving at the easily damaged PSII reaction centres decreased, resulting in a decrease of F^* (Laney *et al.*, 2005). This fluorescence reduction is thus due to nonphotochemical quenching. Variability of irradiance caused changes in the a_ϕ^*, which were attributed to pigment packaging that varied with cell size and pigment content per cell, and changes in relative accessory pigment abundance due to photoadaptation (Sosik and Mitchell, 1991; Marra, 1997). Light variability was thus also responsible for changes in F^* via absorption efficiency changes.

Light limitation can cause decreased efficiency of pigment absorption and energy transfer from light-harvesting pigments to reaction centres (Cleveland and Perry, 1987). Under light limiting conditions reaction centres were fully functional (Kolber *et al.*, 1988), since light deprivation

does not directly prevent protein synthesis (Berges and Falkowski, 1998). However, the capacity of the cell to acquire reduced organic carbon became impaired (*ibid.*).

Diel variability in fluorescence parameters was attributable to PSII damage, namely photoinhibitory damage (Kolber and Falkowski, 1993), or an excess of photoprotectant pigments (Greene *et al.*, 1994) that occurred at high irradiance during midday, and then recovered at lower irradiances. An uncoupling of the variations in ϕ_C and PSII activity can be ascribed to diel changes, especially via photoprotectant pigments (Babin *et al.*, 1995), which affected fluorescence emission through nonphotochemical quenching (Laney *et al.*, 2005).

2.3.6 Summary

Studies indicated that sources of cellular fluorescence variability included changing light levels, and nutrient availability, although not all species were affected equally. Variability could be inferred from fluorescence measurements that indicated cellular responses to altering environmental conditions, especially in the controlled culture experiments. Field studies of phytoplankton assemblages that were subject to complex ocean dynamics were less simple to analyse. It was admitted that, apart from the inseparable nature of relevant environmental factors in the ocean, backscattering of light and instrument limitations could have modified fluorescence signals. Also, fluorescence measurements were made using a variety of techniques and instruments, which means that fluorescence emission quantities and derived parameters were not directly comparable (Kolber *et al.*, 1998). Furthermore, care needed to be taken when results from different seasons and ocean regimes were compared (Stegmann *et al.*, 1992). However, the studies were largely compatible concerning the general deductions that were made.

The impairment of light energy conversion to chemical energy in phytoplankton cells during nitrogen deficiency was reflected in the fluorescence signal. Some studies endeavour to exploit this interaction for the determination of nutrient limitation in phytoplankton by means of fluorescence (Wood and Oliver, 1995).

Although culture studies found an apparent positive linearity between the specific growth rate and ambient temperature of species of phytoplankton cells grown under saturating light and nutrient-

replete conditions (Montagnes and Franklin, 2001; Stramski *et al.*, 2002), no clear relationship was confirmed with regards to fluorescence and temperature.

An important finding from the studies was that the influence of light on fluorescence variability was distinct near the ocean surface where light intensity was relatively high, as compared to the lower euphotic zone. Diel behaviour of fluorescence was a result of the effects of variable intensity of incident light.

Since the environmental attributes affected the fluorescence signal through cellular absorption as well as energy transfer and reaction centre functionality, it can reasonably be assumed that the signal inherently reflects phytoplankton physiological state and adaptation, as determined by the ecological history of cells (Kiefer, 1973a). However, species differences were also intrinsic to the fluorescence signal (*ibid.*), since cellular size and morphology, and pigment composition dictate absorption characteristics. Variations in fluorescence per unit of chlorophyll-a between phytoplankton species were evident in flow cytometric signals of single cells, which were attributed to the differences in the relative abundance of chlorophyll-a and accessory pigments (Sosik *et al.*, 1989). Abbott *et al.* (1995) found that the ultimate cause for spatial and temporal fluctuations in bio-optical properties was modification of the physical environment. They stated that changes in the physical environment are likely the ultimate cause of species change (*ibid.*).

In the ocean the examination of species differences is problematic due to the large number of species found in natural assemblages (Kiefer, 1973a). Analysis of physiological stress experienced by phytoplankton cells is complicated by cellular alterations induced by both nutrient strain and light limitations (*ibid.*).

2.4 Fluorescence Application

Interest in the quantification of sun-induced chlorophyll-a fluorescence originates from the fact that fluorescence measurements can be made without the perturbation of the natural assemblage (Kiefer *et al.*, 1989). Fluorescence measurements can be made rapidly and frequently over large regions of the ocean, and the fluorescence signal is detectable by remote sensors (*ibid.*). Fluorescence emission is specific to chlorophyll-a pigments and chlorophyll-a derivatives, thus

the measured signal excludes the occurrence of other suspended matter in the water (Lin *et al.*, 1984).

Sun-induced fluorescence was first utilised as a means for assessing the distribution and biomass of phytoplankton in the ocean (Neville and Gower, 1977). In this respect the method was considered an improvement from the ocean colour ratio techniques, since the fluorescence signal increases with increasing biomass, in contrast with the diminishing calculated ratios of high biomass waters as a result of increased absorption (Stegmann *et al.*, 1992). In terms of space recordings, correction for background noise proved simpler when fluorescence is detected than for the colour ratios (*ibid.*). Although the mapping of $[chla]$ is a common application of measured *in situ* sun-induced fluorescence, it is known that chlorophyll-a fluorescence is variable, i.e. $[chla]$ is not linearly related to fluorescence emission (Kiefer, 1973a). Sources of variability were discussed in section 2.3. They include photoinhibition as a result of intense light, species differences due to diverse pigment composition and cell sizes and shapes, photoadaptation that causes changes in pigment composition, nutrient fluctuations, and diel forcing (Falkowski and Kiefer, 1985). The rationale for employing sun-induced fluorescence to estimate $[chla]$ through remote techniques requires that the natural variation of ϕ_f, related to photochemical and nonphotochemical quenching processes, and nutrient status, be ignored (Chamberlin *et al.*, 1990). Nonetheless, it is accepted that fluorescence is valuable in providing a semi-quantitative measure of $[chla]$, which is used as a proxy index of biomass (Falkowski and Kolber, 1995). It is known that increases in $[chla]$ measurements can be a result of changes in c_i as a result of photoadaptation, or it can be due to increases in phytoplankton particle concentration (Kiefer *et al.*, 1989). Only in the latter case does $[chla]$ indicate a biomass increase.

Studies have assessed the possible application of the sun-induced fluorescence signal to obtain the photosynthetic rate of a natural phytoplankton assemblage (Kiefer *et al.*, 1989). Derivation of photosynthetic rate from fluorescence measurements is attractive compared to incubation experiments (*ibid.*). Photosynthesis estimation from incubations cause the sample to be perturbed when removed from the natural environment, whilst changes in light and temperature during the experiments can cause imprecise simulation of the ocean environment (*ibid.*). Incubation also does not account for physical ocean dynamics that phytoplankton might be subject to. Possible contamination of samples is ruled out when sun-induced fluorescence is measured. Furthermore, the remote estimation of production is possible via fluorescence measurements (*ibid.*). The

application of sun-induced fluorescence to the derivation of instantaneous primary production is discussed in more detail in section 5.1.

Although active fluorescence techniques can be applied to the estimation of biomass and photosynthesis, variable active fluorometry provides insight to phytoplankton physiology. Physiological state, affected by environmental ambient conditions, is inferred from the actively measured fluorescence yield of phytoplankton through dark adaptation and exposure to bright light (Kiefer, 1973b). Variable fluorescence indicates maximum photochemical quenching of fluorescence within cells, from measurements of the transfer of absorbed quanta to active PSII reaction centres (Cullen *et al.*, 1997). The active fluorescence yield is a measure of the quantum efficiency for photochemistry of PSII (*ibid.*). Fluorescence induction can be related to the absorption cross-section of PSII. Active fluorescence methods are thus useful to infer physiological state of phytoplankton non-invasively and *in situ.*

The shapes of fluorescence excitation spectra obtained from spectrofluorometers are mainly determined by the composition of pigments within the cells (Prézelin and Boczar, 1986 as cited in Johnsen and Sakshaug, 1993). Light-harvesting roles of pigments can be inferred from scaled fluorescence excitation spectra (Sakshaug *et al.*, 1991). These spectra are used to assist in the development of models that predict photosynthetic efficiency (*ibid.*). Excitation spectra assist in the detection of pigments and the assessment of degradation status of chlorophyll-a (Johnsen and Sakshaug, 1993). Peak ratios of normalised absorption spectra and normalised fluorescence excitation spectra are used to assess the effects of photoprotectant pigments (Lutz *et al.*, 2001). Measurements of fluorescence excitation spectra have been used to determine the photoadapted state of phytoplankton and the species composition (Falkowski and Kiefer, 1985).

It has been proposed that actively measured fluorescence responses to nutrient enrichment may be used to detect nutrient limitation within phytoplankton (Wood and Oliver, 1995).

The main applications of fluorescence are thus the estimation of biomass, and photosynthetic rate, as well as phytoplankton physiology assessments, and pigment differentiation.

Chapter 3

Field Study

Field measurements were necessary to obtain an understanding of fluorescence variability of natural phytoplankton assemblages in the dynamic ocean environment. In particular, these measurements were needed for the interpretation of fluorescence calculated by the fluorescence algorithm, and for the validation of fluorescence parameters calculated through the algorithm. Measurements provided insight into the many physiological factors that influenced fluorescence variability, as well as the effect of algorithm assumptions that were necessary.

Although the FRRF instrument has proved to be valuable in studies of *in situ* fluorescence variability, and phytoplankton physiology, the instrument was not used in the present study. It should be emphasised that the fluorescence algorithm is especially useful with application to satellite data, which requires a study of the sun-induced fluorescence. Therefore, passive optical instruments are employed in this field study, as opposed to active instruments.

Field measurements were made off Lamberts Bay on the west coast of South Africa during March and April of 2005. Sampling of the water column was done daily at the surface and at a depth of 5 meters, generally during midmorning. Seawater sampling was concurrent with *in situ* hydrographic and bio-optical measurements of the water column. The location where measurements took place, known as Station 3, remained constant at 32°05.001S and 18°16.072E throughout the field survey. This station is also the location of a multi-sensor bio-optical mooring, BOB, which provides light measurements for near real-time algorithm analysis.

In this chapter the field methods are described, in addition to the necessary parameter derivations that were required for fluorescence interpretations. Approaches to error analyses and statistical treatments are given. Field results are discussed and interpreted. Finally, conclusions obtained from the field study are drawn.

3.1 Field Methods

Discrete field measurements that were analysed in the laboratory included fluorescence emission, hyperspectral absorption coefficients, carbon assimilation, and pigment and nitrate concentrations. In addition, *in situ* CTD and radiometer measurements were made. The fluorescence and carbon assimilation data were used to derive the fluorescence quantum yield and the photosynthetic quantum yield, respectively.

3.1.1 Fluorescence Measurement and ϕ_f Derivation

A Hitachi F-4000 spectrofluorometer was employed for the measurement of fluorescence emission spectra of discrete water samples. The spectrofluorometer was first prepared by ensuring correct lamp positioning. The instrument beam was adjusted such that the exposed sample would be illuminated by a uniformly diffused beam. A performance check was necessary for wavelength calibration and to test sensitivity of the instrument to confirm that the instrument was operating normally. Scan criteria were set to increase the signal-to-noise (S/N) value, as well as the instrument sensitivity: excitation bandwidth was set at 10nm; the emission bandwidth was 20nm; scan speed was 120nm.min^{-1}; and the response time was set at 0.5 seconds. The spectral fluorescence emission was measured between wavelength bands centred at 600nm and 750nm when excited by a beam centred at 457nm to ensure maximal fluorescence emission peaks.

A single quantum correction was applied to the measured fluorescence spectra to account for spectral modification induced by the instrument response (Johnsen *et al.*, 1997). The 'both scan' of a pure Millipore filter pad was made using the spectrofluorometer set to equivalent scan criteria to the samples. In essence the 'both scan' is a reflectance scan that is obtained through the measurement of an emission spectrum, which was produced by identical excitation wavelengths. Investigation of the Millipore filter pad reflectance spectrum measured in a spectrophotometer instrument, described in section 3.1.2, in reflectance mode revealed 100±1.0% reflectance and transmittance for the wavelengths of interest. It can thus be assumed that any deviation from the result observed in the Millipore 'both scan' should be due to the spectrofluorometer instrument response. The following expression describes the correction strategy applied (modified from Lakowicz, 1983):

Chapter 3

Field Study

Field measurements were necessary to obtain an understanding of fluorescence variability of natural phytoplankton assemblages in the dynamic ocean environment. In particular, these measurements were needed for the interpretation of fluorescence calculated by the fluorescence algorithm, and for the validation of fluorescence parameters calculated through the algorithm. Measurements provided insight into the many physiological factors that influenced fluorescence variability, as well as the effect of algorithm assumptions that were necessary.

Although the FRRF instrument has proved to be valuable in studies of *in situ* fluorescence variability, and phytoplankton physiology, the instrument was not used in the present study. It should be emphasised that the fluorescence algorithm is especially useful with application to satellite data, which requires a study of the sun-induced fluorescence. Therefore, passive optical instruments are employed in this field study, as opposed to active instruments.

Field measurements were made off Lamberts Bay on the west coast of South Africa during March and April of 2005. Sampling of the water column was done daily at the surface and at a depth of 5 meters, generally during midmorning. Seawater sampling was concurrent with *in situ* hydrographic and bio-optical measurements of the water column. The location where measurements took place, known as Station 3, remained constant at 32°05.001S and 18°16.072E throughout the field survey. This station is also the location of a multi-sensor bio-optical mooring, BOB, which provides light measurements for near real-time algorithm analysis.

In this chapter the field methods are described, in addition to the necessary parameter derivations that were required for fluorescence interpretations. Approaches to error analyses and statistical treatments are given. Field results are discussed and interpreted. Finally, conclusions obtained from the field study are drawn.

3.1 Field Methods

Discrete field measurements that were analysed in the laboratory included fluorescence emission, hyperspectral absorption coefficients, carbon assimilation, and pigment and nitrate concentrations. In addition, *in situ* CTD and radiometer measurements were made. The fluorescence and carbon assimilation data were used to derive the fluorescence quantum yield and the photosynthetic quantum yield, respectively.

3.1.1 Fluorescence Measurement and ϕ_f Derivation

A Hitachi F-4000 spectrofluorometer was employed for the measurement of fluorescence emission spectra of discrete water samples. The spectrofluorometer was first prepared by ensuring correct lamp positioning. The instrument beam was adjusted such that the exposed sample would be illuminated by a uniformly diffused beam. A performance check was necessary for wavelength calibration and to test sensitivity of the instrument to confirm that the instrument was operating normally. Scan criteria were set to increase the signal-to-noise (S/N) value, as well as the instrument sensitivity: excitation bandwidth was set at 10nm; the emission bandwidth was 20nm; scan speed was 120nm.min^{-1}; and the response time was set at 0.5 seconds. The spectral fluorescence emission was measured between wavelength bands centred at 600nm and 750nm when excited by a beam centred at 457nm to ensure maximal fluorescence emission peaks.

A single quantum correction was applied to the measured fluorescence spectra to account for spectral modification induced by the instrument response (Johnsen *et al.*, 1997). The 'both scan' of a pure Millipore filter pad was made using the spectrofluorometer set to equivalent scan criteria to the samples. In essence the 'both scan' is a reflectance scan that is obtained through the measurement of an emission spectrum, which was produced by identical excitation wavelengths. Investigation of the Millipore filter pad reflectance spectrum measured in a spectrophotometer instrument, described in section 3.1.2, in reflectance mode revealed 100±1.0% reflectance and transmittance for the wavelengths of interest. It can thus be assumed that any deviation from the result observed in the Millipore 'both scan' should be due to the spectrofluorometer instrument response. The following expression describes the correction strategy applied (modified from Lakowicz, 1983):

$$F_{corr}(\lambda) = \left(F_{instr}(\lambda)\right) \cdot \left(\frac{E_{\circ Xe}(\lambda)}{R_{fil}(\lambda)}\right) \tag{3.1}$$

where $F_{corr}(\lambda)$ (Einst.m^{-2}.s^{-1}.nm^{-1}) is the corrected fluorescence emission; $F_{instr}(\lambda)$ is the spectral emission measured by the instrument in counts; $E_{\circ Xe}(\lambda)$ (Einst.m^{-2}.s^{-1}.nm^{-1}) is the xenon lamp scalar emission incident on the sample as measured by a QSL – 100 laboratory scalar quantum irradiance meter (Biospherical Instruments, Inc.); and $R_{fil}(\lambda)$ signifies the filter pad reflectance spectrum in counts as obtained through the 'both scan'.

The total volume fluorescence F (Einst.m^{-3}.s^{-1}) was calculated by incorporating the cuvette pathlength and then integrating the baseline-subtracted volume emission curve between 665nm and 708nm, after quantum corrected blank subtraction.

Roesler and Perry (1995) provide a way to calculate the measured fluorescence quantum yield, ϕ_f (Einst emitted / Einst absorbed). Their relationship was modified such that it may be applied to the spectrofluorometer:

$$\phi_f = \frac{F}{\int_{400}^{700} \left(a_\phi(\lambda)\right) \cdot \left(E_{\circ Xe}(\lambda)\right) \cdot d\lambda} \tag{3.2}$$

where $E_{\circ Xe}(\lambda)$ (Einst.m^{-2}.s^{-1}.nm^{-1}) is the xenon lamp emission measured by means of a QSL – 100 light meter (Biospherical Instruments, Inc.) equipped with a spherical sensor. Measurement of the phytoplankton absorption coefficient, $a_\phi(\lambda)$ (m^{-1}), is described in section 3.1.2.

Surface samples were stored in semi-transparent bottles and kept outdoors in a thermo-regulated bath that simulated the measured ocean surface temperature. The 5m-samples were similarly kept in a bath corresponding to the temperature at 5 meters in bottles that had dimly lit interiors.

Samples were stored for periods ranging from 30 minutes to three hours before analysis. At the time of measurement a volume of carefully mixed sample was transferred into a 10mm quartz cuvette and placed in the cell holder in front of the exit window of the 150W xenon excitation beam. Minimal exposure of the sample to an artificial environment was ensured, whilst phytoplankton cell damage was prevented as far as possible. Using identical scan criteria to the samples, Milli-Q water emission spectra were obtained for the purpose of blank subtraction.

3.1.2 Absorption Measurement

Phytoplankton absorption measurements were made through a quantitative filter pad technique (Yentsch, 1962, as modified by Bernard, 2005). Whatman glass microfibre filters (GF/F) were used for the filtration of samples under pressure of less than 10mm mercury. Volumes of filtered samples were adjusted to ensure substantial amounts of retained material on the filter pads. Volumes of Milli-Q water were filtered for the preparation of blanks. A Shimadzu UV-2501 spectrophotometer with an ISR-2200 internal integrating sphere was employed for the spectral optical density measurements of filter pad samples between wavelengths of 350nm and 750nm. Absorption coefficients were calculated from measured optical densities with the incorporation of a pathlength amplification factor to correct for the use of glass microfibre filters (Roesler, 1998). Methanol extraction was then conducted on the samples, which were reanalysed to allow measurement of the detrital signal (Kishino *et al.*, 1985). The spectral phytoplankton absorption coefficient, $a_\phi(\lambda)$, was obtained by subtraction of detrital absorption from total particulate absorption.

3.1.3 Photosynthesis Measurement and ϕ_C Derivation

For the description of the carbon assimilation experiment and the consequent derivation of the photosynthetic quantum yield (ϕ_c), it is necessary to acquire some background knowledge of the theory behind photosynthesis-irradiance (P/E) experiments. P/E curves obtained from these experiments indicate the rate of photosynthesis of phytoplankton cells as a function of irradiance intensity, which reveal the cellular efficiency of light utilisation for photochemical purposes (Falkowski and Raven, 1997). These curves are typically divided into three distinct regions. The first is the region of light limitation where photosynthetic rates within cells show a positive linear relationship to irradiance. The second and third regions represent light saturation and

photoinhibition, respectively. The initial slope of the P/E curve that defines the light limited region is proportional to the maximum photosynthetic quantum yield (ϕ_m), which in turn provides a means for the calculation of ϕ_c as described below.

Experiments were conducted to obtain P/E curves of discrete samples by measuring carbon fixation rates in a photosynthetron. The photosynthetron consisted of two thermo-regulated bins that are illuminated by a tungsten lamp shining from below. Each bin is partitioned into 30 incubation chambers with metal neutral density screens fixed at the bottom of each chamber, allowing samples to be exposed to varying intensities of light.

The P/E experiment was conducted soon after sampling of the surface and 5m-depth, according to a method resembling Babin *et al.* (1995). Incubation temperatures were adjusted to match measured *in situ* temperatures. The procedure for sample handling of each bin was identical. A 50ml volume of carefully mixed sample was treated with 50 µCi of $H^{14}CO_3^-$ (Saarchem/Merck) before dispensing 1ml of this aliquot into the photosynthetron glass scintillation vials. The bins were then covered and the tungsten lamp switched on. For the purpose of time zero (T_0) control, three aliquots were kept outside the photosynthetron and acidified with 0.5ml 6N HCl (Saarchem/Merck) at the same time that the lamp was switched on. T_0 control samples served to establish the amount of fixation that had taken place before incubation. Aliquots were incubated for 20 minutes during which time the total activity (T_A) samples were prepared. Three vials with 0.1ml of the aliquot each were treated with 10ml Optima Gold XR scintillation cocktail, and 0.01ml of 6N NaOH (Saarchem/Merck). These vials were capped and continuously stirred along with the T_0 control samples. Incubated samples were removed and acidified with 0.5ml 6N HCl and stirred without capping. After an hour had elapsed all uncapped vials were neutralised by adding 0.01ml of 6N NaOH. A volume of 10ml scintillation cocktail was added and the vials were capped. These vials were then stored under low light conditions until they could be radioassayed by scintillation counting.

The tungsten light intensity I (µEinst.m^{-2}.s^{-1}) penetrating each vial positioned in its incubation chamber was measured using a QSL – 100 laboratory scalar quantum irradiance meter (Biospherical Instruments, Inc.). The tungsten lamp spectrum was measured with an Ocean Optics S2000 miniature fibre optic spectrometer, calibrated by an Ocean Optics LS-1-CAL calibrated light source.

P/E experiment count data were converted to the instantaneous rate of photosynthesis P' (mg C.m^{-3}.h^{-1}) in the following way (Parsons *et al.*, 1984):

$$P' = \frac{(R_S - R_b)\cdot(W)}{(R)\cdot(N)} \tag{3.3}$$

where R_S (dpm) is the sample count, and R_b (dpm) is the T_0 count. The weight of total carbon dioxide, W (mg C.m^{-3}), was taken to be constant at 26284mg C.m^{-3} as determined by seawater salinity. A salinity of 34.8 was assumed. R (dpm) is the T_A count, which was assumed constant at a value of 1.42×10^6dpm. The value used is an average of previously acquired data from a field survey to the same region (G. Pitcher, pers. comm.), due to inconsistencies in the measured results. The time of incubation is given by N (hrs).

Measurement of $[chla]$ is described in section 3.1.4. The chlorophyll-a normalised instantaneous photosynthesis rate, P_B (mg C.(mg chl-a)$^{-1}$.h^{-1}), was plotted against I for each experiment to obtain a P/E curve. In order to obtain the functional parameters needed for the derivation of ϕ_c, namely α (mg C.(mg chl-a)$^{-1}$.h^{-1}.(μEinst.m^{-2}.s^{-1})$^{-1}$) and P_S (mg C.(mg chl-a)$^{-1}$.h^{-1}), a P/E equation of the following form was fitted to the plotted data (Cullen *et al.*, 1992):

$$P_B = (P_S)\cdot\left(1 - e^{\left(\frac{-\alpha\cdot I}{P_s}\right)}\right)\cdot\left(e^{\left(\frac{-\beta\cdot I}{P_s}\right)}\right) \tag{3.4}$$

where α denotes the initial linear slope of the P/E curve and P_S is the maximum rate of photosynthesis in the absence of photoinhibition. The parameter β (mg C.(mg chl-a)$^{-1}$.h^{-1}.(μEinst.m^{-2}.s^{-1})$^{-1}$) characterises photoinhibition.

P_S was not directly applied to the calculation of ϕ_c, but it was used in the derivation of the maximum rate of photosynthesis, P_m (mg C.(mg chl-a)$^{-1}$.h^{-1}) as follows (Platt *et al.*, 1980):

$$P_m = (P_S) \cdot \left(\frac{\alpha}{\alpha + \beta} \right) \cdot \left(\frac{\beta}{\alpha + \beta} \right)^{\frac{\beta}{\alpha}} \tag{3.5}$$

The expression needed for derivation of the photosynthetic quantum yield, ϕ_c (mol C.(Einst)$^{-1}$) is shown in equation 3.6 (Kirk, 1996):

$$\phi_c = (\phi_m) \cdot \left(\frac{E_k}{E_{\circ PAR}(z)} \right) \cdot \left(1 - e^{\frac{-E_{dPAR}(z)}{E_k}} \right) \tag{3.6}$$

where $E_{\circ PAR}(z)$ (μEinst.m^{-2}.s^{-1}) and $E_{dPAR}(z)$ (μEinst.m^{-2}.s^{-1}) are the scalar and vector PAR values respectively, at depth z. These variables were derived from downward irradiance above the ocean surface ($E_d(0+, \lambda)$ (μW.cm^{-2}.nm^{-1})) measured using a Satlantic Tethered Hyperspectral Radiometer Buoy (HyperTSRB), accounting for the air-sea interface via an irradiance transmission factor of 0.95 (Maritorena *et al.*, 2000) and applying a geometric factor of 1.30 (*ibid.*).

In the linear part of the P/E curve the irradiance E_k (μEinst.m^{-2}.s^{-1}) is described as (Kirk, 1996):

$$\alpha = \frac{P_m}{E_k}. \tag{3.7}$$

The maximum photosynthetic quantum yield was calculated via equation 3.8 (Kirk, 1996):

$$\phi_m = \frac{\alpha}{\bar{a}_\phi^*} \tag{3.8}$$

where $\bar{a}_\phi^*$ (m^2.(mg chl-a)$^{-1}$) is the measured, spectrally weighted, phytoplankton mean specific absorption coefficient calculated from the spectrophotometer-derived $a_\phi(\lambda)$, as described in section 3.1.2, and corrected for the tungsten spectrum of the photosynthetron lamp (Kyewalyanga *et al.*, 1997). The parameter ϕ_m was converted to units of molC.(Einst)$^{-1}$, which thus also applied to ϕ_C.

3.1.4 Pigment Concentration Measurements

Pigment concentrations were determined according to Barlow *et al.* (2003). Samples were filtered through 25mm Whatman glass microfibre filters (GF/F) such that they contained approximately similar quantities of material. Filtered samples were immediately placed inside cryovials and frozen in liquid nitrogen until High Performance Liquid Chromatography (HPLC) analyses could be performed. Samples were extracted in 90% acetone using ultrasonication and subsequently clarified via centrifugation. A reverse-phase HPLC process was employed using a 3µm Hypersil MOS2 C_8 column, a Varian ProStar tertiary pump, a Thermo Separations AS3000 autosampler, a Thermo Separations UV6000 diode array absorbance detector, and the ChromQuest chromatography software. Extracts were mixed with 1M ammonium acetate in the autosampler prior to injection. Detection of pigments was made at 440nm and 665nm. Pigments were identified by retention time and diode array spectra, and they were then quantified with respect to a carotenal internal standard (*ibid.*).

An additional method was employed to measure $[chla]$, particularly for the P/E analysis. Triplicates were prepared by filtering 100ml of sample, or 50ml in the case of very high biomass, through a 25mm Whatman glass microfibre filter (GF/F) subject to 13mm mercury pressure. Filtered samples were transferred to test tubes and ground in 90% acetone using a glass rod to

extract the pigments. A total volume of 9ml acetone was added to the filter pads. They were then frozen until fluorometric analysis with a Turner 10-AU fluorometer (Parsons *et al.*, 1984).

3.1.5 Effective Diameter Measurement

A moment-based approach is used to define single-parameter equivalent size distributions (Bernard, 2005). Effective diameters of phytoplankton were measured using a 128-channel Coulter Multisizer II instrument in manometer mode (*ibid.*), using a 140μm aperture. A volume of 0.2ml filtered seawater was used as both blank and electrolyte. Dilution of samples was necessary to keep coincidence levels below 10%. Typically a volume of 40ml of sample was counted (*ibid.*). The measured size distributions were then fractionated into algal and non-algal components through numerical techniques, and the phytoplankton effective diameter was derived (Kishino *et al.*, 1985).

3.1.6 Nitrate Measurement

Nitrate concentrations were analysed according to the manual cadmium reduction method (Nydahl, 1976) in which nitrate is reduced to nitrite prior to measurement. The reductor column contained copperised cadmium, screened to 0.5mm – 1mm size. Flow rates were controlled with a peristaltic pump (Eyela). Nitrite was quantified spectrophotometrically (Cecil CE1020) after diazotisation.

3.2 Error Analysis

Errors associated with measured and derived parameters are complex. These errors were introduced in the process of water sampling and sub-sampling, but also as a result of instrument error, and due to assumptions that were made during parameter derivations. Due to the logistical demands of measurement techniques, it was not possible to make repeated identical measurements. Therefore, errors associated with sample acquisition and preparations were not computed. Calculations of total errors introduced at each phase of derivations were not done. For an indication of error propagation, only errors that resulted from instrument imprecision were

calculated. Conservative error estimates associated with the measurements and derivations were thus calculated, which should be regarded as minimum estimates.

3.2.1 Error Estimates of F and ϕ_f

The S/N ratio of the spectrofluorometer indicated instrument performance and it was defined as the ratio of the mean signal detected to its standard deviation. Noise associated with the instrument was assumed to originate from the sample presentation system, the information encoder, the radiation transducer, and the signal processing and readout system. An estimate of error related to a measurement of fluorescence emission was obtained via the calculation of instrument noise. The Raman emission spectrum of Milli-Q water presented a maximal S/N ratio of 40 after optimum positioning of the light source. The error value could thus be seen to comprise 2.5% of the measured signal. Through the propagation of errors in the fluorescence and absorption measurements an estimate of fluorescence quantum yield uncertainty was calculated to be 3%.

3.2.2 Error Estimate of $a_\phi(\lambda)$

Baseline optical density was used as a representation of spectrophotometer noise to achieve a conservative estimate of error in the absorption coefficient measurement. The average background optical density registered by the spectrophotometer was known to be 0.005; this value was treated as a typical noise estimate in order to calculate instrument error. Conversion of this optical density to an absorption coefficient provided a spectrally constant absorption error. This absorption error was converted to a varying spectral percentage error for every sample spectrum. Spectral mean percentage errors of field samples were calculated for a wavelength range of 400nm to 700nm that yielded an average absorption error estimate of 1.7%. Error inherent in the correction of absorption coefficients for pathlength amplification due to the glass microfibre filter was not incorporated into this value.

3.2.3 Error Estimations for P/E Parameters

Errors resulting from instrument uncertainty during the P/E experiments were approximated through the resolved residuals of the measured P/E data versus the modeled curve. Since the

predicted curves fitted the data closely, the residuals were used to represent the random errors resulting from the instruments that provided the plotted data. The average errors of the calculated parameters P_S, α, and β were obtained as 0.12%, 0.03%, and 0.67%, respectively. Equation (3.5) was used in the propagation of these parameter errors for the error estimation of P_m, which was found to be 0.69%. Additional error propagation was necessary to find the error associated with photosynthetic quantum yield derivation (equation (3.6)). Factors influencing irradiance HyperTSRB measurements included not only the inherent instrument uncertainty, but also the tilt and roll that was experienced during data acquisition, and high-frequency variability in the near-surface light field. In order to assess the collective error due to such factors, the mean and standard deviation of numerous measured irradiance spectra were assessed. The average error calculated in this way amounted to 3.8%. The consequent propagated photosynthetic quantum yield error was 2.8%.

3.2.4 Additional Sources of Error

Underestimated errors were obtained in the analysis described above, since only one source of error, namely instrument error, was calculated for each measurement. For data comparisons of different parameters it was born in mind that spatial and temporal differences between water sampling and *in situ* measurements, due to phytoplankton patchiness and advection, could influence these assessments. However, sampling and *in situ* measurements were kept as coincident as possible. Comparison of measured fluorescence and photosynthesis data is complicated by the fact that the fluorescence measurement is instantaneous, whilst photosynthesis incubations lasted for 20 minutes (Chamberlin and Marra, 1992). The time lag between sample collection and sample analysis is known to affect the interpretation of *in situ* conditions (Babin *et al.*, 1995). Careful sub-sampling was done, and when measurements could not be performed immediately, samples were kept in a simulated light and temperature environment until measurement.

3.3 Statistical Analysis

All statistical analyses were done using a bootstrap technique. This technique was necessary since much of the data was not normally distributed, as determined by a Lilliefors test (Conover, 1980).

A bootstrap analysis using 1000 resampled replicates was done; a Fisher transform (Fisher, 1921) was performed on correlation data to ensure a normal distribution. Coefficients of determination were found using median replicate values, whilst significance levels were calculated at a 95% confidence level. The 2.5th and 97.5th percentiles of the replicated correlation data were thus used, i.e. $p < 0.05$.

3.4 Field Results

The ocean region under consideration is a dynamic and productive system. Advective mechanisms impacted upon Eulerian observations that were made. The direct physical environment influenced fluorescence variability, for example through changes in nutrient availability, and due to assemblage-related variability. It was therefore essential to measure the ambient light regime, water temperature changes, nitrate availability, and biomass dynamics. Furthermore, phytoplankton groups present in the water had to be assessed for effective fluorescence evaluation. Initial analyses are presented in a descriptive and qualitative manner to better introduce and describe the dataset as a whole. In addition to qualitative assessment of the data, quantitative analyses aimed to determine dominant factors governing fluorescence variability. The data were assessed to determine whether it was possible to isolate observable trends in the relationships between possible causal factors and fluorescence variability.

The prevailing daily light regime at Station 3 during the March-April 2005 Lamberts Bay field survey is shown in figure 3.1. Light measurements were made during midmorning, which corresponded to the time that water sampling was done, using a Satlantic HyperTSRB instrument. Measurements of $E_d(0+,\lambda)$ indicated the hyperspectral ambient light field as a result of atmospheric light conditions. The majority of sampling periods coincided with fine weather conditions. On 16/03 and 18/03, sampling was done in foggy conditions, whilst 23/03 sampling concurred with fine and cloudless skies. Rain and overcast dense cloud prevailed during sampling on 20/03 and 06/04.

Measured $L_u(0.66,\lambda)$ ($\mu W.cm^{-2}.nm^{-1}.sr^{-1}$), the upward radiance at 0.66 meters, seemed to match $E_d(0+,\lambda)$ in terms of the intensity of light upwelled in the green region of the electromagnetic spectrum. With more light available in the water column due to sunny atmospheric conditions,

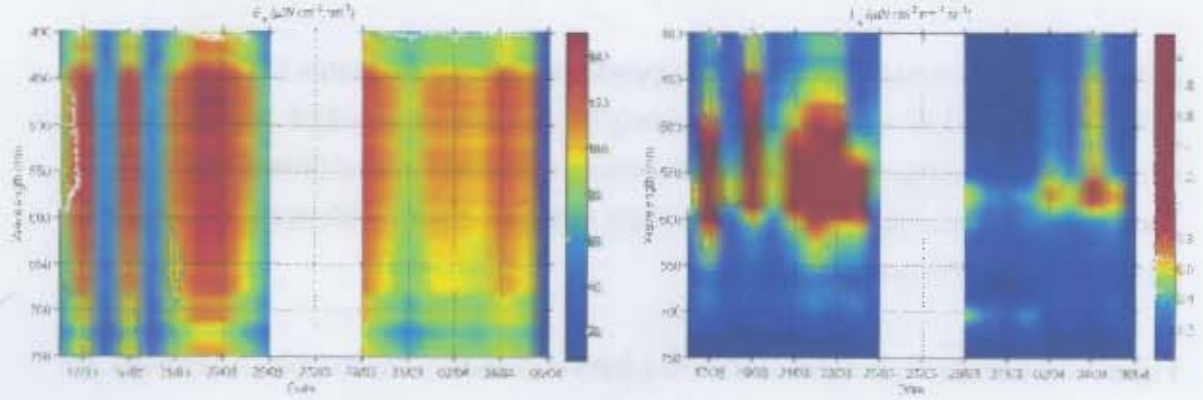

Figure 3.1: Satlantic HyperTSRB measurements of $E_d(0+,\lambda)$ and $I_u(0.66,\lambda)$ for the duration of the Lamberts Bay 2005 field survey. The measurements were made daily during midmorning in conjunction with water sampling.

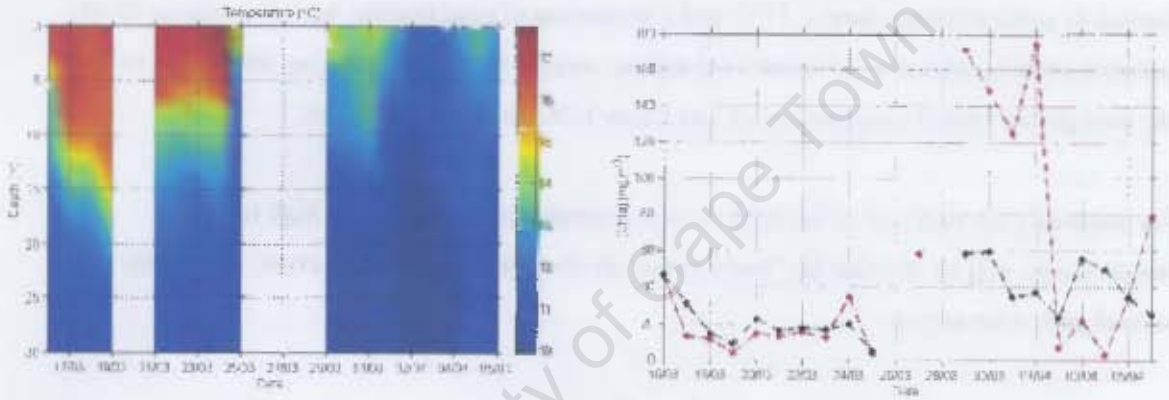

Figure 3.2: Station 3 CTD measurement of water column temperature at the time of sampling. Fluorometric [chla] is given at 0m-depth (red) and 3m-depth (black) for the duration of the survey.

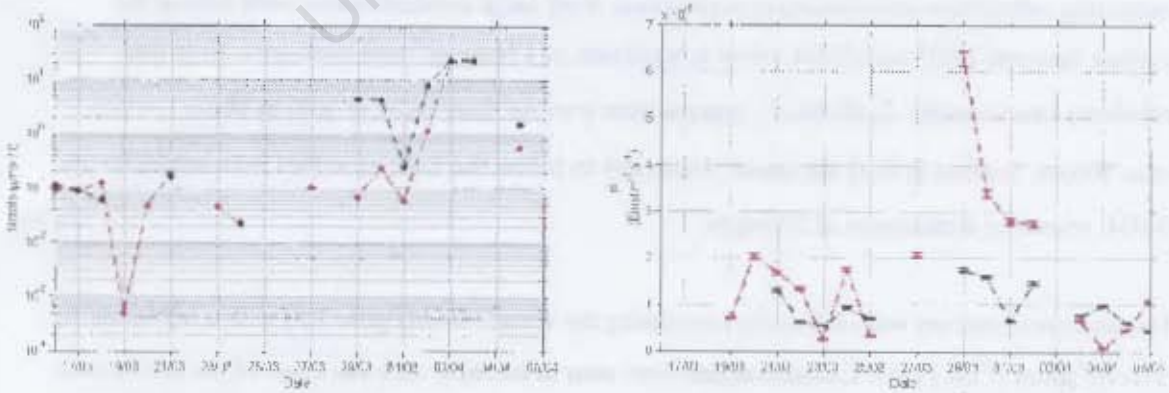

Figure 3.3: Daily nitrate concentrations at the surface (red) and at 5 meters (black) are shown, as well as fluorescence emission, F, as analysed by the Hitachi spectrofluorometer at 0 meters (red) and 5 meters (black).

more light could be scattered upward by phytoplankton and water molecules. Exceptions were 29/03, 30/03, and 01/04 when, although relatively bright conditions prevailed, upward light was minimal and confined to a small region of the spectrum. The peak around 685nm due to fluorescence emission was apparent on most days, except for 29/03, 30/03, and 01/04 when a shifted peak near 700nm replaced it.

Figure 3.2 reveals the temperature profiles to a depth of 30 meters obtained using a Sea Bird CTD instrument, and $[chla]$ as measured fluorometrically (see section 3.1.4) at two distinct depths, namely the surface (red) and 5 meters (black). It was evident that during the first half of the survey the upper water column was relatively warm, and stratified. On 17/03 the surface temperature was 17°C and it remained near this temperature between 19/03 and 24/03. A rapid decline in surface temperature to 14°C and a weakening of stratification was observed on 25/03, possibly showing effects of advected cold surface waters. A cold event during the second half of the time period caused temperatures of just below 12°C on 02/04 and 03/04.

For simplicity the first half of the field survey, corresponding to relatively high water temperatures, will be denoted the 'warm event', as distinct from the 'cold event' during the second part of the survey.

Relatively low $[chla]$ was seen during the warm event at both sampled depths. There was only a minor difference in $[chla]$ between these two depths in agreement with a mixed upper water column on most days. During the cold event $[chla]$ was somewhat elevated at 5 meters, indicating subsurface phytoplankton populations. Very large concentrations were seen at the surface between 29/03 and 01/04, when a maximum of 174mg.m^{-3} was measured. Note that relatively low intensity $L_u(0.66,\lambda)$ spectra were seen on these days, as well as shifted peaks near 700nm. Surface $[chla]$ decreased drastically to below the 5-meter values between 02/04 and 04/04, revealing a minimum of 2.9mg.m^{-3}.

Nitrate concentrations were relatively low during the warm event (figure 3.3) with a minimum of 5.0×10^{-4}µmol.l^{-1} on 19/03. Concentrations were seen to increase with the onset of the cold event, reaching maxima on 02/04 and 03/04 of about 23µmol.l^{-1} at the surface and at 5 meters, although 31/03 and 05/04 experienced drops in nitrate concentration.

Volume fluorescence emission, F, obtained from discrete measurements with the Hitachi spectrofluorometer suggested some trends (figure 3.3). Emission at the surface (red) and at 5-meter depth (black) on 02/04 was undetectable, and therefore the data point was omitted from the diagram. The low F value at the surface occurred in conjunction with low $[chla]$ of 6.6mg.m^{-3} (figure 3.2), as well as a low phytoplankton absorption coefficient at 440nm, $a_\phi(440)$, of 0.2m^{-1} (not shown). At 5 meters $[chla]$ was 23.7mg.m^{-3}, but $a_\phi(440)$ was a relatively low value of 0.5m^{-1}. $a_\phi(440)$ represents the typical Soret absorption peak due to absorption by the majority of chlorophyll and carotenoid pigments (Jeffrey *et al.*, 1997).

Figure 3.4 shows bubble plots of F against $[chla]$, with the phytoplankton absorption coefficient at 675nm, $a_\phi(675)$, represented as relative bubble sizes. Relationships at the surface and at 5 meters are shown. Parameter $a_\phi(675)$ indicates the chlorophyll-a related absorption peak in the red part of the electromagnetic spectrum (Jeffrey *et al.*, 1997).

A positive linear trend was seen to exist between F and $[chla]$ at the surface. An r^2 of 0.69 was determined using the bootstrapping technique (see section 3.3). Surface F minima typically corresponded to lowest measured $a_\phi(675)$ at minimum $[chla]$ values, in a varying range of light conditions. Highest F values at the surface were seen to correspond to relatively high $a_\phi(675)$ and $[chla]$ at comparable light conditions. The data point with $[chla]$ of 57.9mg.m^{-3} coincided with foggy, low light conditions, whilst the 78.2mg.m^{-3} data point was measured in overcast conditions. The lower relative light conditions appeared not to affect the relationships depicted.

The two points of highest $[chla]$ on 29/03 (171mg.m^{-3}) and 01/04 (174mg.m^{-3}) displayed similar $a_\phi(675)$ and light conditions, yet F was lower than expected on 01/04 as compared to 29/03. Observable differences between these two dates included a 2.5°C temperature difference, an order of magnitude difference in nitrate concentrations, and 01/04 revealed a higher relative concentration in accessory pigments (not shown); peridinin was three times higher, whilst diadinoxanthin was double the concentration measured on 29/03. Based on the pigment concentration data, and additional phytoplankton count data, the dinoflagellate *Prorocentrum*

triestinum dominated the phytoplankton assemblage on 29/03, whilst the large dinoflagellate *Ceratium furca* dominated on 01/04.

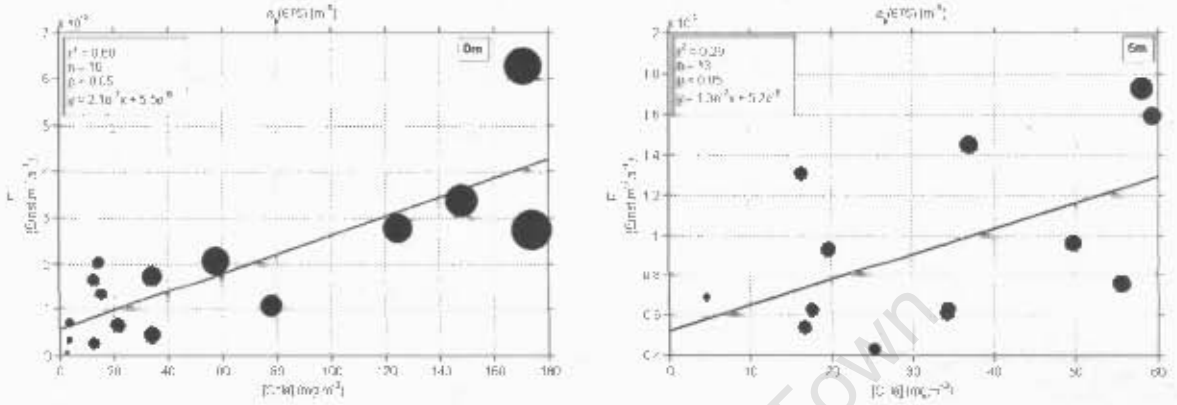

Figure 3.4: Surface and 5m-depth fluorescence emission, F, derived from the Hitachi spectrofluorometer plotted against fluorometric chlorophyll-a concentration, $[chla]$, with sizes of bubbles indicating relative values of the spectrophotometer-measured phytoplankton absorption coefficient, $a_\phi(675)$.

The 5-meter data shown in figure 3.4 suggested a positive linear trend between F and $[chla]$ that was consistent with the surface trend for the relative values seen, although an r^2 of 0.29 was calculated for these few data points. Values of $a_\phi(675)$ increased slightly towards higher $[chla]$ and F, and were consistent with relative $a_\phi(675)$ for a similar $[chla]$ range at the surface. The point with 25mg.m^{-3} corresponded to overcast conditions: it had a value of F that was lower than expected, and $a_\phi(675)$ was somewhat lower than expected.

When plotting the 5m-depth F values against PAR measured with a PNF-300 (Biospherical Instruments, Inc.)(not shown), an approximate negative linear trend was seen. The surface and 5-meter F data seemed to confirm the finding of Babin *et al.* (1996) that at low light intensities F depends largely on PAR, but at relatively high light intensities F depends strongly on $[chla]$. It

appeared that on overcast days, i.e. 20/03 and 06/04, $[chla]$ had a stronger effect on F variability than PAR.

Fluorescence emission variability of the assemblage as a whole was considered in combination with data relating to the phytoplankton cells. Data describing cellular characteristics included effective diameter, chlorophyll-a specific absorption, and chlorophyll-a specific accessory pigment composition, which allowed the assessment of chlorophyll-a specific fluorescence, as well as fluorescence and photosynthetic quantum yields, and the quantum yield ratio.

Coulter counter size data revealed that the effective diameter of phytoplankton cells at the surface was generally higher during the cold event, except for one incidence on 20/03 during the warm event, when the effective diameter was 23.5μm (figure 3.5). The higher relative effective diameters during the cold event were due to the dominance of the large dinoflagellate, *Ceratium furca*, as revealed by phytoplankton count data. A minimum of 8.7μm occurred on 16/03, due to a dominance of the coccolithophorid, *Syrachosphaera pulchra.*

The hyperspectral chlorophyll-a specific phytoplankton absorption coefficient, $a_{\phi}^{*}(\lambda)$ shown in figure 3.6 corresponds to the effective diameter data of figure 3.5. Relative high $a_{\phi}^{*}(440)$ values corresponded to relatively small effective diameters during the warm event, whilst lower $a_{\phi}^{*}(440)$ values were seen during the cold event. On 04/04 the surface $a_{\phi}^{*}(\lambda)$ data were distinct from the other days with a maximum value of $0.1 m^2.(mg\ chl\text{-}a)^{-1}$ at 440nm, and a relatively small effective diameter of 14.6μm. Large effective diameters corresponded to low $a_{\phi}^{*}(440)$. At 5 meters, $a_{\phi}^{*}(440)$ values were relatively higher during the warm event, suggesting that relatively small phytoplankton cells were also found at this depth during this time. During the cold event very low $a_{\phi}^{*}(\lambda)$ at 5 meters suggested that populations with larger cells were situated at this depth.

Chlorophyll-a specific accessory pigment concentrations analysed through the HPLC technique (figure 3.7) show differences between the warm and cold events. The warm event corresponded to a mixture of dominating cellular photosynthetic accessory pigments, namely alloxanthin (green), 19'-hexanoyloxyfucoxanthin (pink), fucoxanthin (red), and peridinin (blue), along with

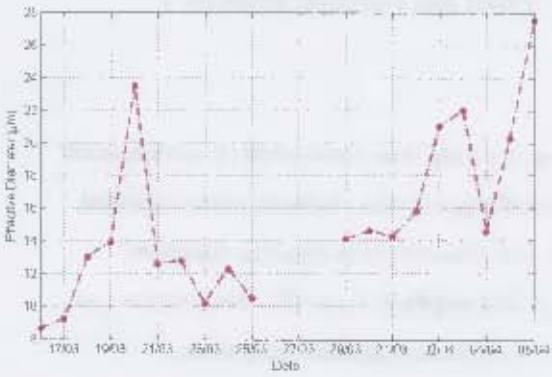

Figure 3.5: Daily Coulter counter effective diameter surface data.

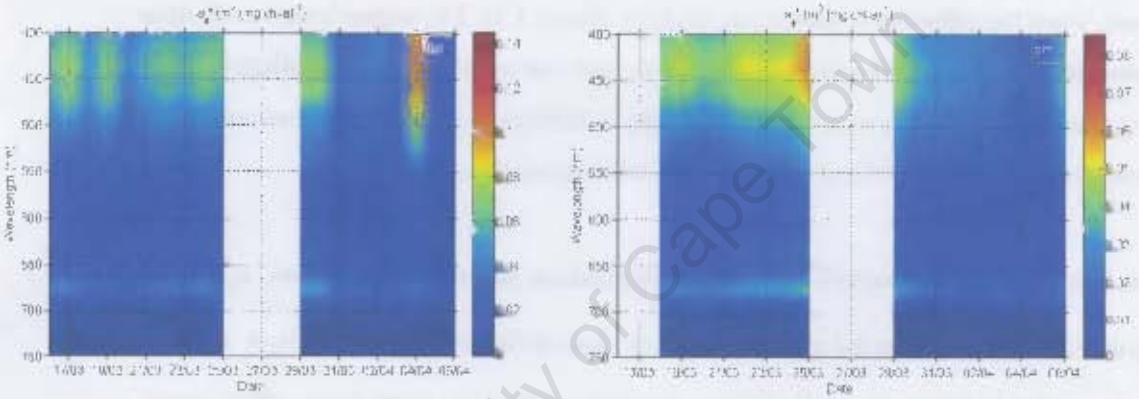

Figure 3.6: Chlorophyll-a specific hyperspectral phytoplankton absorption coefficient, $a_\phi^*(\lambda)$, at the surface and at a depth of 5 meters for wavelengths of 400nm to 750nm.

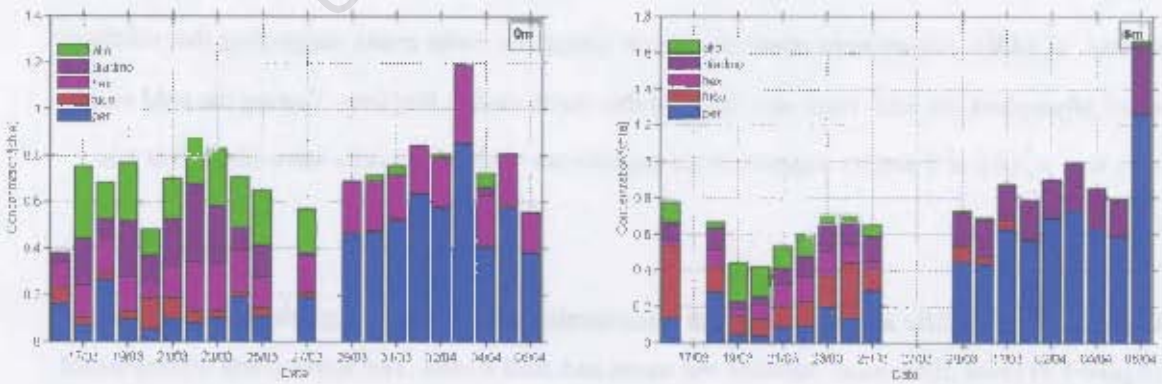

Figure 3.7: Chlorophyll-a specific pigment concentrations for five dominant accessory pigments at 0 meters and 5 meters, namely alloxanthin (green), diadinoxanthin (purple), 19'-hexanoyloxyfucoxanthin (pink), fucoxanthin (red), and peridinin (blue).

the photoprotectant diadinoxanthin (purple), both at the surface and at 5 meters. Phytoplankton count data confirm the alternating dominance of the dinoflagellate, *Prorocentrum triestinum*, and the coccolithophorid, *Syrachosphaera pulchra*, during this period. Higher relative concentrations of the photoprotectant pigment, diadinoxanthin, at the surface suggest differential photoadaptation of cells at the surface compared to the 5-meter cells. During the cold event, cellular peridinin and 19'-hexanoyloxyfucoxanthin dominated at the surface, but peridinin and diadinoxanthin were most prominent at 5 meters. The count data indicate a dominance of the dinoflagellate, *Ceratium furca*, during this time.

In summarising the events observed during the field survey, it was clear that the event with warmer and stratified upper column water corresponded to low biomass, relatively low nutrient concentrations, and small cellular effective diameters, identified as predominantly coccolithophorid and small dinoflagellate. Marker pigments were 19'-hexanoyloxyfucoxanthin and peridinin. Note that the relatively low chlorophyll-a specific peridinin seen during the warm event as compared to the cold event is due to the fact that *Ceratium furca* has a much higher peridinin to chlorophyll-a ratio than *Prorocentrum triestinum*. Diatoms were prominent only during the first two days of the field survey, i.e. 16/03 and 17/03. With the introduction of colder water to the upper column there was an increase in nitrate concentrations, concurrent with a large initial increase in biomass and cellular effective diameters that was identified as a red tide. Large dinoflagellate cells were seen to dominate the phytoplankton population, as confirmed by the peridinin marker pigment. The surface biomass decreased abruptly following the red tide occurrence, whilst the subsurface population persisted.

Parameters of fluorescence and photosynthesis, obtained from derivations of Hitachi fluorescence emission measurements and P/E experiments, varied from day to day as shown in figure 3.8. Surface data are shown in red, and 5-meter data are indicated in black. The chlorophyll-a specific spectrally integrated fluorescence emission, F^*, was higher at both depths during the warm event as compared to the cold event. Literature values of F^* are quoted as $0.05\mu Einst.mg^{-1}.s^{-1}$ – $1.05\mu Einst.mg^{-1}.s^{-1}$ (Abbott *et al.*, 1995). The measured range shown in figure 3.8 is $0.14\mu Einst.mg^{-1}.s^{-1}$ – $1.84\mu Einst.mg^{-1}.s^{-1}$. Maximum F^* appeared on 19/03 and the warm event minimum was on 23/03. The maximum is seen to coincide with a minimum nitrate concentration, and the minimum occurred in intense light conditions. Data of F^* at the surface are not consistently higher than the 5-meter data, as would be expected for large depth differences. The

cold event shows much less variability in F^* at both depths and less discrepancy in the values of the two depths.

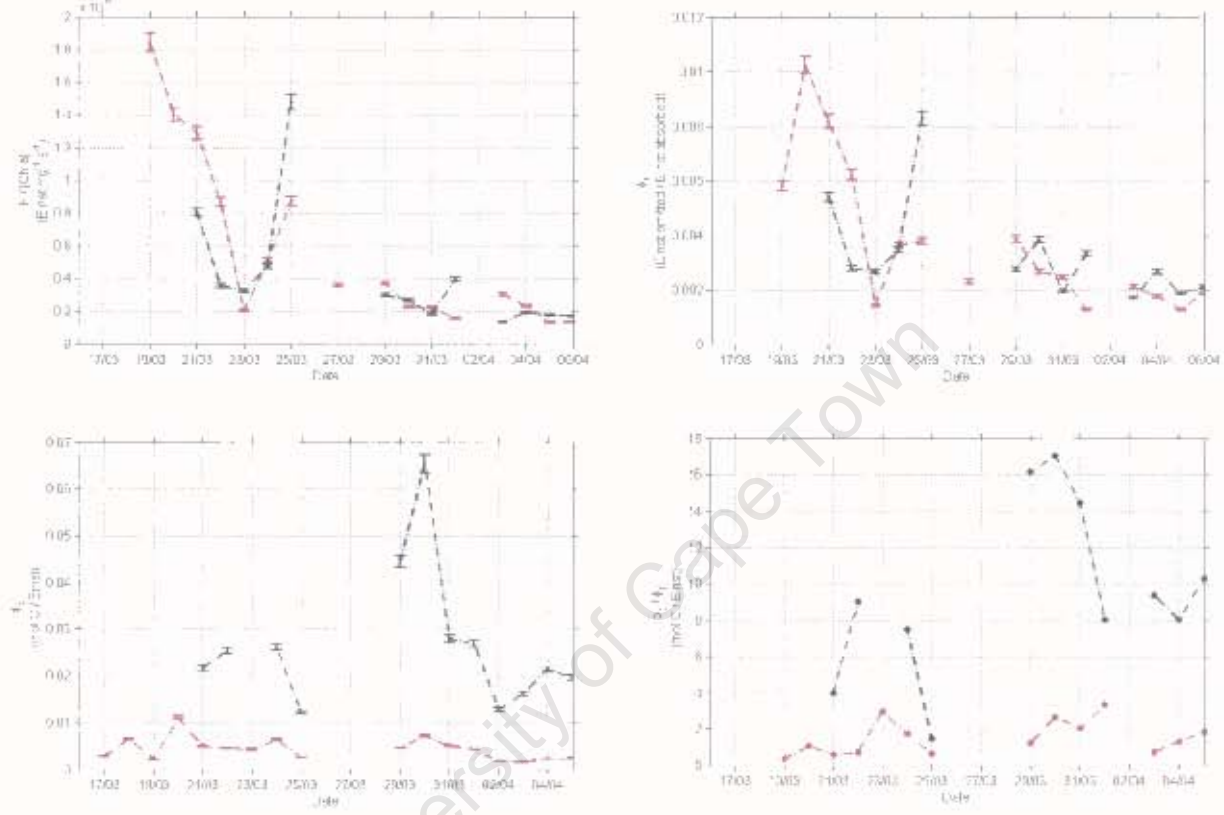

Figure 3.8: Clockwise from top left are chlorophyll-a specific fluorescence emission, F^*, the fluorescence quantum yield, ϕ_f, the quantum yield ratio, ϕ_c / ϕ_f, and the photosynthetic quantum yield, ϕ_C, as derived from measurements at 0 meters (red) and 5 meters (black).

Values of the fluorescence quantum yield, ϕ_f, and photosynthetic quantum yield, ϕ_c, (figure 3.8) agree with measured parameters recorded in the literature. A theoretical maximum of ϕ_f was recorded to be 0.05 (Falkowski and Kiefer, 1985). A study that measured ϕ_f near the ocean surface, approximately at solar noon, found it to be around 0.01 (Maritorena *et al.*, 2000). Values

of ϕ_f derived from measurements of the present study, were found to be within the range 0.001 – 0.01. Literature studies recorded ϕ_c to have values between 0.0015molC.(Einst)$^{-1}$ and 0.051 molC.(Einst)$^{-1}$, and averaged 0.012molC.(Einst)$^{-1}$ through the water column (Lizotte and Priscu, 1994). Maximum ϕ_c was found to vary from 0.004molC.(Einst)$^{-1}$ to 0.08molC.(Einst)$^{-1}$ (Babin *et al.*, 1995). Values seen in figure 3.8, derived from measurements of the present study, range between 0.002 – 0.07molC.(Einst)$^{-1}$.

Similar to the F^* trend, values of ϕ_f were generally higher during the warm event. There was no significant divergence between surface and 5 meter values. ϕ_c on the other hand revealed consistently lower values at the surface. At 5 meters ϕ_c was higher and it fluctuated by larger amounts. Higher ϕ_c was observed during the cold event. For most days, fluctuations in ϕ_f roughly corresponded to fluctuations in ϕ_c at the surface, and at 5 meters. Some surface ϕ_c maxima were seen to correspond to days of lower relative irradiance (figure 3.1), but this was not true on other maxima days.

The quantum yield ratio, ϕ_c / ϕ_f, consistently revealed higher values at 5 meters. At 5m-depth, values of ϕ_c / ϕ_f were higher during the cold event, while the surface did not reveal a clear distinction between the two events. Values of ϕ_c / ϕ_f were slightly high (0.36molC.(Einst)$^{-1}$ – 17 molC.(Einst)$^{-1}$) as compared to modeled literature recordings that ranged from zero to about 8molC.(Einst)$^{-1}$ through the water column (Stegmann and Lewis, 1997).

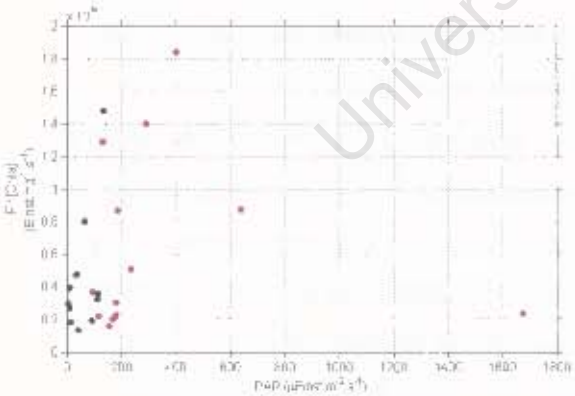

Figure 3.9: The chlorophyll-a specific fluorescence emission, F^*, plotted against PNF PAR for surface data (red) and 5-meter data (black).

Figure 3.9 shows F^* plotted against PAR measured with a PNF-300 (Biospherical Instruments, Inc.) for the surface (red) and at 5 meters (black). At relatively low light

levels, a positive linear trend was discerned, but this trend seemed to break down in relatively high light conditions. At high light intensities a trend resembling a hyperbolic function could be seen. Although few data points were available in the assessment, it seemed possible that two trends existed for different light regimes. F^* thus increased roughly linearly with PAR below approximately 300μEinst.m^{-2}.s^{-1}, but above this light intensity the correlation appeared to change. This deduction is discussed in more detail in section 5.1.3.

3.5 Field Discussion

Data relating to the whole phytoplankton assemblage revealed F trends that closely corresponded to $[chla]$ data, especially at the surface. As expected, the phytoplankton absorption increased with an increase in biomass, resulting in an increase of fluorescence. This relationship affirms the use by some researchers of fluorescence as a biomass proxy (Neville and Gower, 1977) as discussed in section 2.4. This relationship was seen to be valid also on overcast days. However, the 5-meter F data seemed to vary more closely with PAR, which agreed with the findings of Babin *et al.* (1996).

Some deviation from the F versus $[chla]$ relationship appeared to exist at the surface on the days 29/03 and 01/04. It did not seem likely that nonphotochemical quenching was responsible for reduced fluorescence emission at the surface on 01/04. Proportionately, the diadinoxanthin concentration showed no significant increase on this day as compared to previous days, and $E_d(0+,\lambda)$ was not high. With the introduction of new nutrients via colder water to the surface, efficient photochemistry might have caused higher photochemical quenching of fluorescence on 01/04, but this would have produced quenching of fluorescence also at 5 meters. Nitrate trends shown in figure 3.3 suggested increased concentrations at the surface and at 5 meters on 01/04. However, surface pigment concentrations of diadinoxanthin and peridinin on 29/03 were much higher on 01/04. This seemed to suggest that the relative difference in accessory pigment concentrations between these days could be accountable for the difference in fluorescence emission. The dinoflagellate *Prorocentrum triestinum* dominated the phytoplankton assemblage on 29/03, whilst the large dinoflagellate *Ceratium furca* dominated on 01/04.

At the cellular level some additional inferences could be made regarding fluorescence parameters. Phytoplankton effective diameters were seen to vary with $a_\phi^*(\lambda)$ values, especially near 440nm. Maximum surface $a_\phi^*(\lambda)$ near 440nm on 04/04 corresponded to a relatively small effective diameter, whilst effective diameter maxima were seen to be consistent with relatively low $a_\phi^*(\lambda)$ near 440nm

The warm and cold events showed distinct characteristics in F^*, ϕ_f, ϕ_c, and ϕ_c / ϕ_f. Distinctions between the warm and cold events were reflected in other parameters, namely $[chla]$, accessory pigment concentrations, nitrate concentrations, and effective diameter. Chlorophyll-a specific accessory pigment concentrations and effective diameter data suggested that a change in dominant phytoplankton species occurred between the two events. Phytoplankton count data confirmed that the dinoflagellate, *Prorocentrum triestinum*, and the coccolithophorid, *Syrachosphaera pulchra*, dominated during the warm event, whilst the dinoflagellate, *Ceratium furca*, was dominant during the cold event. Fluorescence and photosynthesis variability between the two events was thus concurrent with distinct biomass, temperature, nitrate, and phytoplankton group regimes.

The following scenarios could therefore be considered to explain the principal reasons for the general variability of these parameters between the two events. Variability of $a_\phi^*(\lambda)$ as a result of changing phytoplankton effective diameters, and thus phytoplankton groups, could reasonably be responsible for changes in F^*, although similar variability is seen in values of ϕ_f, which did not vary with $a_\phi^*(\lambda)$. Water temperature changes were not considered to directly cause variability in the fluorescence parameters, since the literature had been inconclusive about parameter variability subject to fluctuating temperatures (see section 2.3.2). Plotting fluorescence parameters with nitrate concentrations revealed no clear trends. Increased nitrate during the cold event could explain the overall increase in ϕ_c values during this period at 5m-depth. Similarly, low nitrate concentrations during the warm event could explain relatively high ϕ_f (see section 2.3.2). Values of ϕ_c at the surface seemed to change independently from nitrate. Maximum F^* on 19/03 corresponded with a minimum nitrate concentration. If nitrate availability regulated the fluorescence and photosynthesis differences between the warm and cold events, then one would

expect higher $a_\phi^*(\lambda)$ during the warm event (see section 2.3.2). Higher $a_\phi^*(\lambda)$ was generally detected during the warm event as compared to the cold event.

Ambient light effects on fluorescence and photosynthesis variability seemed to cause variability from day-to-day. Surface variability of ϕ_c and ϕ_c / ϕ_f appeared to be largely affected by light intensity, due to the large difference in these values between the surface and 5 meters. F^* plotted against PAR seemed to indicate variability according to two different light regimes. Values of F^* and ϕ_f during the warm event roughly showed reductions in ambient high intensity light, whilst increases were observed with decreasing irradiance, as proposed by the literature (see section 2.3.3). Similarly, ϕ_c surface data of the warm and cold events generally showed peaks on relatively low irradiance days. Since PAR was used in the derivations of ϕ_f and ϕ_c, a completely independent comparison was not possible. However, trends between these parameters and PAR are discussed in more detail in section 5.1.3. P/E curves showed that cells did not experience photoinhibition on days of high irradiance. Photoadaptation of cells should therefore also be considered in the analysis, but it was not measured.

3.6 Field Conclusion

Total fluorescence emission of the entire phytoplankton assemblage generally provided an indication of biomass regardless of the prevailing ambient light regime, except at relatively low light levels where fluorescence emission was more closely related to PAR. Differences in fluorescence emission due to a difference in species were suggested. It should be born in mind that variability of c_i due to photoadaptation, which could not be specifically measured, would have complicated the supposition that $[chla]$, and thus fluorescence, indicated biomass.

At the cellular level of investigation several viable explanations for fluorescence parameter variability were possible. Biomass dynamics, nitrate availability, and species differences were all considered, along with the daily irradiance effect. It was found that large changes in the parameters between the two events were possibly related to changes in phytoplankton groups,

and/or changes in nitrate concentrations. Fluctuations in these parameters from day-to-day were attributed to variability of the ambient light.

In conclusion, the causality of fluorescence parameter variability of phytoplankton assemblages in the natural, dynamic ocean environment was complex. No dominant signatures could be inferred with confidence, and even atypical data points were not easily explained. It seemed that different causal factors might dominate in different circumstances, for example when depth distinctions were made, and that all the influencing factors collectively determined the variability.

Chapter 4

Fluorescence Algorithm

The fluorescence algorithm is designed to extract a fluorescence signal from near real-time spectroradiometric data acquired via *in situ* buoy systems and from ocean colour satellite systems. It enables the derivation of both the fluorescence line height (FLH), which quantifies fluorescence emission, and the fluorescence quantum yield, ϕ_f, which is a valuable phytoplankton physiological parameter.

The theory is discussed in this chapter with regard to fluorescence remote optical detection and fluorescence quantum yield derivation. A distinction between algorithm developments is drawn for data acquired from *in situ* moored platforms, in contrast with satellite data. Nesting of the fluorescence algorithm within a hyperspectral inverse reflectance algorithm (Bernard, 2005) is examined. The chapter concludes with algorithm validation and testing. Validation was attempted by comparison of calculated parameters to measured field data. A small field dataset was available for FLH and ϕ_f validations, given that fluorescence parameters were only measured during one field excursion. A larger field dataset, incorporating several field studies to the southern Benguela, was employed to test algorithm performance with field data input, as compared to algorithm-generated input. All field data were obtained through the methods described in section 3.1.

4.1 Model Theory

The mathematical model that is required for the quantification of phytoplankton assemblage fluorescence emission as parameterised by FLH, and ϕ_f, is initiated by the formulation that describes emitted sun-induced fluorescence of phytoplankton in the ocean as follows (Babin *et al.*, 1996):

$$E_{\circ F}(z) = \left(E_{\circ PAR}(z)\right) \cdot \left([chla]\right) \cdot \left(\bar{a}_{\phi}^{*}\right) \cdot \left(Q_a^{*}(685)\right) \cdot \left(\phi_f\right) \cdot dz \qquad (4.1)$$

where $E_{\circ F}(z)$ (Einst.m^{-2}.s^{-1}) is the rate of emitted chlorophyll-a fluorescence of phytoplankton, which occurs at an instant, and emanates isotropically from an infinitesimally thin layer of seawater dz (m) at some depth z (m). This spectrally integrated fluorescence emission is thus a function of the following variables: $E_{\circ PAR}(z)$ is the photosynthetically available scalar radiation (PAR) (Einst.m^{-2}.s^{-1}); $[chla]$ signifies chlorophyll-a concentration (mg.m^{-3}); $\overline{a}_{\phi}^{*}$ is the spectrally weighted mean chlorophyll-a specific phytoplankton absorption coefficient (m^{2}.(mg chl-a)$^{-1}$); $Q_{a}^{*}(685)$ denotes the fluorescence reabsorption factor, also known as the package effect parameter, at 685nm (dimensionless); and ϕ_f is the fluorescence quantum yield (Einst emitted/Einst absorbed).

Main sources of fluorescence variability are accounted for in equation (4.1): species dependence and photoadaptation are indirectly accounted for via $\overline{a}_{\phi}^{*}$; light variability is justified through ϕ_f change, which varies with photochemical and nonphotochemical quenching processes; and nutritional status is reflected in ϕ_f (Babin *et al.*, 1996).

PAR diminishes with depth in an exponential manner through the water column. As shown in equation (4.2), the scalar PAR value at a specified depth z, namely $E_{\circ PAR}(z)$, is determined by the attenuation of excitation irradiance from just below the ocean surface, $E_{\circ PAR}(0)$ (Babin *et al.*, 1996):

$$E_{\circ PAR}(z) = E_{\circ PAR}(0) \cdot e^{-K_{PAR} \cdot z} \qquad (4.2)$$

where K_{PAR} (m^{-1}) is the vertical diffuse attenuation coefficient for PAR.

An upwelling radiance sensor mounted upon an *in situ* buoy detects a signal of fluorescence attributable to the aggregate of all infinitesimal layers emitting fluorescence in its direction from

below the sensor, with the emission undergoing attenuation on the way up to the sensor. Due to the isotropic nature of fluorescence, the fluorescence in an upward vertical direction as a result of emission from one layer can be expressed as follows (Babin *et al.*, 1996):

$$L_F(z) = \frac{E_{\circ F}(z)}{4\pi} \tag{4.3}$$

where $L_F(z)$ (Einst.m^{-2}.s^{-1}.sr^{-1}) represents the radiance at depth z due to fluorescence emitted by phytoplankton from an infinitesimal layer dz in a single direction, i.e. of one steradian solid angle. For the correct interpretation of the measured signal, the upward emitted and attenuated fluorescence from all depths below the sensor should be incorporated. All $L_F(z)$ values below the sensor are integrated and attenuated according to the following mathematical working (modified from Babin *et al.*, 1996):

$$\begin{aligned} L_F(d) &= \int_d^\infty L_F(z)\cdot e^{-c(685)\cdot z}\cdot dz \\ &= \int_d^\infty \left(\frac{1}{4\pi}\right)\cdot\left(E_{\circ PAR}(z)\right)\cdot\left([chla]\right)\cdot\left(\bar{a}_\phi^*\right)\cdot\left(Q_a^*(685)\right)\cdot\left(\phi_f\right)\cdot e^{-c(685)\cdot z}\cdot dz \\ &= \left(\frac{1}{4\pi}\right)\cdot\left([chla]\right)\cdot\left(\bar{a}_\phi^*\right)\cdot\left(Q_a^*(685)\right)\cdot\left(\phi_f\right)\cdot\left(E_{\circ PAR}(0)\right)\int_d^\infty e^{-\left(K_{PAR}+c(685)\right)z}\cdot dz \end{aligned} \tag{4.4}$$

where $L_F(d)$ is the radiance due to fluorescence measured at the depth of the sensor, d, and $c(685)$ (m^{-1}) represents a beam attenuation coefficient. The upper bound of integration is infinity, since sun-induced fluorescence decreases with depth and then becomes insignificant (Stegmann *et al.*, 1992). Feasibility of the model necessitates the assumption that $[chla]$, $\bar{a}_\phi^*$, $Q_a^*(685)$, and ϕ_f are constant through the vertical integrated depth at the instant that the measurement is made. K_{PAR} and $c(685)$ are also assumed to be invariable with depth, as implied by equation (4.4). Due to exponential attenuation of the upward signal, the measured signal is dominated by

the contribution of $L_F(z)$ from layers nearest to the sensor, thus making the assumption viable (Kiefer *et al.*, 1989; Maritorena *et al.*, 2000).

After integration and rearranging of equation (4.4), ϕ_f can be expressed in terms of sensed emitted fluorescence and absorbed irradiance:

$$\phi_f = \frac{(4\pi)\cdot(L_F(d))}{([chla])\cdot(\overline{a}_\phi^*)\cdot(Q_a^*(685))\cdot(E_{\circ PAR}(0))\cdot\left(\frac{1}{K_{PAR}+c(685)}\right)\cdot e^{-d\cdot(K_{PAR}+c(685))}} \quad (4.5)$$

4.2 *In Situ* Model Development

The fluorescence model is developed for near-surface hyperspectral radiometer buoys, such as the Satlantic HyperTSRB and BOB, as these are the most commonly used in the southern Benguela (Bernard, 2005). Near-surface hyperspectral radiometric buoys provide *in situ* observational platforms for the acquisition of radiometric data that can be input into the fluorescence algorithm. With the mathematical model elucidated, the necessary procedures for parameter input and derivation can be considered.

4.2.1 Parameter Computation

Measurements of above-surface hyperspectral downward vector irradiance, $E_d(0+,\lambda)$ ($\mu W.cm^{-2}.nm^{-1}$) and upward subsurface radiance $L_u(d,\lambda)$ ($\mu W.cm^{-2}.nm^{-1}.sr^{-1}$) are obtained from radiometric sensors. Radiance sensors are typically situated between 0.4 m and 0.66m below the water surface and cosine irradiance collectors are typically at 0.5m to 0.7m above the surface. The photosynthetic process does not discriminate between photons of differing energy, but depends on the quantity of photons that are absorbed by chlorophyll-a (Mobley, 1994). As a result, PAR is defined in terms of quanta (*ibid.*). It is therefore necessary that optical variables of equation (4.1) be expressed in quantum units. Radiometric quantities of measured $E_d(0+,\lambda)$ and $L_u(d,\lambda)$ are converted to quantum units via the formulation $\lambda/(h\cdot c_v)$ (Morel and Smith,

1974) where λ (nm) denotes wavelength in a vacuum, h (joules.s^{-1}) is Planck's constant, and c_v (nm.s^{-1}) is the velocity of light in a vacuum. When a radiometric value is multiplied by this energy factor it generates the number of photons that impact upon the sensor.

For the estimation of $L_F(d)$ in equation (4.5) a fluorescence line height (FLH) approach (Gower *et al.*, 1999) is employed to the measured upward radiance spectra at the sensor depth, d. It involves the spectral integration of the fluorescence peak as it appears in the radiance spectra after the subtraction of an interpolated baseline. The baseline represents an approximate spectrum assumed to exist in the absence of fluorescence. This background is a result of elastically backscattered radiation and it can be represented as a straight line, given that water absorption increases in a monotonic way within the fluorescence emission spectral interval (Chamberlin *et al.*, 1990; Maritorena *et al.*, 2000). Morrison (2003) showed that at 683nm the relative contribution of backscattered light to the $L_u(d,\lambda)$ signal compared to the fluorescence signal is small, even at the surface. At any wavelength λ_2 (nm) that falls within the spectral range of fluorescence emission, the corresponding radiance intensity L_{u2} (Einst.m^{-2}.s^{-1}.nm^{-1}.sr^{-1}) is subtracted from the background to give the fluorescence line height $FLH(\lambda_2)$ (Einst.m^{-2}.s^{-1}.nm^{-1}.sr^{-1}) at that point. By adding $FLH(\lambda_2)$ calculated at all points along the fluorescence emission curve, the spectrally integrated fluorescence line height FLH_{int} (Einst.m^{-2}.s^{-1}.sr^{-1}) is obtained. Equation (4.6) illustrates the calculation of FLH_{int} (modified from Gower *et al.*, 1999):

$$FLH_{\text{int}} = \sum_{\lambda_2=665nm}^{705nm}\left[FLH(\lambda_2)\cdot\Delta\lambda\right] = \sum_{\lambda_2=665nm}^{705nm}\left[L_{u2} - L_{u3} - (L_{u1} - L_{u3})\cdot\left(\frac{\lambda_3-\lambda_2}{\lambda_3-\lambda_1}\right)\cdot\Delta\lambda\right] \quad (4.6)$$

where the wavelength λ_1 and radiance intensity L_{u1} characterise the lower boundary of the fluorescence peak, while λ_3 and L_{u3} identify the upper boundary. $\Delta\lambda$ signifies the spectral width of integrated areas. Figure 4.1 assists in visualising the FLH procedure. For application to

the *in situ* data, a lower boundary is adopted at 665nm and an upper boundary at 705nm. *In situ* hyperspectral radiometric systems can typically offer a wavelength resolution of ~1nm, so $\Delta\lambda$ is typically defined at 1nm. Visual inspection of measured *in situ* upward radiance spectra from a variety of water types confirmed the use of this spectral range.

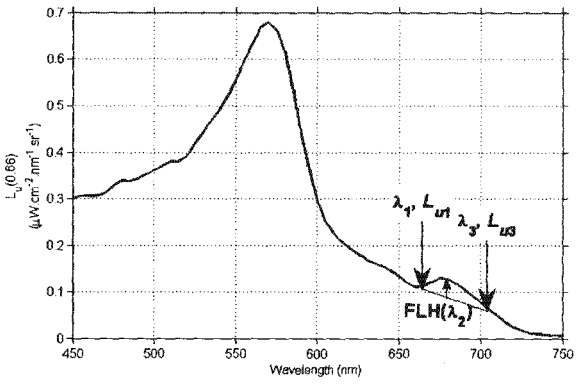

Figure 4.1: Radiance spectrum for the demonstration of the FLH technique

An alternative means to acquire FLH_{int} is through nesting of the fluorescence algorithm within a hyperspectral inverse reflectance algorithm (Bernard, 2005), which is explained in more detail in section 4.4. The reflectance algorithm can fit a mathematically derived curve to the measured radiance data based on simulated inherent optical properties of the water and its constituents, whilst excluding the effect of fluorescence. The fitted curve thus provides the spectral shape of a mathematically computed background in the fluorescence emission spectral interval, which can be subtracted from the measured fluorescence curve and integrated as discussed above. A potential advantage of this method is that a more accurate estimate of the fluorescence signal is obtained due to the calculated backscattering.

FLH_{int} calculated via the latter method will be denoted $FLH_{\text{int}\,2}$ and FLH_{int} calculated by way of the first method will be denoted $FLH_{\text{int}\,1}$, only when the need arises to make the distinction. FLH_{int} calculated via either method is assumed to correspond directly to $L_F(d)$. One can thus equate FLH_{int} and $L_F(d)$.

For *in situ* calculations, $E_d(0+,\lambda)$ is transmitted through the air-sea interface via an irradiance transmission factor of 0.95 (Maritorena *et al.*, 2000) to account for the loss of light as a result of reflection at the air-sea interface. After transmission, the vector downward irradiance just below the surface, $E_d(0,\lambda)$, can be used for the derivation of PAR. The following expression calculates PAR just below the surface, $E_{o\,PAR}(0)$ (Einst.m^{-2}.s^{-1}) (Sakshaug *et al.*, 1998):

$$E_{\circ PAR}(0) = \int_{400nm}^{700nm} E_{\circ}(0,\lambda) \cdot d\lambda \qquad (4.7)$$

where $E_{\circ}(0,\lambda)$ represents the spectral scalar irradiance just below the surface. Scalar irradiance is acquired by the conversion of $E_d(0,\lambda)$ through a geometric factor of 1.30 (Maritorena *et al.*, 2000). The use of this factor is justified in section 4.2.2. From equation (4.7) it is clear that PAR is a broadband quantity that represents all available light for absorption, and the subsequent excitation energy for fluorescence emission.

The vertical diffuse attenuation coefficient of PAR namely K_{PAR} is empirically related to $[chla]$ by means of euphotic depth (Z_e (m)) for case I waters (Morel, 1988). A linear relationship was found as (*ibid.*):

$$K_{PAR} \cdot Z_e = 4.605 \qquad (4.8)$$

and from the definition of Z_e the following expression was obtained (*ibid.*):

$$K_{PAR}(Z_e) = 0.121 \cdot [chla]^{0.428} \qquad (4.9)$$

where $[chla]$ is an output parameter of the hyperspectral inverse reflectance algorithm and can thus directly be fed to the fluorescence algorithm through algorithm nesting.

Another parameter acquired through algorithm nesting is the spectral *in vivo* phytoplankton absorption coefficient, $a_{\phi}(\lambda)$ (m^{-1}). The chlorophyll-a specific *in vivo* phytoplankton absorption

coefficient $a_\phi^*(\lambda)$ (m^2.(mg chl-a)$^{-1}$) is used in the derivation of $\overline{a}_\phi^*$ of equation (4.5) (Babin *et al.*, 1996). Weighted by the *in situ* irradiance spectrum, $\overline{a}_\phi^*$ is given by (*ibid.*):

$$\overline{a}_\phi^* = \frac{\int_{400nm}^{700nm} \left(a_\phi^*(\lambda)\right) \cdot \left(E_\circ(0,\lambda)\right) \cdot d\lambda}{E_{\circ PAR}(0)} \qquad (4.10)$$

Fluorescence within cells may be partially reabsorbed before escaping the cells, as the absorption of chlorophyll-a in the red part of the spectrum coincides partly with fluorescence emission wavelengths. To ensure calculation of the true extracellular yield the reabsorption of fluoresced light within cells is accounted for in equation (4.5) by means of the reabsorption factor $Q_a^*(685)$, which can be expressed in the following way (Morel and Bricaud, 1981):

$$Q_a^*(685) = \frac{a_\phi^*(685)}{a_{sol}^*(685)} \qquad (4.11)$$

where $a_\phi^*(685)$ is the chlorophyll-a specific *in vivo* phytoplankton absorption coefficient at 685nm and $a_{sol}^*(685)$ is the chlorophyll-a specific absorption coefficient in solution at 685nm, which represents the absorption of the cellular material ideally dispersed in solution.

A discrepancy exists between the *in vivo* spectral absorption of phytoplankton cells in suspension compared to the hypothetical absorption of pigments in solution. Absorbing pigments and protein complexes in suspension are clustered within chloroplasts, which in turn exist inside cells, such that they are 'packaged'. This phenomenon, known as the package effect, can cause cellular pigments to be less efficient in capturing ambient light, particularly with an increase in intracellular pigment content and cell diameter (Duysens, 1956). The ratio a_{sus} / a_{sol} characterises the extent of the package effect (Morel and Bricaud, 1981). It is related to the

efficiency factor for absorption, defined as the ratio of the energy absorbed within a spherical phytoplankton cell to the radiant energy arriving at its geometrical cross-section (*ibid.*). The parameter $Q_a^*(685)$ of equation (4.11) represents the fraction of fluorescence that is not reabsorbed at 685nm (Collins *et al.*, 1985).

The value of $a_{sol}^*(685)$ calculated from an acetone solution of chlorophyll-a is known to be $0.011 m^2.(mg\ chl\text{-}a)^{-1}$ (Babin *et al.*, 1996). For the purpose of this study the value was adjusted to a more typical value of $0.016 m^2.(mg\ chl\text{-}a)^{-1}$ based on a previous study of phytoplankton packaging in the southern Benguela (S. Bernard, pers. comm.). An alternative method for the acquisition of $Q_a^*(685)$ is through nesting of the fluorescence algorithm into the hyperspectral inverse reflectance algorithm, which can be configured to return package effect parameters (Bernard, 2005).

The parameter $c(685)$ represents the attenuation of the fluorescence signal on its vertical, upward passage through the water column. After application of the FLH method, scattering at fluorescence emission wavelengths is known to be negligible compared to absorption, which is largely a result of the very high pure water absorption at these wavelengths (Maritorena *et al.*, 2000). In addition to the pure water absorption, the attenuation can also significantly be affected by the absorption of phytoplankton cells at these wavelengths, especially in high biomass waters. Thus, $c(685)$ is calculated by the addition of the absorption coefficient of pure water, $a_w(685)$, to $a_\phi(685)$. A value of $0.495 m^{-1}$ is adopted for $a_w(685)$ (*ibid.*). Values of $a_\phi(685)$ are calculated during the hyperspectral inverse reflectance algorithm operation, and made available to the fluorescence algorithm through nesting.

4.2.2 Assessment of Assumptions

The *in situ* fluorescence algorithm consists predominantly of derived and calculated parameters, light spectra being the only measured input. It is necessary to assess the origin and validity of the assumptions associated with these approximated parameters.

Measurement of $L_u(d,\lambda)$ for the extraction of a fluorescence signal is advantageous since it maximises the ratio of fluorescence to scattered sunlight at all depths (Kiefer *et al.*, 1989). The

FLH calculation becomes problematic in conditions of very low fluorescence due to a low S/N ratio, which can cause equation (4.6) to produce a negative result. $FLH_{\text{int}1}$ is calculated using a constant spectral range. Inspection of radiance spectra reveals that the fluorescence emission curve can shift slightly along the spectral domain, causing imprecise derivations of $FLH_{\text{int}1}$. In waters of very high biomass the intense elastically backscattered light at higher wavelengths may contaminate the fluorescence emission signal. The method that produces $FLH_{\text{int}2}$ provides a more accurate estimation of the background light and therefore a more reliable baseline for subtraction. However, inaccurate values of $FLH_{\text{int}2}$ are still obtained due to the spectral shifting of the fluorescence signal, and due to very low or very high biomass conditions. The FLH technique can therefore only be applied to biomass conditions that fall within a specified $[chla]$ range. This $[chla]$ range and the shifted peaks are assessed in section 4.5.1.

Phytoplankton cells collect light from all directions due to scattering and internal reflection of the light field by the water. Cells are thus best described as spherical collectors (Kiefer *et al.*, 1989). PAR is defined as a scalar irradiance to account for the changing angular distribution of the submarine light field (Morel, 1991), and it is broadband, implying that equation 4.1 assumes ϕ_f to be independent of spectral excitation (Kiefer *et al.*, 1989). The factor used for the conversion of instrument vector irradiance, $E_d(0,\lambda)$, to scalar irradiance, $E_\circ(0,\lambda)$, depends on depth, wavelength, and light conditions above the surface. An approximate value of 1.30 was adopted as derived by Maritorena *et al.* (2000) using radiative transfer modeling. It was derived for oligotrophic, case I conditions where maximal $[chla]$ reached 4.5mg.m^{-3}. Although the area considered in this study is assumed to be case I, $[chla]$ observed is often considerably higher than 4.5mg.m^{-3}. The light field, and therefore the conversion factor, can thus be significantly different in this study as compared to the conditions relevant to the derivation of the Maritorena conversion factor. The vector-to-scalar irradiance factor is known to reach values of up to 2 (Morel, 1991). Green, eutrophic waters can reveal values much higher than 1.20, due to high scattering and relatively low absorption (*ibid.*).

The parameter K_{PAR} depends both on the medium and on the angular structure of the surrounding light field. It is defined in terms of the decrease with depth of ambient PAR. It is strongly associated with $[chla]$ of phytoplankton (Mobley, 1994), since biomass is the main cause of attenuation in natural waters. K_{PAR} relates to the whole photosynthetic spectrum that is

specified in the definition of PAR (Morel, 1988). The Morel empirical formulation used calculates an average K_{PAR} for the euphotic zone, defined as the column of water that reaches to a depth where 1% of the surface light intensity persists (*ibid.*). This vertical region is assumed to have sufficient light to permit phytoplankton photosynthesis. Regression analysis of $[chla]$ versus euphotic layer depth (Z_e) of predominantly case I waters allowed the estimation of K_{PAR} (*ibid.*). Linearity between K_{PAR} and $[chla]$ is only valid for small ranges of biomass concentration (Kirk, 1996).

4.3 Satellite Model Development

In addition to *in situ* buoy sensors, satellite spectrometers are functional in providing optical data for input into the fluorescence algorithm. Whilst *in situ* hyperspectral radiometer buoy data are necessary for algorithm development and validation, a more widespread application of the algorithm emerges through ocean colour satellites. The focus here is on the MERIS sensor as it is configured with three appropriate bands for fluorescence determination. Algorithm adaptation for input of satellite imagery is discussed below.

4.3.1 Parameter Computation

Satellite sensors measure a signal from the very upper layer of the ocean, typically the upper optical depth (Gordon and McLuney, 1975). Therefore, an upward fluorescence signal detected via satellite, represented here as the parameter $L_F(0)$, emanates from just below the water surface. All emitting infinitesimal depth layers contributing to that signal from below are integrated and propagated to the surface, i.e. at 0 meters, such that a simplified version of equation (4.5) is obtained (modified from Babin *et al.*, 1996):

$$\phi_f = \frac{(4\pi)\cdot\left(K_{PAR} + c(685)\right)\cdot L_F(0)}{\left(E_{\circ PAR}(0)\right)\cdot\left([chla]\right)\cdot\left(\bar{a}_\phi^*\right)\cdot\left(Q_a^*(685)\right)} \qquad (4.12)$$

MERIS provides normalised water-leaving reflectance (ρ_{norm}) imagery measured at fifteen discreet channels. The remote sensing reflectance (R_{rs}) is defined as the ratio of the upward radiance to the downward irradiance (Albert and Mobley, 2003). R_{rs} is used in the reflectance algorithm, which necessitates the conversion of ρ_{norm} to R_{rs} (Bernard *et al.*, 2005). With application to satellites and ocean colour, a description of remote sensing reflectance is given in equation (4.13) (Mobley, 1994):

$$R_{rs}(\xi) = \frac{L_W(0+,\xi)}{E_d(0+,\lambda)} \tag{4.13}$$

The remote sensing reflectance, R_{rs} (sr^{-1}), is dependent on ξ that denotes the direction from which the measured light originates and the wavelength that is evaluated. Water-leaving radiance $L_W(0+,\xi)$ ($W.m^{-2}.nm^{-1}.sr^{-1}$) is measured in the air just above the ocean surface, and similarly $E_d(0+,\lambda)$ ($W.m^{-2}.nm^{-1}$) is the downward irradiance above the water's surface.

It is necessary to derive a value for $L_F(0)$ in equation (4.12). The first step is to determine $E_d(0+,\lambda)$, which facilitates the calculation of $L_W(0+,\xi)$ from equation (4.13) and the derivation of $E_{\circ PAR}(0)$. The Gregg and Carder (1990) simple spectral solar irradiance model for cloudless maritime atmospheres is employed to calculate diffuse plus direct spectral irradiance incident onto the sea surface, as $E_d(0+,\lambda)$ is not a standard geophysical satellite product. The available Gregg and Carder Fortran code was translated into Matlab and modified to ensure compatibility with the fluorescence algorithm. The model procedure includes the correction for earth-sun orbital distance of extraterrestrial irradiance, and the consequent attenuation through the atmosphere due to Rayleigh scattering, ozone, oxygen, water vapour, and marine aerosol. Reflectance at the air-sea interface is also accounted for. $E_d(0+,\lambda)$ is calculated at 1nm-resolution in the spectral interval of 350 – 700nm.

Data input of spectral, mean extraterrestrial solar irradiance for the required wavelengths were obtained from Gregg and Carder (1990) and from Bird and Riordan (1986). Meteorological

conditions are known to affect the attenuation of the irradiance through the atmosphere. For the purpose of this study the meteorological input is kept constant at suggested default values. The meteorological quantities used for parameterisation of the model are listed in table 4.1. In addition, the model uses the appropriate date and earth position to derive total atmospheric ozone.

Pressure	29.92mbar
Air-mass type	marine aerosols
Relative humidity	80%
Precipitable water	1.5cm
Mean windspeed	$4 m.s^{-1}$
Current windspeed	$6 m.s^{-1}$
Visibility	15km

Table 4.1: Meteorological input to the Gregg and Carder model

Gregg and Carder (1990) performed a sensitivity analysis to assess the relative importance of meteorological input to the performance of the model. See section 4.3.2 for more detail. According to the authors, the spectral irradiance produced by the model agrees well with observed data.

The modeled Gregg and Carder $E_d(0+,\lambda)$ values are used to calculate $L_w(0+,\xi)$ through equation (4.13). An air-sea transmission factor of 0.7346 (Kirk, 1996) for radiances is applied to acquire the upward radiance just below the surface, $L_u(0,\lambda)$. Radiometric quantities are then converted to quantum units, such that $E_d(0+,\lambda)$ has units of $Einst.m^{-2}.s^{-1}.nm^{-1}$ and $L_u(0,\lambda)$ has units of $Einst.m^{-2}.s^{-1}.nm^{-1}.sr^{-1}$. Transmission of $E_d(0+,\lambda)$ through the air-sea interface to just below the surface is obtained through the conversion factor 0.95 (Maritorena *et al.*, 2000) and

scalar conversion is achieved through the geometrical factor 1.30 (*ibid.*). Calculation of PAR just below the surface, $E_{\circ PAR}(0)$ (Einst.m^{-2}.s^{-1}), is enabled via equation (4.7).

MERIS is equipped with three wavebands that are dedicated to fluorescence detection. Data collected in these three channels are employed in the FLH calculation. Values of $L_u(0,\lambda)$ corresponding to a 10nm-wide band centred at 665nm, a 7.5nm-wide band centred at 681.25nm, and a 10nm-wide band centred at 708.75nm are applied to calculate $FLH(\lambda_2)$ only at a single waveband, such that λ_1 = 665nm, λ_2 = 681.25nm, and λ_3 = 708.75nm (Gower *et al.*, 1999):

$$FLH(\lambda_2) = L_{u2} - L_{u3} - (L_{u1} - L_{u3}) \cdot \left(\frac{\lambda_3 - \lambda_2}{\lambda_3 - \lambda_1} \right) \qquad (4.14)$$

The interpolated linear baseline is now defined between 665nm and 708.75nm, as compared to the *in situ* application of equation 4.6. A Gaussian curve is then used to simulate the fluorescence peak for a spectral range of 665nm to 708.75nm, assuming a maximum L_{u2} at 681.25nm (Gower *et al.* 1999). Fitting Gaussian curves to the fluorescence peaks of a variety of measured *in situ* radiance spectra determined the width of the Gaussian curve. The magnitude of the integrated area below this idealised curve, when the maximum value is normalised to 1, is assumed to represent the area of a typical fluorescence peak. This integrated peak area, which was found to be 15, can be used as a scaling factor for the integration of the Gaussian peaks fitted to measured L_{u1}, L_{u2}, and L_{u3} data. Applying the scaling factor to $FLH(\lambda_2)$ produces the integrated fluorescence emission, FLH_{int}, which in turn represents $L_F(0)$ in equation (4.12).

The alternative means of FLH_{int} calculation applied in section 4.2.1 that requires nesting of the fluorescence algorithm into the hyperspectral inverse reflectance algorithm (Bernard, 2005) can also be applied to multispectral satellite reflectance data. The reflectance algorithm uses an inversion technique to simulate measured reflectance data from the inherent optical properties parameterisations, excluding the fluorescence affected spectral range. The simulated reflectance from the inversion algorithm can thus be used to provide a baseline in the fluorescence range, as it accounts for the effects of absorption and backscattering without fluorescence. Subtraction of

the modeled background at λ_2 = 681.25nm from measured L_{u2} at 681.25nm can be performed to obtain $FLH(\lambda_2)$. Application of the scaling factor produces FLH_{int}.

Where necessary FLH_{int} calculated via the linear baseline method will be denoted $FLH_{\text{int}\,1}$, whilst FLH_{int} obtained from the inverse reflectance method will be known as $FLH_{\text{int}\,2}$.

Remaining variables of equation (4.12), namely K_{PAR}, $c(685)$, $[chla]$, $\bar{a}_{\phi}^{*}$, and $Q_a^{*}(685)$, are calculated for each detected pixel as described in section 4.2.1. Data of $[chla]$ and hyperspectral $a_{\phi}(\lambda)$ are available to the fluorescence algorithm by means of algorithm nesting.

4.3.2 Assessment of Assumptions

As discussed in section 4.2.2 the fluorescence algorithm is developed mainly through parameterisations of the model terms, given that light spectra provide the only measured input. The assessment of assumption validity in the case of the satellite model is similar to section 4.2.2 where the *in situ* model is discussed.

In contrast with the *in situ* model, the satellite model does not receive hyperspectral radiance and irradiance data. Reflectance data at discreet satellite sensor bands are fed into the model. The fluorescence emission peak is characterised through three channels only, which limits the representation of the actual shape of the peak. Representation of the fluorescence emission peak with a Gaussian form therefore has greater uncertainty, although this approach has been applied previously (Maritorena *et al.*, 2000). Additional limitations of the FLH approach have been discussed in section 4.2.2.

The Gregg and Carder (1990) model is applicable to any cloudless oceanic or coastal region. $E_d(0+,\lambda)$ calculated via the model was found by Gregg and Carder to agree spectrally with observed surface spectral irradiances to within ±6.6% (rms) under various atmospheric conditions for the range 400nm – 700nm. The model is constrained by the assumed constant meteorological conditions. Model sensitivity to meteorological input parameters (Gregg and Carder, 1990) revealed that air-mass type, visibility, and total ozone produced differences in surface spectral irradiance that exceeded the model error. Besides restrictions imposed via the irradiance model,

the calculation of PAR is affected by the transmission and conversion factors as discussed in section 4.2.2.

4.4 Algorithm Nesting

The *in situ* radiometer system radiance and irradiance sensors and MERIS spectrometers provide the only available measured input to the fluorescence algorithm. All other parameters required are derived from this measured data. Most parameter inputs have been explained, but the calculations of $[chla]$ and $a_\phi(\lambda)$ remain to be elucidated. By nesting of the fluorescence algorithm into an existing hyperspectral inverse reflectance algorithm (Bernard, 2005) these parameters can be obtained. It is instructive to consider the functioning of the reflectance algorithm, as well as the theory behind it. A brief explanation of the reflectance algorithm is provided.

The basis of the reflectance algorithm is the simulation of reflectance using detailed information on the inherent optical properties of the phytoplankton population. The mechanism of the hyperspectral inverse reflectance algorithm is to simulate reflectance spectra measured by the ocean colour sensor system through standard size distributions of cells assumed to have two-layered spherical geometries, in order to represent the optical properties of phytoplankton populations (Bernard, 2005). The algorithm employs spectral refractive index data and intracellular pigment concentrations of three phytoplankton groups, intended to correspond to the three major phytoplankton classes in upwelling regions, to calculate the efficiency factors for cell sizes ranging between 1μm and 100μm diameters. Refractive index data are derived from field measurements of particle size distributions and particle absorption.

Input to the reflectance algorithm includes the measured hyperspectral upward subsurface radiance and the above surface downward irradiance in the case of *in situ* hyperspectral radiometer buoys, or measured discrete MERIS reflectance imagery. A number of solvable unknowns are then returned as output, namely chlorophyll-a concentration, phytoplankton effective diameter, absorption of gelbstoff and detritus, small particle backscattering, and the fractional contribution of the three phytoplankton groups. A Simplex solution method with constant initial values is used to match remotely measured light spectra. (Bernard, 2005)

Resulting calculated outputs, $a_\phi(\lambda)$ and $[chla]$ are available as input into the fluorescence algorithm, along with the measured light spectra. $Q_a^*(\lambda)$ can also be calculated via the reflectance algorithm as an alternative to equation (4.11).

4.5 Model Validation and Testing

The performance of the developed algorithm is assessed below in the following manner. The effect that the spectral shifts, which occur under high biomass conditions, have on the usefulness of the model will be considered. As a first assessment, parameters that are calculated via the model can be compared to values quoted in the literature. Algorithm evaluation will be done in different parts. The 'fluorescence algorithm' refers to the section of the model that calculates fluorescence parameters without nesting into the reflectance algorithm, and it operates through the input of measured variables. The 'reflectance-fluorescence algorithm' refers to the fluorescence algorithm that is nested within the hyperspectral inverse reflectance algorithm, or 'reflectance algorithm' for short. Input variables for the calculation of fluorescence parameters are generated through the operation of the reflectance algorithm.

Validating the fluorescence model requires the input of field variables and comparison of the calculated fluorescence parameters with the field-measured fluorescence parameters. Very limited data was available for this assessment, since field-measured fluorescence parameters are only available from the Lamberts Bay 2005 survey. As a result of this limitation, output from the different parts of the *in situ* model will be compared. For this purpose the fluorescence algorithm is input with all available discrete sample field data, whilst the reflectance-fluorescence algorithm is input only with the reflectance spectra corresponding to these field measurements. Two versions of the reflectance-fluorescence algorithm are compared; the relative performance between the $FLH_{\text{int}1}$ and $FLH_{\text{int}2}$ methods are assessed. Table 4.2 provides a summary of the field data employed, whilst table 4.3 compares the forms of algorithm discussed. Field measurements were made according to the methods described in section 3.1.

Finally, fluorescence products will be compared to environmental variables to test potential algorithm application.

Date	Location	Dominant Algal Groups	[*Chla*] (mg.m^{-3})
October 2002	Southern Benguela	Mixed	0.24 – 23
October 2002	Shore based Lamberts Bay	*Alexandrium catenella*	309
January 2003	Shore based Saldanha Bay	*Aureococcus anophagefferens*	12 – 14
March 2003	Shore based Lamberts Bay	Mixed	1 – 17
March 2004	Shore based Lamberts Bay	Mixed *Mesodinium rubrum* *Pseudo-Nitzschia* spp.	3 – 70
March & April 2005	Shore based Lamberts Bay	Mixed *Syrachosphaera pulchra* *Prorocentrum triestinum* *Ceratium furca*	3 – 173

Table 4.2: Field surveys of data used as input into the algorithm for testing and comparison of calculated parameters to measured data (modified from Bernard, 2005).

Algorithm	Input	Test
Fluorescence algorithm (Lamberts Bay 2005 – see table 4.2)	**Discreet field data:** $a_\phi(\lambda)$, $[chla]$ ***In situ* data:** $E_d(0+,\lambda)$, $L_u(d,\lambda)$	Validation through comparison of: Measured F and modeled $FLH_{\text{int}1}$ Measured and modeled ϕ_f
Fluorescence algorithm (All field data – see table 4.2)	**Discreet field data:** $a_\phi(\lambda)$, $[chla]$ ***In situ* data:** $E_d(0+,\lambda)$, $L_u(d,\lambda)$	Compare output to the reflectance-fluorescence algorithm output
Reflectance-fluorescence algorithm (All field data – using the $FLH_{\text{int}1}$ method)	***In situ* data:** $E_d(0+,\lambda)$, $L_u(d,\lambda)$	Validation through comparison with measured F and ϕ_f data For algorithm methods comparison; compare modeled F and $FLH_{\text{int}1}$ with measured environmental variables
Reflectance-fluorescence algorithm (All field data – using the $FLH_{\text{int}2}$ method)	***In situ* data:** $E_d(0+,\lambda)$, $L_u(d,\lambda)$	Validation through comparison with measured F and ϕ_f data For algorithm methods comparison

Table 4.3: Table describing the different forms of the algorithm employed, necessary input required, and the purpose of operation.

4.5.1 Restrictions of the FLH Method

One of the limitations of the fluorescence algorithm occurs through the FLH estimation. The typical upward radiance peak in the red part of the spectrum, characterising fluorescence, is a result of the combination of fluorescence emission and elastically backscattered light. In high biomass conditions a peak shifted along the spectral domain to higher wavelengths can be observed, which contaminates the fluorescence emission peak. It thus becomes impossible to separate fluorescence emission via a subtracted baseline. The apparent shifted peak is a result of the combination of high water absorption at these wavelengths, along with the high backscattering of phytoplankton in the same spectral range in high biomass conditions (Bernard, 2005).

Figure 4.2 (a) shows the $L_u(0.66,\lambda)$ spectra measured by the Satlantic HyperTSRB from field surveys done at Station 3 off the coast of Lamberts Bay (see chapter 3). Thin solid lines represent the peaks that are assumed to correspond mainly to fluorescence. Maxima occur from 680nm to 685nm and the spectral range of the peaks is approximately 665nm – 705nm. Dotted lines reveal altered spectra that have maxima near 695nm, whilst the thick solid lines portray peaks of maxima above 700nm within a spectral range of about 685nm – 725nm.

The FLH technique is effective in calculating fluorescence from the peaks that are illustrated by thin solid lines in figure 4.2 (a). However, when the FLH method is applied to peaks shown in dots or thick solid lines, the result is erroneous. Some control needs to be integrated into the algorithm to prevent ambiguous results due to the red shift. When the wavelength corresponding to maximum $L_u(0.66)$ of each peak is compared to $[chla]$ (figure 4.2 (b)) it can be seen that the majority of maxima occur between 678nm and 683nm in conjunction with relatively low $[chla]$. The fluorescence algorithm can therefore be restrained to process data of $L_u(d,\lambda)$ in assemblages with $[chla]$ below 30mg.m^{-3}. Note that this restriction will be inherent in the operation of the algorithm in the remainder of this chapter. The implication of the considerable biomass restriction is that the FLH technique, and thus the algorithm, is not useful for direct HAB assessments. However, it remains useful to the study of formative stages before the high biomass conditions set in. Close inspection of the data in figure 4.2 (b) suggests that maxima at higher wavelengths can also occur in conditions of relatively low $[chla]$. Examination of this signal in

relation to pigment-derived chemotaxonomy shows no discernable patterns. It can be concluded that caution is required with the application of the FLH method, particularly at high $[chla]$ values.

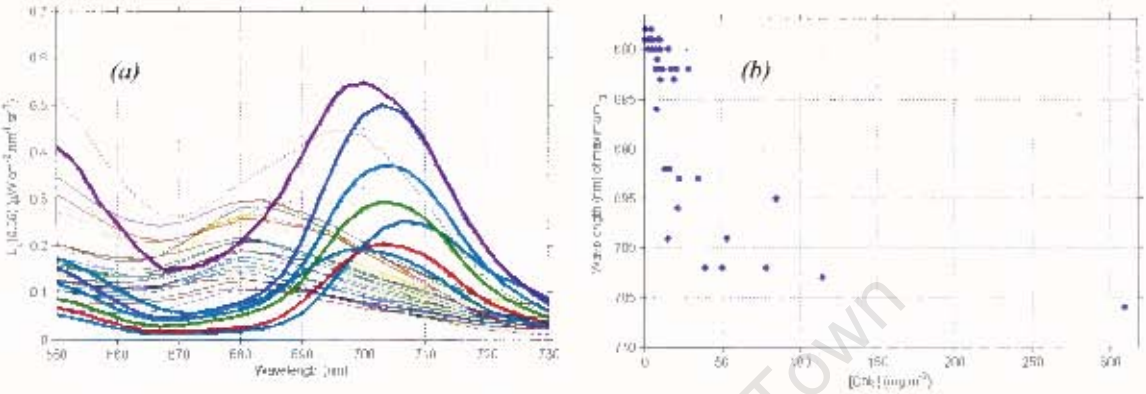

Figure 4.2: (a) Demonstration of the tendency for shifted peaks along the fluorescence emission spectral interval. Thin solid lines represent peaks that provide reliable fluorescence. Dotted and thick lines cannot be used to derive fluorescence. (b) Wavelength of the maximum observed upward radiance peak between 675nm and 710nm plotted against measured $[chla]$ is shown.

4.5.2 Algorithm Validation

In order to assess the performance of the algorithm in its different forms (table 4.3), measured field data can be input into the algorithm with the purpose of comparing calculated output to field measured fluorescence data. Measured fluorescence data are only available from the Lamberts Bay field survey of 2005 (see table 4.2), which is a small dataset for the purpose of validation. Moreover, this dataset reflects only certain ocean conditions with particular phytoplankton assemblages. Ideally, validation should be done using a large dataset, incorporating many ocean- and phytoplankton assemblage conditions. Methods of field data acquisition, measurement, and analysis are discussed in chapter 3.

The size of the dataset is further decreased by the 30mg.m^{-3} $[chla]$ restriction that ensures the omission of possible red shifted spectra for valid calculations of FLH_{int}. Also, one measurement of spectrofluorometer fluorescence emission is omitted due to a very low signal.

Figure 4.3 (a) shows the modeled FLH_{int} versus measured F. Input of the fluorescence algorithm (green) include 1nm-resolution Satlantic HyperTSRB $L_u(0.66,\lambda)$ and $E_d(0+,\lambda)$ data, 1nm-resolution surface $a_\phi(\lambda)$ data, and surface $[chla]$ data, all measured simultaneously during each acquisition. The reflectance-fluorescence algorithm employing $FLH_{\text{int}1}$ (blue) and $FLH_{\text{int}2}$ (red) has input of the field-measured $L_u(0.66,\lambda)$ and $E_d(0+,\lambda)$ data only. A regression analysis was not performed, since too few data points are available, but a line is shown that indicates the best qualitative correspondence obtained from the limited dataset. The line applies to the reflectance-fluorescence algorithm employing $FLH_{\text{int}2}$. Figure 4.3 (b) displays the modeled ϕ_f according to the models mentioned above, as compared to the measured ϕ_f. A line of good qualitative comparison is fitted to the reflectance-fluorescence algorithm that employs $FLH_{\text{int}2}$. The reflectance-fluorescence algorithm also seems to provide a positive linear trend in ϕ_f of figure 4.3 (b). However, reflectance-fluorescence modeled values of ϕ_f (blue and red) are higher than the measured ϕ_f. Values of ϕ_f calculated via the fluorescence algorithm (green) follows a rough positive linear trend with the measured ϕ_f, and there is a smaller difference between these values.

Although the dataset is not large enough to provide a conclusive indication of the validity of the algorithm, or the accuracy with which it estimates ϕ_f, the general trends of figure 4.3 indicate that each of the three models provide plausible estimates of this parameter, although they differ slightly in magnitude. Considering the errors inherent in the derivations of both the measured and the modeled fluorescence parameters, the relationships depicted are considered to be good. The fact that the fluorescence algorithm ϕ_f estimates are closer to the measured values indicates that the $FLH_{\text{int}1}$ method provides a good estimation of fluorescence emission when appropriate biomass restrictions are in place, and that the relatively larger difference in ϕ_f values calculated via the two reflectance-fluorescence models is due to the generating of input variables necessary

for fluorescence parameter calculations. The combination of algorithm-generated input parameters and the FLH_{int2} method causes the largest difference in values of modeled and measured ϕ_f.

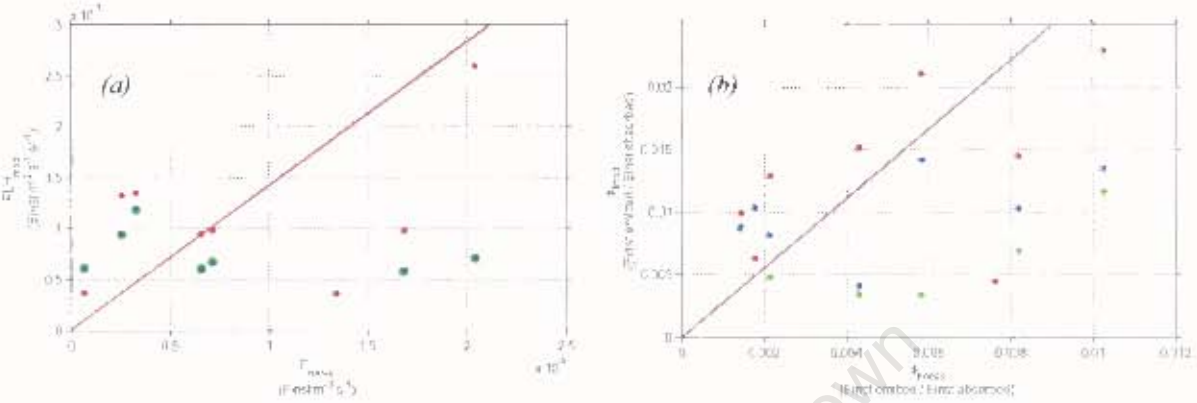

Figure 4.3: (a) Measured F plotted against modeled FLH calculated via the fluorescence algorithm (green), and the reflectance-fluorescence algorithm according to FLH_{int1} (blue) and FLH_{int2} (red). (b) The same models are shown depicting calculated and measured ϕ_f.

4.5.3 Comparison of Algorithm Methods

The relative performance of the different algorithm methods can be explored further. The fluorescence algorithm cannot be applied in a remote operational sense, since nesting is required to ensure the necessary input for fluorescence parameter calculations. It is nonetheless instructive to compare the fluorescence algorithm to the two versions of the reflectance-fluorescence algorithm, since fewer errors are associated with the fluorescence algorithm. Due to a lack of field-measured fluorescence parameters, the fluorescence algorithm thus provides the data against which the reflectance-fluorescence output can be assessed. It is necessary to determine which of the two reflectance-fluorescence techniques provide the best estimates of ϕ_f, such that it may be used in remote sensing applications.

Surface discreet sample data of $a_\phi(\lambda)$ and $[chla]$, as well as concurrently measured HyperTSRB $L_u(0.66,\lambda)$ and $E_d(0+,\lambda)$ measurements from all field surveys described in table 4.2, are considered in the assessment. The data were acquired on separate field surveys in the southern Benguela during the summer season. Field methods were similar to the methods described in section 3.1. Measured field data of $a_\phi(\lambda)$, $[chla]$, $L_u(0.66,\lambda)$, and $E_d(0+,\lambda)$ are necessary as input into the fluorescence algorithm. Reflectance-fluorescence algorithm input consist of $L_u(0.66,\lambda)$ and $E_d(0+,\lambda)$ only.

For relative comparison, figure 4.4 (a) shows reflectance-fluorescence algorithm-calculated $FLH_{\text{int}1}$ (blue), $FLH_{\text{int}2}$ (red), and fluorescence algorithm-calculated $FLH_{\text{int}1}$ (green), all in units of Einst.m^{-2}.s^{-1}.sr^{-1}, plotted against measured $[chla]$. Measured F (black) is in units of Einst.m^{-3}.s^{-1}. Figure 4.4 (b) shows ϕ_f calculated and measured in the same way.

Literature values of fluorescence emission of assemblages compare well with the data seen in figure 4.4 (a). F is seen to be in the range 0.67μEinst.m^{-3}.s^{-1} – 17.5μEinst.m^{-3}.s^{-1}, whilst the modeled values are in the range 0.01μEinst.m^{-2}.s^{-1}.sr^{-1} – 0.31μEinst.m^{-2}.s^{-1}.sr^{-1}. Values reported from different regions and at different depths include 0.0004μEinst.m^{-2}.s^{-1} – 0.5μEinst.m^{-2}.s^{-1} (Chamberlin *et al.*, 1990), as well as volume emissions of 0.16μEinst.m^{-3}.s^{-1} – 1.2μEinst.m^{-3}.s^{-1} (Stegmann *et al.*, 1992; Stegmann and Lewis, 1997) and 0.03μEinst.m^{-3}.s^{-1} – 5.0μEinst.m^{-3}.s^{-1} (Roesler and Perry, 1995). Chlorophyll-a specific volume emissions of 0.05μEinst.mg^{-1}.s^{-1} – 1.05μEinst.mg^{-1}.s^{-1} were measured (Abbott *et al.*, 1995).

Calculated ϕ_f data displayed in figure 4.4 (b) are within the expected range as confirmed by the literature. Values are in the range 0.001 – 0.048. A study conducted in the central South Pacific, the western Sargasso Sea, and two sheltered bays found values of ϕ_f between 0.01 and 0.09, as derived from a PNF (Chamberlin *et al.*, 1990). Values of ϕ_f modeled from reflectance spectra that were measured in various ocean regions yielded values ranging from 0.008 to 0.09 (Roesler and Perry, 1995). A similar method implemented in another study of phytoplankton near the ocean surface produced ϕ_f of 0.005 – 0.01 (Maritorena *et al.*, 2000). A radiance reflectance inversion method was used to calculate profiles of ϕ_f, which produced values of 0.004 – 0.06

(Morrison, 2003). Another author estimates ϕ_f to have values between 0.0005 and 0.05 (Babin, 2003).

Modeled data of figure 4.4 (a) do not vary much between the different models, and a positive trend with $[chla]$ can be discerned for all three models. Values of $FLH_{\text{int }2}$ are generally higher, as compared to the other models.

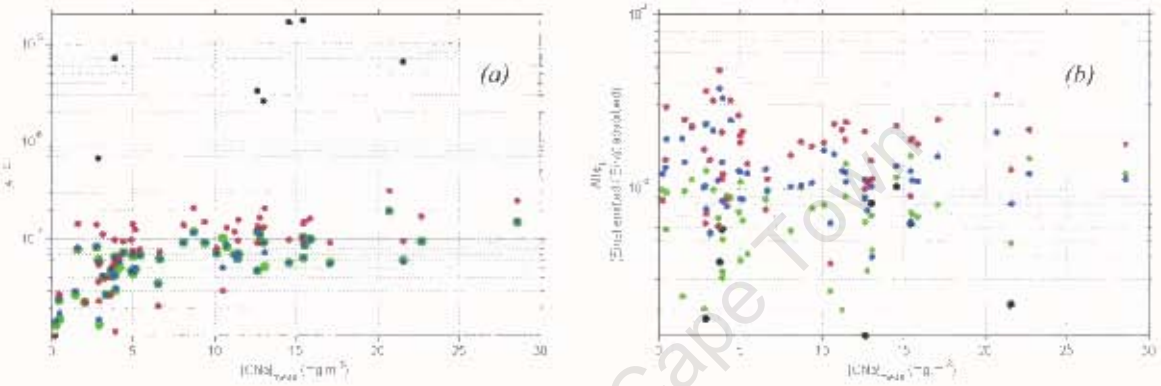

Figure 4.4: (a) Plot of measured F (Einst.m^{-2}.s^{-1}) (black) and modeled FLH (Einst.m^{-2}.s^{-1}.sr^{-1}) calculated via the fluorescence algorithm (green), and the reflectance-fluorescence algorithm according to $FLH_{\text{int }1}$ (blue) and $FLH_{\text{int }2}$ (red) against measured $[chla]$. (b) Similarly, calculated ϕ_f and measured ϕ_f are plotted against measured $[chla]$.

As the near surface layer is considered, values of ϕ_f are expected to be relatively low (see section 2.3.3). At the high light intensities experienced near the surface, photoadaptation of phytoplankton ensures that a larger number of photoprotectant pigments are present within cells, as compared to deeper populations, such that a smaller fraction of excitation energy is available for fluorescence and photosynthesis. As seen in figure 4.4 (b), data of ϕ_f calculated via the $FLH_{\text{int }1}$ method (shown in green and blue), as well as the measured ϕ_f (shown in black), appear viable for the surface layer. The majority of these points are below 0.01. Calculated ϕ_f values of the fluorescence algorithm compare well with measured data. Calculations of ϕ_f via

the reflectance-fluorescence algorithm, using the $FLH_{\text{int}1}$ method, correspond more closely to the fluorescence algorithm calculations than do ϕ_f values calculated via the $FLH_{\text{int}2}$ method. The majority of ϕ_f values calculated via the $FLH_{\text{int}2}$ method are within the range 0.01 – 0.048, which is high for phytoplankton near the surface.

Although $FLH_{\text{int}2}$ is expected to be more accurate than $FLH_{\text{int}1}$, given that the background light is calculated based on reflectance modeling of inherent optical properties, the reflectance algorithm is still in an experimental phase and weighting optimisation needs to be considered further. For the remainder of the chapter, and as an initial study, only the method yielding $FLH_{\text{int}1}$ will be used, since $FLH_{\text{int}1}$ provides results that are more consistent with expected surface data and they are comparable to literature evaluations of FLH_{int}.

4.5.4 Fluorescence as a Tool: Potential Application

Calculated fluorescence products of the reflectance-fluorescence algorithm, with input of $L_u(0.66,\lambda)$ and $E_d(0+,\lambda)$ from all field surveys (table 4.2) as discussed above, can be assessed in comparison with the measured environmental variables to determine functionality of fluorescence as a remote sensing tool. Comparisons of calculated fluorescence parameters to measured data such as temperature, effective diameter, and pigment concentrations, which correspond to the optical measurements, provide an opportunity to examine possible trends. Trends can be assessed in terms of phytoplankton physiology and assemblage group composition. Note that although a large dataset is used, the biomass restriction imposed on the FLH technique (see section 4.5.1) prevents the assessment of high biomass assemblages, and thus HABs.

Bootstrap regression analysis (see section 3.3) of $FLH_{\text{int}1}$ versus measured $[chla]$ provides confirmation of a relatively strong positive correlation, which indicates the fluorescence-biomass proxy (Neville and Gower, 1977) as discussed in section 2.4. A value for r^2 is calculated to be 0.41 (figure 4.5 (a)). A positive correlation is also detected between $FLH_{\text{int}1}$ and total fucoxanthin concentrations, which presents an r^2 of 0.49 (figure 4.5 (b)). Fucoxanthin is the dominant accessory pigment within diatoms. The correlation seen in figure 4.5 (b) necessitates the investigation of a potential premise that diatoms fluoresce more intensely than dinoflagellates. This idea is based on inspection of certain reflectance spectra. Fucoxanthin and peridinin are

carotenoids that can be used as biomarkers of diatoms and dinoflagellates, respectively. However, bootstrap regression of measured $[chla]$ versus fucoxanthin concentrations reveals an r^2 of 0.81, which indicates that diatoms are the dominant phytoplankton group in the data set. Diatoms are generally expected to dominate in an upwelling system, but more so in this dataset, since high biomass assemblages and thus red tides, typically consisting of dinoflagellates, are not

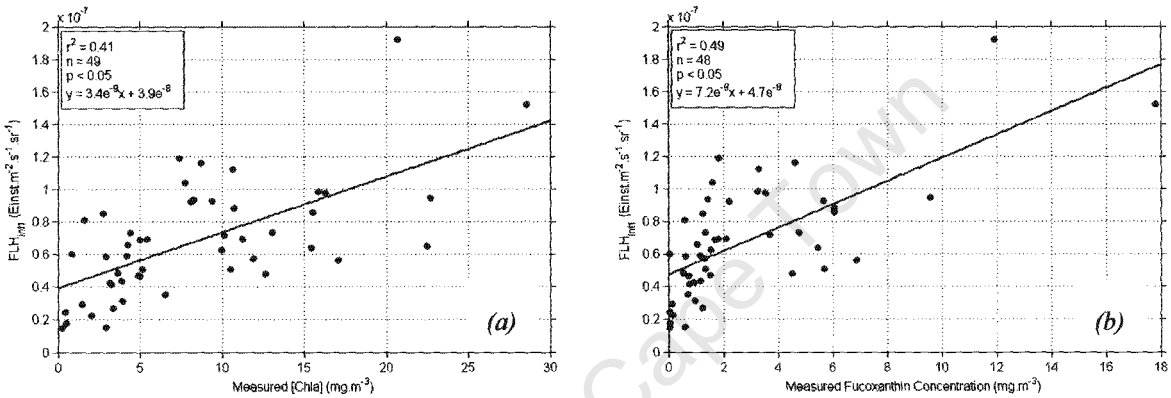

Figure 4.5: (a) Modeled $FLH_{\text{int}1}$ plotted against measured $[chla]$. (b) Modeled $FLH_{\text{int}1}$ plotted against measured fucoxanthin concentrations. Regression lines are shown.

considered. The dataset is thus not sufficient to comment on the hypothesis in this way.
A further assessment regarding the above-mentioned hypothesis is seen in figure 4.6. The chlorophyll-a specific $FLH_{\text{int}1}$ plotted against chlorophyll-a specific fucoxanthin concentrations is seen in figure 4.6 (a). This figure can be compared to the chlorophyll-a specific $FLH_{\text{int}1}$ plotted against chlorophyll-a specific peridinin concentrations. Variability in cellular fluorescence seems not to be related to cellular concentrations of either these accessory pigments. Moreover, data of cellular fluorescence generally falls within a range that is common to both accessory pigments, regardless of the relative concentrations. Note that by considering fucoxanthin in figure 4.6 (a) the presence of prymnesiophytes may affect the analysis. Prymnesiophytes contain relatively high fucoxanthin and 19'-hexanoyloxyfucoxanthin concentrations. Therefore the comparison is repeated, disregarding data points of high chlorophyll-a specific 19'-hexanoyloxyfucoxanthin concentrations. The above interpretation of the data remains unchanged after the omission of this data.

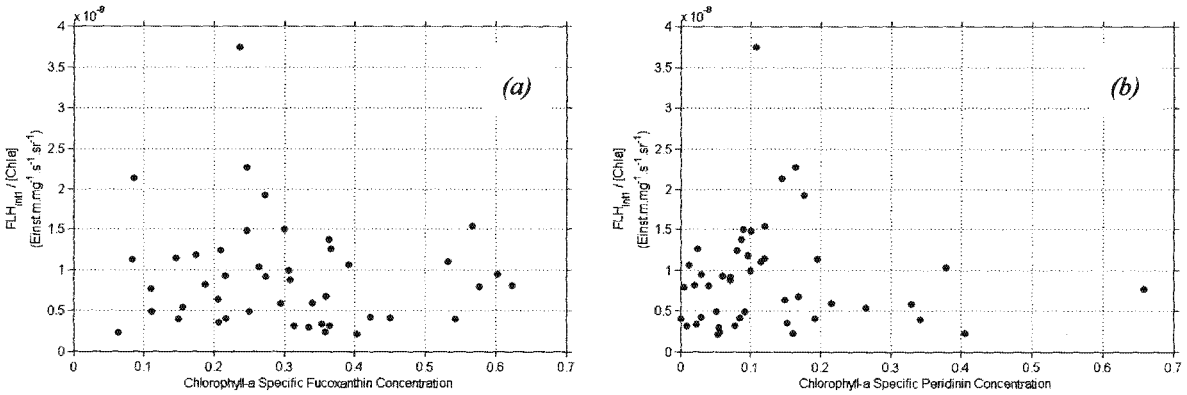

Figure 4.6: (a) Chlorophyll-a specific $FLH_{\text{int}1}$ plotted against chlorophyll-a specific fucoxanthin concentration. (b) Chlorophyll-a specific $FLH_{\text{int}1}$ plotted against chlorophyll-a specific peridinin concentration.

Comparison of the derived ϕ_f to measured surface temperatures (figure 4.7 (a)) suggests a negative trend, but a regression analysis provides no indication that a correlation exists between ϕ_f and the ambient water temperature. In the literature there exists disagreement about temperature effects on fluorescence parameters, as discussed in section 2.3.2. In the southern Benguela system the apparent temperature effect may be a result of, for example, effective diameter variability. The bootstrap analysis of measured temperature versus measured effective diameter during the Lamberts Bay 2005 field survey produces a negative linear correlation with an r^2 of 0.63. As discussed in section 3.4, the period of relatively high temperatures was associated with relatively small cells, whilst cooler water concurred with larger cells. Also, inherent in the temperature comparison with fluorescence parameters is the variability of nutrient concentrations. In the southern Benguela nutrient concentrations are typically higher during cold events, as compared to warm events, due to upwelling from deeper levels. Considering the temperature data it should be born in mind that trends suggested by comparison to fluorescence parameters do not exclusively represent a temperature effect on cellular fluorescence. Figure 4.7 (b) shows that there exists no predictable relationship between measured effective diameter and ϕ_f. Highest ϕ_f values seem to correspond to relatively small effective diameters, but otherwise the data is scattered.

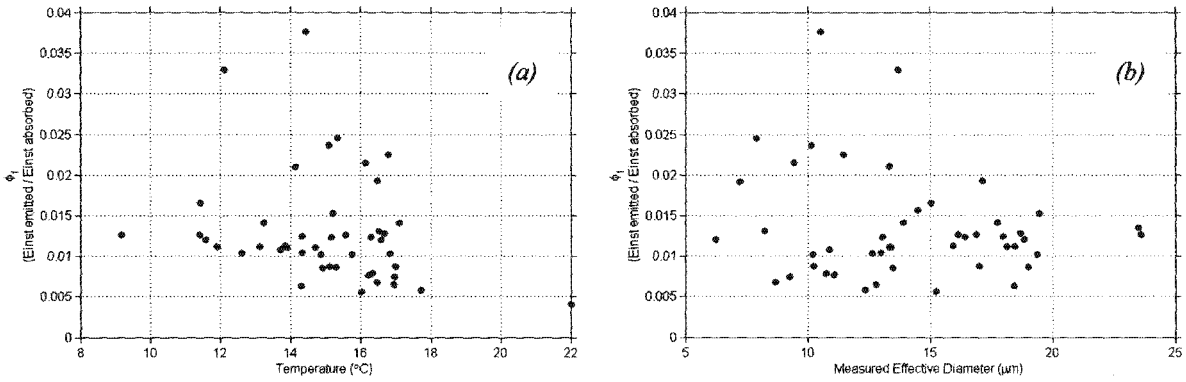

Figure 4.7: (a) Calculated ϕ_f compared to measured temperature. (b) Calculated ϕ_f compared to measured effective diameter.

4.6 Summary

In this chapter the algorithm developed for the derivation of fluorescence products from remotely acquired data is seen to produce viable results that compare well with literature assessments, and with field-measured fluorescence parameters. The algorithm is found to be unreliable in waters of very high biomass, and it is thus appropriately constraint to analyse lower biomass waters only. The implication of this constraint is that fluorescence characteristics of HABs cannot be assessed remotely through the use of the algorithm. However, the formative stages of HAB development can still be considered, which might provide valuable insight into the development of HABs on a physiological level. From comparisons of calculated fluorescence parameters with temperature, effective diameters, and pigment compositions, an easily identifiable environmental- or group-related trend cannot be discerned. Based on the discussion in section 4.5.4, the value of algorithm fluorescence parameters as remote environmental-, physiological-, or assemblage proxies is not obvious. Nonetheless, the algorithm provides quantitative data of FLH_{int}, and ϕ_f of phytoplankton assemblages for remote sensing applications.

Chapter 5

Application

Individually, the parameter ϕ_f is very useful in the investigation of phytoplankton characteristics. In combination with the parameter ϕ_c, another application of phytoplankton fluorescence emerges. In section 2.1.3 the fact that fluorescence is related to photosynthesis at the phytoplankton cellular level is discussed. The relationship between fluorescence and photosynthesis depends upon the probability that excitation energy will be used for fluorescence, photochemistry, or heat dissipation, after light is absorbed by the phytoplankton cell (Chamberlin *et al.*, 1990). Changes in the rate of photosynthesis, due to physiological changes of the cells, light availability, and/or pigment composition, will coincide with changes in the rate of fluorescence (Kiefer *et al.*, 1989). This covariance depends on the ratio ϕ_c / ϕ_f (*ibid.*), which is known to vary in a complex manner with environmental variables (Chamberlin and Marra, 1992; Stegmann and Lewis, 1997), species variation (Stegmann *et al.* 1992) and light intensity (Chamberlin *et al.*, 1990) as described in section 2.3. Thus, the possibility exists to predict primary production from fluorescence, depending on the ability to parameterise this ratio (*ibid.*). Existing literature methods used to suitably parameterise ϕ_c / ϕ_f for primary production estimation from fluorescence are experimental and these methods are probably associated with large errors (Chamberlin and Marra, 1992). In this chapter, estimations of instantaneous primary production are obtained via the reflectance-fluorescence algorithm by applying parameterisations suggested in the literature. The algorithm is also employed to derive *in situ* continuous time series fluorescence products and instantaneous primary production from autonomous moorings, which offer the potential for high frequency, real-time Eulerian monitoring and investigation of phytoplankton dynamics. Satellite application of the reflectance-fluorescence algorithm is assessed last. From the satellite application the ability exists to provide a physiological proxy, i.e. ϕ_f, or primary production estimates on synoptic, large spatial scales. Satellite application of the algorithm is potentially a very powerful tool for HAB monitoring and assessment of phytoplankton dynamics.

5.1 Primary Production

5.1.1 Model Theory and Implementation

Photosynthesis can be related to the instantaneous rate of sun-induced fluorescence based on the principle that cellular excitation energy can be channelled along three pathways to be utilised for photochemistry, emitted as fluorescence, or dissipated as heat. It was seen in equation 4.1 that the rate of fluorescence is expressed, in general terms, through the product of the fluorescence quantum yield and the rate of light absorption within cells. The instantaneous rate of photosynthesis at a particular depth can similarly be expressed via absorption rate and the photosynthetic quantum yield (Kiefer *et al.*, 1989):

$$P(z) = \left(E_{\circ PAR}(z)\right) \cdot \left([chla]\right) \cdot \left(\bar{a}_{\phi}^{*}\right) \cdot \left(\phi_{c}\right) \cdot dz \qquad (5.1)$$

where $P(z)$ (molC.m^{-2}.s^{-1}) represents the instantaneous rate of carbon fixation; $E_{\circ PAR}(z)$ is the photosynthetically available scalar radiation (PAR) (Einst.m^{-2}.s^{-1}); $[chla]$(mg.m^{-3}) signifies chlorophyll-a concentration; $\bar{a}_{\phi}^{*}$ (m^{2}.(mg chl-a)$^{-1}$) is the spectrally weighted mean chlorophyll-a specific absorption coefficient of phytoplankton; and ϕ_{c} (molC(Einst)$^{-1}$) is the photosynthetic quantum yield. The models shown in equation 5.1 and equation 4.1 assume that the parameters that govern fluorescence emission rate and photosynthetic rate are the same, except for the respective quantum yields (Stegmann and Lewis, 1997). Equation (5.1) can be combined with equation 4.1 in the following way (Babin *et al.*, 1996):

$$P(z) = \left(\frac{\phi_{c}}{\phi_{f}}\right) \cdot \left(\frac{E_{\circ F}(z)}{Q_{a}^{*}(685)}\right) \qquad (5.2)$$

To enable the estimation of primary production from equation (5.2), it is necessary to assume that $E_{\circ F}(z)$ and $P(z)$ are the only variable parameters, or that $\phi_c/(\phi_f \cdot Q_a^*(685))$ is predictable (Kiefer *et al.*, 1989). In an attempt to acquire a photosynthesis-fluorescence relationship, one approach is to use an empirical formulation obtained through the correlation between measured $E_{\circ PAR}(z)$ and measured $P(z)/E_{\circ F}(z)$ (Chamberlin *et al.*, 1990):

$$\left(\frac{P(z)}{E_{\circ F}(z)}\right)=\left(\frac{k_{cf}}{k_{cf}+E_{\circ PAR}(z)}\right)\cdot\left(\frac{\phi_c}{\phi_f}\right)_{\max} \tag{5.3}$$

where $(\phi_c/\phi_f)_{\max}$ is the maximum value of the ratio of quantum yields, and k_{cf} is the value of irradiance when the ratio is equal to half of its maximum value. Both these parameters are empirical constants with values that differ between literature assessments, as determined by best-fit rectangular hyperbolic functions. The k_{cf} parameter was given values of 133μEinst.m^{-2}.s^{-1} (Chamberlin *et al.*, 1990), 116μEinst.m^{-2}.s^{-1} (Chamberlin and Marra, 1992), 187μEinst.m^{-2}.s^{-1} (Garcia-Mendoza and Maske, 1996), and 128.6μEinst.m^{-2}.s^{-1} (Stegmann and Lewis, 1997). The $(\phi_c/\phi_f)_{\max}$ parameter was calculated to be 2.3Catoms.(photon)$^{-1}$ (Chamberlin *et al.*, 1990), 1.5Catoms.(photon)$^{-1}$ (Chamberlin and Marra, 1992), 1.9Catoms.(photon)$^{-1}$ (Garcia-Mendoza and Maske, 1996), and 5.94 Catoms.(photon)$^{-1}$ (Stegmann and Lewis, 1997). The wide ranges obtained for these constants are a result of field studies conducted in different ocean regions, and measurements made at different depths. For the purpose of this study, equation (5.3) can be integrated with depth and applied to fluorescence signals that are detected *in situ* or via satellite sensors. The integrated formulation derived from equation (5.3) is given in equation (5.4):

$$P(d)=([chla])(\bar{a}_\phi^*)(Q_a^*(685))(\phi_f)\left(\frac{\phi_c}{\phi_f}\right)_{\max}\left(-\frac{k_{cf}}{K_{PAR}}\right)\left(\ln\frac{k_{cf}}{k_{cf}+E_{\circ PAR}(0)\cdot e^{-(d\cdot K_{PAR})}}\right) \tag{5.4}$$

where $P(d)$ is the vertically depth-integrated instantaneous rate of carbon fixation within the column of fluorescing cells to below the sensor depth, d, assumed to be the ocean surface for satellite detection. To account for the isotropic nature of fluorescence emission, 4π has been factored into the $P(d)$ calculation of equation (5.4). All parameters in equation (5.4) necessary for the calculation of $P(d)$ are available from the reflectance-fluorescence algorithm, or assumed constant, as described in section 4.2.1 for *in situ* algorithm application, and section 4.3.1 for satellite algorithm application.

The approach described in equations (5.3) and (5.4) will be referred to as the 'Chamberlin method'. Another approach implemented by Stegmann *et al.* (1992), referred to as the 'Stegmann method', presents the following expression:

$$\int_{d}^{\infty} P(z) \cdot dz = (4\pi) \cdot (L_F(d)) \cdot \left(\frac{\phi_c}{\phi_f}\right) \cdot \left(\frac{K_t + K_f}{K_t}\right) \tag{5.5}$$

where $P(z)$ is integrated with respect to depth such that the contribution of all detected fluorescing layers below the sensor is incorporated into the estimation; the upper boundary of integration is infinity, since sun-induced fluorescence decreases with depth and then becomes insignificant (*ibid.*); $L_F(d)$ is the radiance due to fluorescence measured at the depth of the sensor, d, detected through a steradian solid angle, necessitating the factor 4π to account for isotropic fluorescence emission at all depths; K_t (m^{-1}) is the total diffuse attenuation coefficient over the PAR spectrum; and K_f (m^{-1}) is the total diffuse attenuation coefficient for fluorescence at 685nm radiance.

Stegmann *et al.* (1992) acquired an estimated constant value for ϕ_c / ϕ_f empirically from the regression of measured production, fluorescence, and the ratio $(K_t + K_f)/K_t$ in accordance with equation (5.5). The ϕ_c / ϕ_f parameter was found to be 0.39molC.(Einst)$^{-1}$ for a combination of 1645 data points obtained from a variety of ocean regions at different times of the day (Stegmann and Lewis, 1997). They concluded that a relative invariance observed in ϕ_c / ϕ_f data

between different locations implied that a single ϕ_c / ϕ_f value could be applied to various geographical locations.

Therefore, this constant ϕ_c / ϕ_f value of 0.39molC.(Einst)$^{-1}$ is adopted here to permit the calculation of instantaneous primary production from nesting of equation (5.5) into the reflectance-fluorescence algorithm. Nesting provides necessary input to the formulation. Diffuse upward radiance attenuation coefficients required for input to equation (5.5) are calculated via the reflectance algorithm using the Albert and Mobley (2003) formulation. $L_F(d)$ is calculated according to the FLH method outlined in section 4.2.1 for *in situ* application of the algorithm, and section 4.3.1 for satellite application.

5.1.2 Assessment of Assumptions

The rates of fluorescence and photosynthesis are related due to the fact that both these processes depend on the number of absorbed photons by the phytoplankton cell. However, for a robust correlation of fluorescence and photosynthesis with absorption, heat dissipation has to be accounted for. Estimates of heat dissipation are not easily quantifiable.

The two methods considered to calculate instantaneous primary production differ in their treatment of ϕ_c / ϕ_f. Determining the relationship between photosynthesis and fluorescence from equation (5.2) would require the assumption that the $\phi_c /(\phi_f \cdot Q_a^*(685))$ factor is constant (Kiefer *et al.*, 1989). Similarly, ϕ_c / ϕ_f is assumed constant according to the Stegmann method (equation 5.5). Alternatively the variability of the quantum yield ratio can be parameterised as a function of measured environmental variables such as PAR, e.g. according to the Chamberlin method (equation 5.3) (Chamberlin *et al.*, 1990).

The Stegmann method of photosynthetic rate estimation is limited by the unpredictability of the ϕ_c / ϕ_f term, due to the variability of ϕ_c / ϕ_f (Babin *et al.*, 1996) with environmental variables (Chamberlin and Marra, 1992; Stegmann and Lewis, 1997), species variation (Stegmann *et al.*, 1992) and light intensity (Chamberlin *et al.*, 1990) as described in section 2.3. The Chamberlin method requires the adoption of empirical constants that vary among studies. Variability in these parameters seen in published data is attributable to empirical derivations made in different ocean

systems, with different water types, and phytoplankton assemblages, and thus due to phytoplankton physiological variability (Garcia-Mendoza and Maske, 1996). Both methods are limited with respect to primary production estimation.

Calculated $P(d)$ relates to instantaneous production, whereas daily production is more commonly used, and is normally of greater interest (Behrenfeld and Falkowski, 1997). Scaling problems can be overcome to some extent with high frequency *in situ* derivations through multiple estimates of the instantaneous rate. However, for single *in situ* or satellite acquisitions the problem remains. In terms of satellite and *in situ* applications it must be considered that the observed fluorescence signal might originate from a relatively thin layer of the ocean, whilst carbon fixation occurs throughout an extensive part of the water column (Morel and Berthon, 1989). This problem is a source of contention in the field of bio-optics. It should be noted that the application of the reflectance-fluorescence algorithm to the estimation of instantaneous primary production in this study is a preliminary analysis, and it is intended to contribute in an experimental sense towards operational monitoring purposes. The main interest of the study is to characterise phytoplankton physiology, and assemblage structure, and not to produce a robust estimation of production.

Consistent with the assumptions regarding the reflectance-fluorescence algorithm, the Chamberlin method (equation 5.4) assumes that all parameters, apart from $E_{\circ PAR}(z)$, are independent of depth (Stegmann *et al.*, 1992). All parameters are assumed to be wavelength-independent (*ibid.*). These two assumptions also apply to the Stegmann method (equation 5.5). The Stegmann method does not account for nonlinearities in the photosynthesis-irradiance and fluorescence-irradiance relationships (*ibid.*).

In-depth assessments of the performance and inherent errors of the Chamberlin and Stegmann methods are discussed in the appropriate literature.

Assumptions discussed in section 4.2.2 with regard to relevant algorithm parameter calculations are also inherent in the calculation of $P(d)$ according to equation (5.4).

5.1.3 Parameterisation of ϕ_c / ϕ_f

It is apparent from equation (5.2) that the ability to predict instantaneous primary production from sun-induced fluorescence depends on the ratio ϕ_c / ϕ_f (Chamberlin and Marra, 1992), which is a variable parameter. An assessment of measured ϕ_c / ϕ_f data of the southern Benguela might indicate an appropriate parameterisation that is specific to this region. In this section the measured ϕ_c / ϕ_f data from the Lamberts Bay 2005 field survey (see chapter 3) are examined together with measured environmental variables to see if it is possible to parameterise ϕ_c / ϕ_f. Methods regarding data acquisitions and parameter derivations are described in section 3.1. Since measured ϕ_c / ϕ_f data are only available from the Lamberts Bay 2005 field survey, no rigorous assessment is possible in this regard. The dataset is very small, and it relates to specific ocean and phytoplankton assemblage conditions. It is thus not representative of the system in general, and any parameterisation derived from the data would be considered inadequate. Nonetheless, the data are examined as a first analysis of possible ϕ_c / ϕ_f parameterisation in the southern Benguela.

Plotting measured ϕ_c / ϕ_f against $[chla]$ for both the surface and 5-meter data together does not reveal a clear trend. However, separate depth treatments are shown in figure 5.1 with bootstrap regression analyses (see section 3.3) performed on measured ϕ_c / ϕ_f versus measured $[chla]$ surface and 5-meter data. Simple linear trends are shown, since they provide the highest r^2 values. Since few data points are available for regression, the relationship is considered uncertain. In the case of surface data the r^2 is found to be 0.37, whilst the 5-meter data have an r^2 of 0.58. The ϕ_c / ϕ_f data of phytoplankton at the surface is much lower compared to the 5-meter data, and it varies within a much smaller range. The difference between ϕ_c / ϕ_f at these two depths is expected, since this parameter is known to behave in a distinct way near the surface where light intensity is high (see section 2.3.3). Both ϕ_f and ϕ_c decrease with increasing light intensity (Chamberlin *et al.*, 1990), i.e. an increase is seen in these parameters with depth (Babin *et al.*, 1995). Similarly, ϕ_c / ϕ_f is known to decrease with an increase in light intensity (Chamberlin *et al.*, 1990). Near the surface, due to photoadaptation, a larger proportion of photoprotectant pigments within cells cause a relative paucity in excitation energy to be fluoresced or used in

photochemistry. In conditions of light limitation, assumed to apply to phytoplankton at 5m-depth, a more robust parameterisation is achieved of ϕ_C / ϕ_f with $[chla]$.

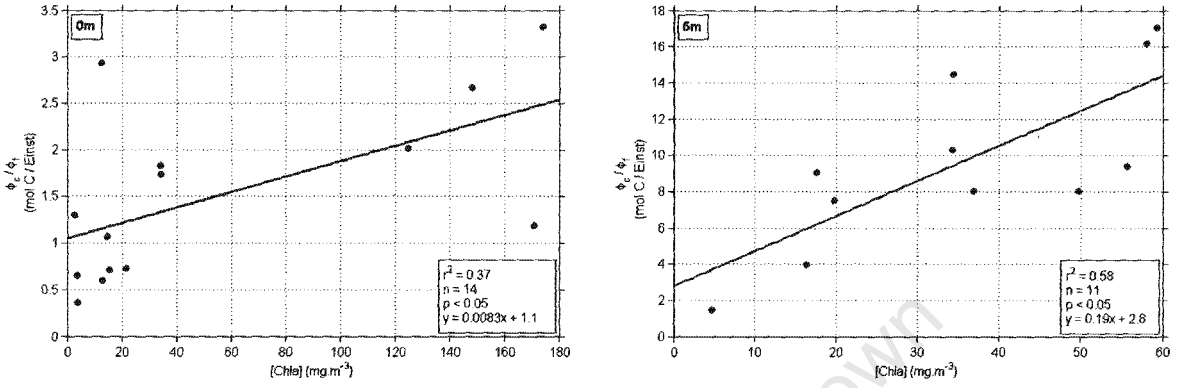

Figure 5.1: Bootstrap regression analyses of ϕ_c / ϕ_f against $[chla]$ for surface data, and data obtained from 5 meters.

Expanding the discussion of ϕ_C / ϕ_f variability with light, figure 5.2 (a) indicates a noticeable trend between ϕ_C / ϕ_f and PAR, when data at both depths are considered. Surface data are shown in red, and 5-meter data are shown in black. A value of r^2 is found to be 0.63 when the relationship between ϕ_C / ϕ_f and PAR is approximated by a power law function. It appears that ϕ_C / ϕ_f varies distinctly according to two separate light regimes. Below approximately 300μEinst.m^{-2}.s^{-1}, ϕ_C / ϕ_f is seen to decrease roughly linearly with PAR, but above this light intensity ϕ_C / ϕ_f decreases at a slower rate with increasing light intensity. Comparable trends are also evident in the literature (Chamberlin *et al.*, 1990; Chamberlin and Marra, 1992; Garcia-Mendoza and Maske, 1996). The Chamberlin method of parameterisation is based on a similar relationship. The relationship seen in figure 5.2 (a) reinforces the knowledge that PAR is a major determinant of ϕ_C / ϕ_f.

The effects of PAR and $[chla]$ on ϕ_c / ϕ_f can be assessed on the same graph. Figure 5.2 (b) shows PAR plotted against $[chla]$ on a bubble plot. The areas of the bubbles indicate relative magnitudes of ϕ_c / ϕ_f. The PAR versus $[chla]$ relationship is comparable to a depiction of Babin *et al.* (1996) of PAR versus $[chla]$, where F is plotted in the third dimension. The authors state that at low PAR values, F depends primarily on PAR, whereas at high PAR values, F depends primarily on $[chla]$. However, in the case of ϕ_c / ϕ_f, which indicates cellular changes as opposed to biomass dynamics, the relationship is expected to be distinct. Despite few data points, it appears that at very high $[chla]$ and low PAR, values of ϕ_c / ϕ_f are relatively low and unvarying; a comparable value of ϕ_c / ϕ_f is seen at very high PAR and low $[chla]$. For data falling below PAR of 500µEinst.m^{-2}.s^{-1} and $[chla]$ of 60mg.m^{-3}, a trend of increasing ϕ_c / ϕ_f with increasing $[chla]$ and decreasing PAR can be discerned. Considering the present study, this trend might be useful in terms of the $[chla]$ restrictions necessary for the operation of the reflectance-fluorescence algorithm (see section 4.5.1), but less useful for the high intensity light environment detected at the surface by satellite sensors, and *in situ* radiometric systems.

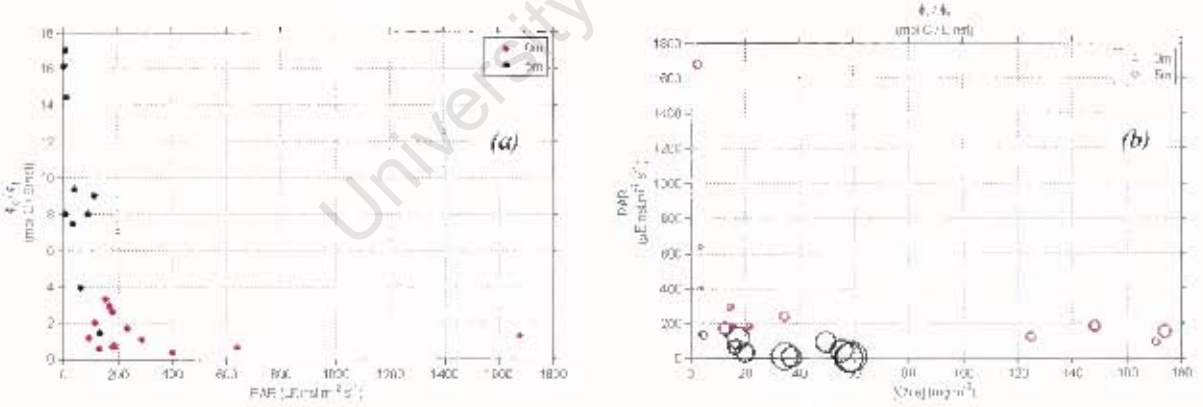

Figure 5.2: (a) Measured ϕ_c / ϕ_f plotted against PAR at the surface (red) and at 5m-depth (black). (b) Bubble plot of PAR versus $[chla]$ with ϕ_c / ϕ_f represented as relative bubble sizes (0m and 5m).

The determinant of the relationship observed in figure 5.2 (a) appears to be the variability of ϕ_c with PAR (figure 5.3 (a)). Chamberlin *et al.* (1990) found a similar trend of these two parameters. Data of ϕ_f with PAR (figure 5.3 (b)) suggest once again that two light regime-related trends could exist. Below 300μEinst.m^{-2}.s^{-1} values of ϕ_f increase according to a linear trend with increasing PAR. Above approximately 300μEinst.m^{-2}.s^{-1} values of ϕ_f suggest a hyperbolic trend with PAR.

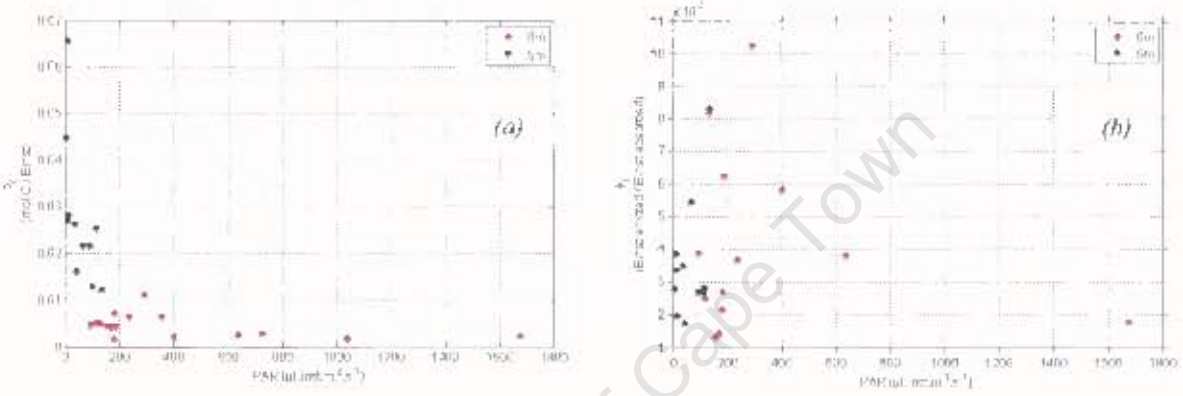

Figure 5.3. (a) Data of ϕ_c against PAR at the surface (red) and at 5m-depth (black). (b) Data of ϕ_f against PAR at the surface (red) and at 5m-depth (black).

It should be noted that PAR and [*chla*] are implicit in the derivation of measured ϕ_c, so these parameters are not completely independent. Nevertheless, trends observed here compare well with trends described in the literature.

None of these possible means of parameterisation will be used in this study, since they are based on very few data points that only relate to a specific ocean regime, but they are useful as a first analysis of possible parameterisations.

A depiction of ϕ_c / ϕ_f with nitrate concentrations at the surface is given in figure 5.4. A bootstrap linear regression performed on these parameters gives an r^2 of 0.33. The analysis is somewhat inconclusive, since there are only ten data points available. Nitrate is an important

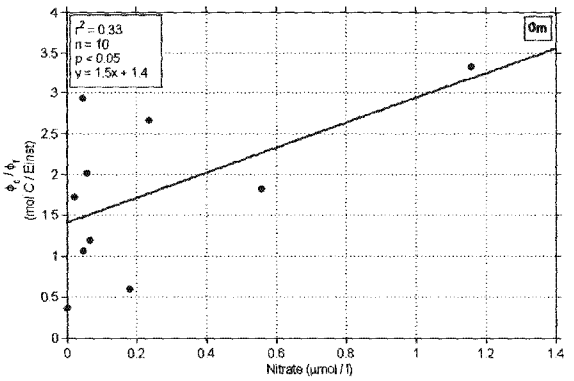

Figure 5.4: Data of measured ϕ_C / ϕ_f plotted against nitrate concentrations.

variable in upwelling systems, where its variability is typically linked to water temperature. However, nitrate is much more useful in nitrate limiting conditions. In the southern Benguela nitrate is not always limiting and it is possible to have considerable phytoplankton growth on reduced nitrogen nutrients (Probyn *et al.*, 1990); it is therefore not an appropriate parameter for parameterisation with ϕ_C / ϕ_f. Assessment of ϕ_C / ϕ_f with water temperature and phytoplankton effective diameter data revealed no clear trends.

In an attempt to uncover a predictable quantum yield ratio, the regression analysis of measured ϕ_c versus ϕ_f is also examined (not shown). Values of linear r^2 of both the surface data and the 5-meter data are low, revealing no clear trends between these parameters. Few data points are available for the analysis, thus rendering the result somewhat inconclusive.

5.1.4 Initial Comparison of Production Methods

The limitations of the few measured data available from this study prevent the prediction of variable ϕ_C / ϕ_f in the southern Benguela. The Chamberlin and Stegmann methods are therefore implemented as an experimental approach to estimate instantaneous primary production through the reflectance-fluorescence algorithm, although these methods have been derived empirically from data specific to other ocean regions. Nesting of these formulations into the reflectance-fluorescence algorithm enables the calculation of instantaneous primary production from *in situ* optical near real-time buoys, and from space via satellite.

Values for the empirical constants, k_{cf} and $\left(\phi_c / \phi_f\right)_{\max}$ of equation (5.4) are adopted from field studies expressed in the literature, since the available field data are also not sufficient to calculate appropriate constants for the southern Benguela system. The adopted constant values are from

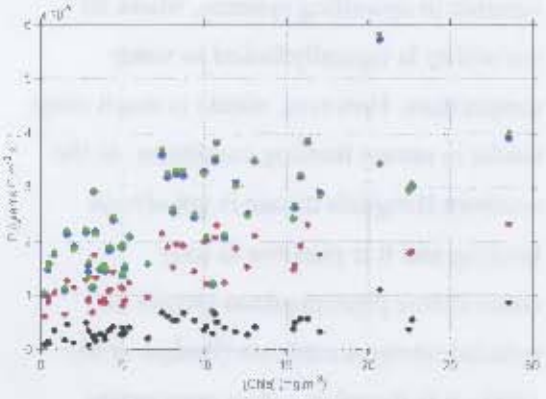

Figure 5.5: Calculated P using the Chamberlin method, and three literature estimations of the empirical constants (blue, green, red) plotted against measured $chla$. Data of P calculated using the Stegmann method is shown in black.

Chamberlin *et al.* (1990), Chamberlin and Marra (1992), and Garcia-Mendoza and Maske (1996). All available Satlantic HyperTSRB field-acquired optical data (see table 4.2) are input into the reflectance-fluorescence algorithm in order to calculate P according to equation (5.4) and equation (5.5). Figure 5.5 shows the results obtained, plotted against measured $[chla]$. Blue data points indicate P calculated via the Chamberlin method applying constants of Chamberlin *et al.* (1990); red data points represent values of P according to the Chamberlin method using constants of Chamberlin and Marra (1992); green data points are obtained from the Chamberlin method with Garcia-Mendoza and Maske (1996) constants; black data points are calculated using the Stegmann method.

The P values acquired via both formulations vary according to similar trends, and they show a general increase with biomass. The Chamberlin method gives the highest values, as compared to the Stegmann method, which is also less varied. A range expected for P values can be obtained from the literature, incorporating data measured for a variety of ocean regions. A typical range appears to be $0.0 gramsC.m^{-2}.s^{-1} - 2.4\times10^{-5} gramsC.m^{-2}.s^{-1}$, with the large majority of P values falling below $1.2\times10^{-5} gramsC.m^{-2}.s^{-1}$ (Stegmann *et al.*, 1992; Stegmann and Lewis, 1997). Since the field optical data were collected during the highly productive spring/summer seasons of the Benguela upwelling region, relatively large P estimates are assumed appropriate. However, since the function described by Chamberlin *et al.* (1990) was developed for depths below 2 meters, care should be taken when near-surface depths are considered. Cullen and Lewis (1995) advise that the function expressed in equation (5.3) should not be applied to data obtained from near the surface, even if a backscatter correction is employed. Nonlinearities in measured fluorescence and production observed by Stegmann *et al.* (1992) at high irradiance intensities caused them to consider the future incorporation of the nonlinear component into equation (5.5).

5.2 Fluorescence Algorithm with Bio-Optical Moorings

The reflectance-fluorescence algorithm can be applied to *in situ* measured hyperspectral optical data that is acquired near real-time via sensors on the BOB mooring. It enables the semi-continuous assessment of fluorescence parameters, and the instantaneous primary production for the assessment of phytoplankton dynamics and HAB development.

Two time series, each of approximately one-month duration, are considered in the assessment of *in situ* application of the reflectance-fluorescence algorithm. Half-hourly radiance and irradiance daytime data acquired from BOB are input into the reflectance-fluorescence algorithm to obtain calculated output of $[chla]$, phytoplankton effective diameter, $FLH_{\text{int}1}$, ϕ_f, and P. Since the mooring is equipped with a thermistor chain it is also possible to acquire temperature data at the same frequency.

The first time series is of data acquired during the summer from 27 January 2005 to 22 February 2005. This period was characterised by an extensive warm event with a stratified upper column, and several upwelling events. Wind data from the South African Weather Service for the Lamberts Bay Nortier Station reveal that moderate northerly winds, thus not conducive to upwelling, predominated during the warm event, with short intermittent occurrences of southwesterly winds. Halfway through the time series the wind became persistently southwesterly and relatively strong, causing a major upwelling event. Towards the end of the time series, warming of the upper water column coincided with moderate northerlies. No field-measured data are available for this time series. The second time series occurred during autumn from 01 April 2005 to 04 May 2005. Initially southeasterly winds were associated with cooler waters, which became southerly for an extensive period, during which the water column warmed slightly, showing weak and deep stratification. With northwesterly winds halfway through the time series, the upper water column became approximately mixed in terms of temperature, and relatively warm. Towards the end of the series the wind changed rapidly from southerly to northerly, and then from southeasterly to northerly. A field survey overlaps with the first week of the time series, so some measured data are available for interpretation. High biomass HAB events occurred during this time, which was dominated by the dinoflagellates, *Prorocentrum triestinum* and *Ceratium furca*. The occurrence and relative extent of HABs are known to be greatest during the latter part of the upwelling season (Pitcher and Calder, 2000).

Data for the period 27 January 2005 to 22 February 2005 is seen in figure 5.6. Measured data include temperature and wavelength-integrated $E_d(0+,\lambda)$, denoted $E_{d\,\mathrm{int}}(0+)$. Reflectance-fluorescence algorithm-derived parameters are also shown.

The following information can be inferred from the data. The last stage of an upwelling event occurs at the onset of the time series considered. Values of $[chla]$, derived from the reflectance algorithm, are seen to increase significantly as the water temperature increases, and then decrease again for the duration of the quiescent phase of stratified, high upper water column temperatures. It is these stratified waters that are most typically associated with HAB events in the southern Benguela, which are normally dinoflagellate bloom events (Pitcher *et al.*, 1998). A brief incidence of cooler surface waters follows the warm spell, concurrent with increased $[chla]$, which subsequently fluctuate with relatively high surface temperatures. An extensive upwelling period causes $[chla]$ to decrease appreciably. The end of the time series suggests a slight increase in temperatures, and a consequent increase in $[chla]$. Effective cell diameter data fluctuates considerably, although maximum diameters are seen to persist at the onset of the final cold event.

The general trend detected in $FLH_{\mathrm{int\,l}}$ seems to correspond roughly to $[chla]$, consistent with the analysis of measured data in section 3.4, and literature analyses (Neville and Gower, 1977). Note that the assessment of fluorescence emission through the FLH technique is assumed here to be valid for data points of $[chla]$ no higher than 50mg.m^{-3}; all data points above 50mg.m^{-3} are neglected. Relative intensities of $E_{d\,\mathrm{int}}(0+)$ from day-to-day show no clear trend with $FLH_{\mathrm{int\,l}}$, but over the period of one day the diurnal $FLH_{\mathrm{int\,l}}$ patterns are evident as is suggested in literature field studies (Kiefer *et al.*, 1989). Minimum $FLH_{\mathrm{int\,l}}$ is seen during the morning in concurrence with lowest $E_{d\,\mathrm{int}}(0+)$ intensities. Both parameters show parallel increases during the morning to become maximal around midday, followed by decreasing trends towards evening (*ibid.*). ϕ_f values reveal no obvious trends from day-to-day, but diurnal depressions can be detected on most days, which is discussed in terms of literature findings in section 2.3.3. A possible cause for the maximum peak observed in the ϕ_f data cannot easily be assessed from the available data. The chlorophyll-a specific instantaneous primary production, P^*, calculated from

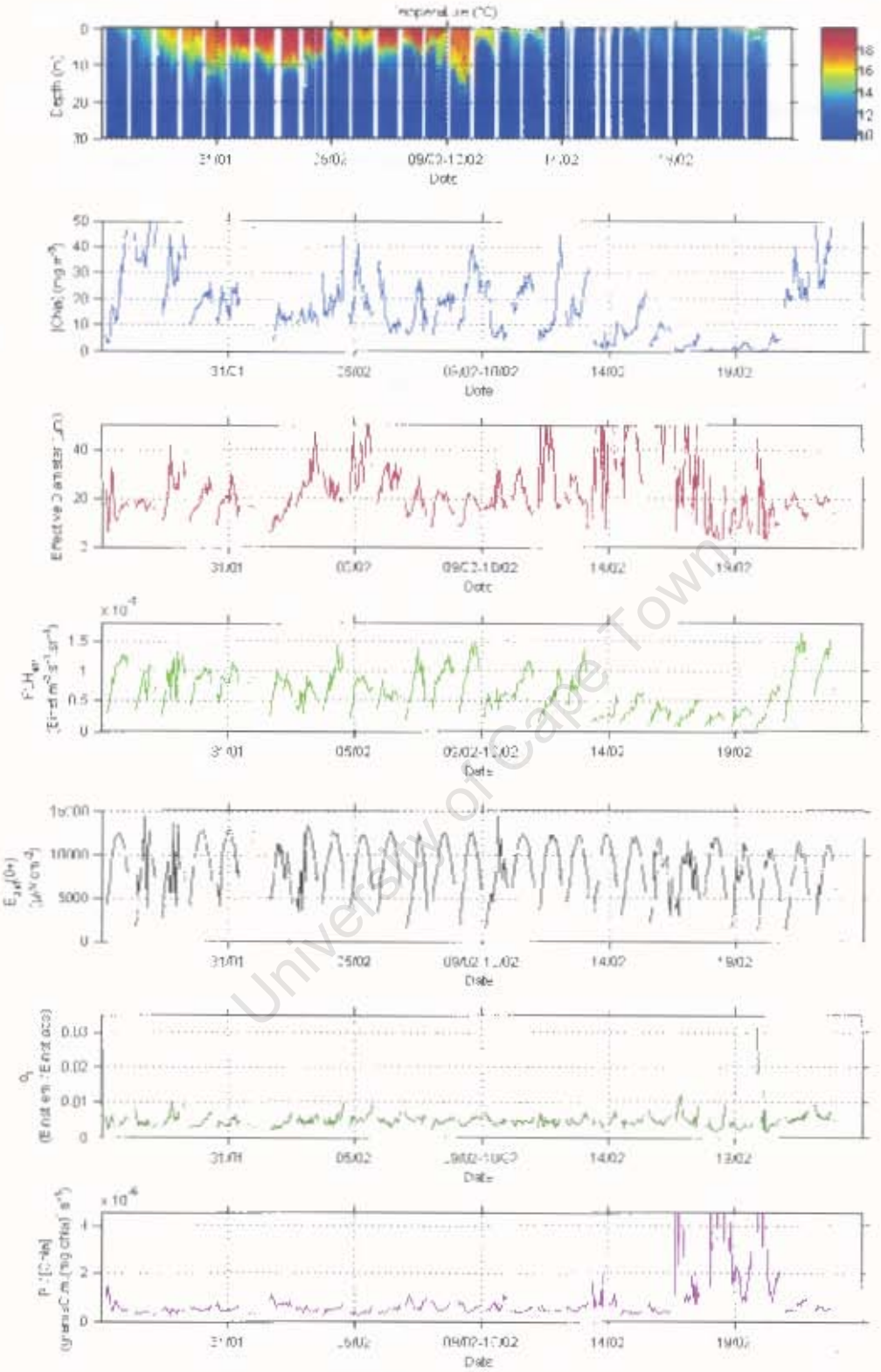

Figure 5.6: BOB-measured temperature and wavelength-integrated downward irradiance just above the ocean surface, and reflectance-fluorescence algorithm derived parameters for the summer period of 27 January 2005 to 22 February 2005. Only daytime data is presented, processed at half-hourly intervals.

equation 5.4 (Chamberlin *et al.*, 1990) is relatively unvarying for most of the time series, but values are observed to increase drastically during the period of extensive upwelling, when $[chla]$ is lowest. Diurnal midday depressions of P^* are evident on most days as seen in the literature (Stegmann and Lewis, 1997).

Between 13/02 and 18/02 a prominent event can be seen. High effective phytoplankton cell diameters suggest that diatoms dominated the cold, newly upwelled surface waters. This period is associated with relatively low $[chla]$ and thus low values of $FLH_{\text{int}1}$, but P^* increased dramatically towards the end of this event.

Assessment of the reflectance-fluorescence algorithm during the autumn period of 01 April 2005 to 04 May 2005 is shown in figure 5.7. The same measured and calculated parameters are represented as is shown in figure 5.6.

Temperature data reveal a brief period of cooler upper column water, which becomes replaced with relatively warm water that persists through the remainder of the observable temperature series. A warm surface mixed layer is suggested in the relatively uniform water column temperatures observed, which deepens toward the final measured segment of the series. Calculated $[chla]$ values are relatively higher than data observed in the time series of figure 5.6, which occurs earlier in the upwelling season, confirming the higher occurrence of blooms later in the upwelling season (Pitcher and Calder, 2000). These high $[chla]$ values corresponded to HAB events. Large effective cell diameters are seen to dominate throughout the majority of the time series. During the first week the large diameters are known to correspond to *Ceratium furca.*

Calculated parameter data appear messy due to the 50mg.m^{-3} $[chla]$ restriction that was necessary for the viable operation of the FLH technique of the algorithm (see section 4.5.1), and due to the fact that the data is characterised by very high biomass waters and HAB events. It is thus not easy to identify trends in the data. In contrast with figure 5.6, $FLH_{\text{int}1}$ does not show an obvious trend with $[chla]$. Instead, $FLH_{\text{int}1}$ appears to relate more to $E_{d\,\text{int}}(0+)$ on a day-to-day basis. Values of $E_{d\,\text{int}}(0+)$ are generally lower during the autumn series than observed through the summer period. This confirms the literature findings, mentioned in section 5.1.3, which show that under low intensity light conditions fluorescence emission of phytoplankton assemblages

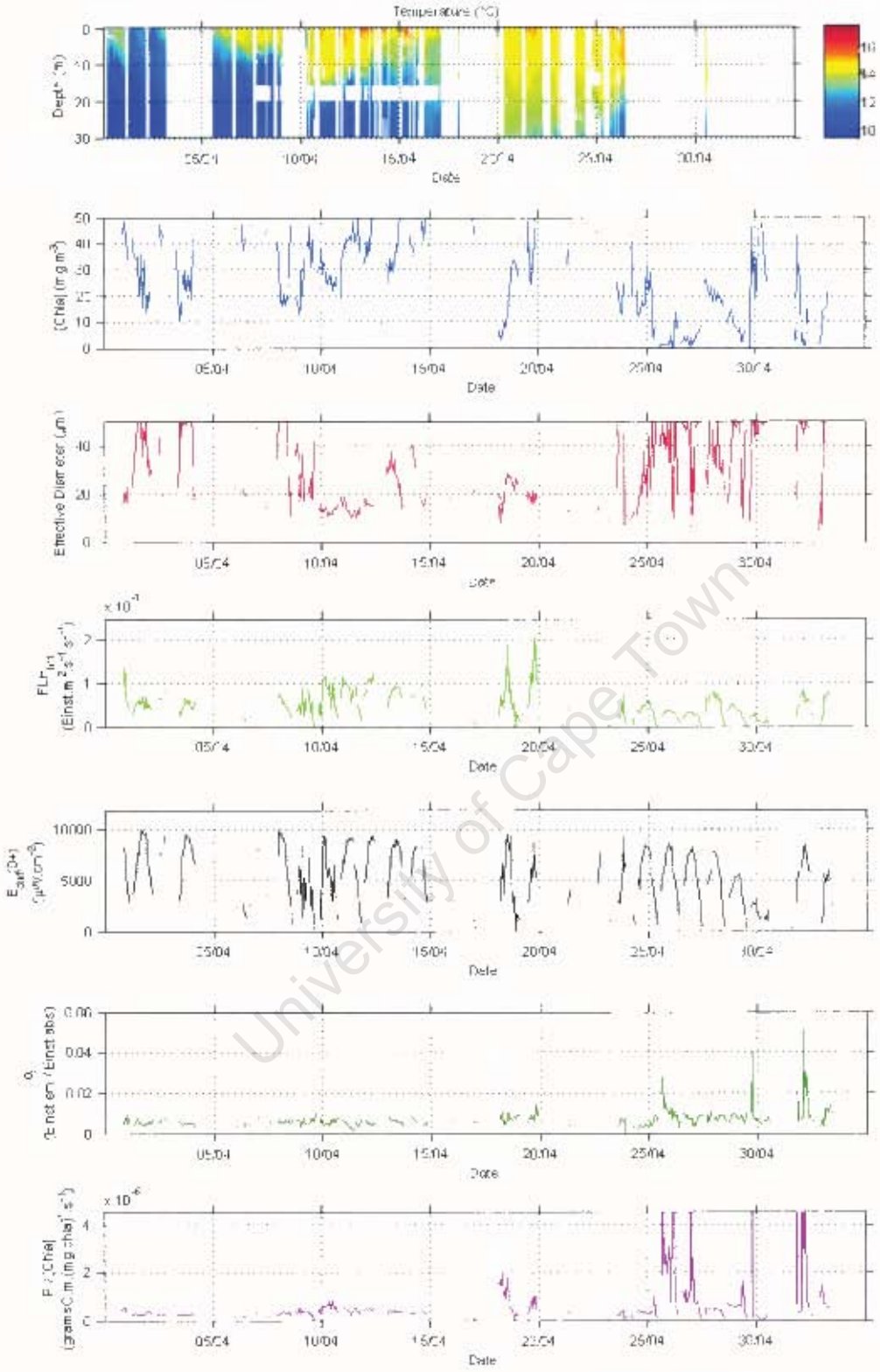

Figure 5.7: BOB-measured temperature and wavelength-integrated downward irradiance just above the ocean surface, and reflectance-fluorescence algorithm calculated parameters for the autumn period of 01 April 2005 to 04 May 2005. Only daytime data is presented, processed at half-hourly intervals.

depends on the incoming light, whilst at high intensity light conditions fluorescence emission is closely correlated with biomass (Babin *et al.*, 1996). $FLH_{\text{int}\,l}$ data show a diurnal response on most days, manifested in midday maxima. ϕ_f is relatively invariable from day-to-day during most of the time series, but higher variability corresponding to lower biomass is observed towards the end of the series. Periods of invariability show ϕ_f values that fall within a relatively narrow and similar range than ϕ_f values during the summer period. This range is roughly between 0.002 and 0.008, which agree well with surface measured ϕ_f quoted in the literature, e.g. the measured ϕ_f range of 0.005 – 0.01 (Maritorena *et al.*, 2000). Values of ϕ_f derived from measurements of the Lamberts Bay 2005 field survey (see chapter 3) were found to be within the range 0.001 – 0.01. Small variability in ϕ_f and messy data prevent a significant ϕ_f diurnal trend to be identified. Large variability in P^* can be seen towards the end of the series.

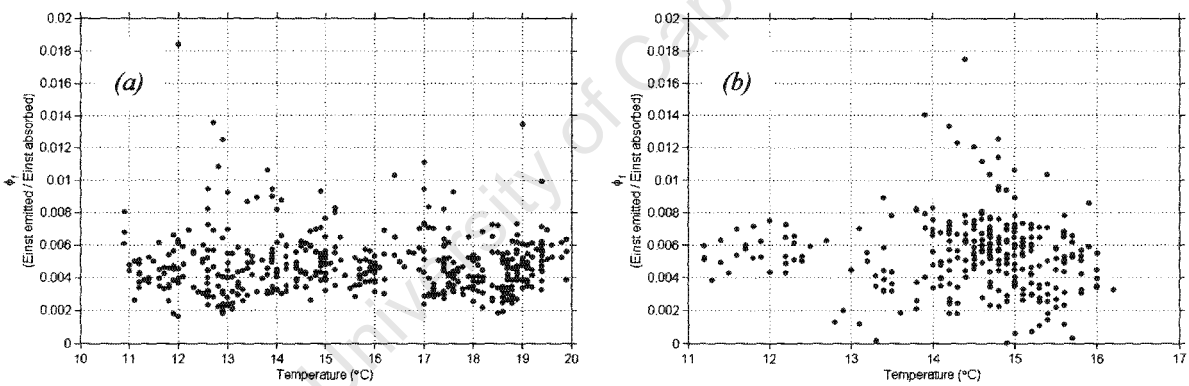

Figure 5.8: Calculated ϕ_f versus measured surface temperature (a) for the series 27 January 2005 to 22 February 2005, and (b) for the series 01 April 2005 to 04 May 2005.

To further assess the possibility of using calculated ϕ_f as a remote sensing physiological proxy, calculated ϕ_f values obtained from the two time series are plotted against measured surface temperatures in figure 5.8. Temperature data are available from thermistor chains on *in situ* radiometric mooring systems, as well as from satellite imagery. Temperature is thus an

independent remote sensing environmental parameter that can be used in comparison with ϕ_f, which is calculated through the algorithm. A temperature trend with ϕ_f might also indirectly suggest changes in assemblage structure, due to the temperature-nitrate link in the southern Benguela. Large scatter is observed in both the summer (figure 5.8 (a)) and the autumn (figure 5.8 (b)) series, and no useful trends are discernable.

Two algorithm parameters that are independent in terms of their respective derivations are FLH_{int} and $[chla]$. To assess whether anything can be deduced from a comparison of these parameters, they are plotted as seen in figure 5.9 for both the time series. The summer series (figure 5.9 (a)) reveals an identifiable fluorescence-biomass relationship as discussed in section 2.4, but only at $[chla]$ values that are below approximately 25mg.m^{-3}. Relatively more scatter seen in the FLH_{int} data at higher $[chla]$ might be due to slight occurrences of red shifts of the integrated peaks (see section 4.5.1). Additionally, the fluorescence signal might be more severely attenuated in high biomass water, causing FLH_{int} to be depressed in these waters. The positive linear trend is less obvious in data of the autumn series (figure 5.9 (b)), which are more scattered. It should be born in mind that during this period $[chla]$ values were on average much higher than during the summer period. There are thus fewer data points below 25mg.m^{-3}, and more data points above this concentration. It therefore appears that the overall trend might be similar to the trend seen in figure 5.9 (a).

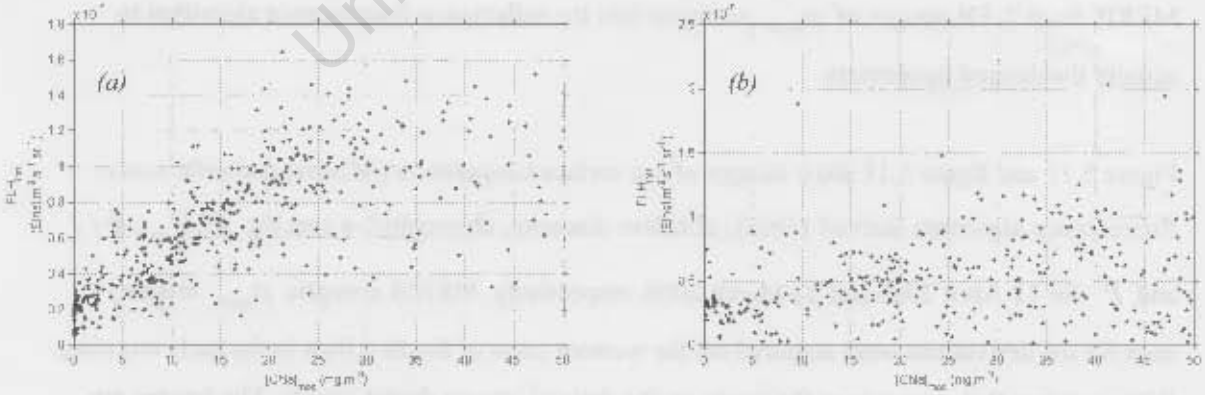

Figure 5.9: Plots of FLH_{int} versus algorithm-derived $[chla]$ for (a) the period 27 January 2005 to 22 February 2005, and (b) the period 01 April 2005 to 04 May 2005.

The reflectance-fluorescence algorithm is a useful tool for assessing remote *in situ* time series data, or *in situ* near real-time continuous fluorescence products, including ϕ_f that might be used as a physiological proxy, and the instantaneous primary production. Considering the summer and autumn time series, it still appears that the complexity of the southern Benguela system hinders the ability to distinguish causal factors of fluorescence variability within natural assemblages. Some of this apparent complexity might be due to the fact that light measurements are made on a Eulerian mooring within a highly dynamic system, which can cause parameter interpretation to be difficult. Variability in the calculated values of ϕ_f and $FLH_{\text{int}1}$ are seen to correspond to literature assessments of the variability. Magnitudes of these parameters are also seen to agree with published data. It can therefore be deduced that the algorithm provides a good estimation of these parameters in the southern Benguela. The two time series suggest that natural assemblage ϕ_f as a sensitive, remote Eulerian estimation of phytoplankton physiology is not easily interpreted, and it does not straightforwardly indicate broad phytoplankton group distinctions. These aspects would have to be studied further.

5.3 Satellite Application

Deriving fluorescence parameters from satellite images of ρ_{norm} is very valuable. It is the only independent means of physiologically related measurements from space. Phytoplankton physiology can thus be assessed synoptically over extensive regions of the globe. For this study MERIS level 2, FR images of ρ_{norm} are input into the reflectance-fluorescence algorithm to acquire the desired parameters.

Figure 5.10 and figure 5.11 show images of sea surface temperature (NOAA) and reflectance-fluorescence algorithm derived $[chla]$, effective diameter, chlorophyll-a specific FLH_{int}, ϕ_f, and P^* for 12 April 2005 and 28 March 2006, respectively. MERIS synoptic ρ_{norm} imagery used for the derivations were acquired off the western coast of South Africa in the early morning. White patches that appear over the ocean on the derived images depict clouds. The images are mostly cloud free. The fluorescence portion of the reflectance-fluorescence algorithm was restricted to the analysis of ρ_{norm} data that corresponded to pixels with $[chla]$ values below

50mg.m^{-3}. Images of ϕ_f, chlorophyll-a specific FLH_{int}, and P^* show dark blue regions that represent pixels exceeding the $[chla]$ limitation and were therefore not analysed.

Interpretation of satellite products derived from the reflectance-fluorescence algorithm can be done in a simplistic way by making certain crude assumptions. It is assumed that the various phytoplankton assemblages depicted in an image have similar light histories, and that they are photoadapted to their surface environment. Also, it is assumed that the ambient light intensity is not excessive for phytoplankton, which is viable for images acquired in the morning, and that the light field does not vary significantly over the region depicted in the image.

The temperature image of 12 April 2005 in figure 5.10 depicts upwelling along the coast. Very cold 11°C and 12°C, recently upwelled water is seen south of Cape Columbine, stretching to south of Cape Town. Newly upwelled water of 12°C can also be seen near the coast in the most northern coastal region depicted in the image. A very large and high biomass phytoplankton bloom is seen right outside St. Helena Bay as depicted in the $[chla]$ image, and a slightly lower biomass bloom is elongated northward. The algorithm associates the cores of these blooms with cells of large effective diameters. The oceanic northwestern part of the image that corresponds to ~17°C water has effective diameters that are also reasonably high.

The image of chlorophyll-a specific FLH_{int} of figure 5.10 seems to correspond to the effective diameter image in some respects. Large effective diameters of the elongated northern bloom, as well as the northwestern oceanic region, correspond to relatively low chlorophyll-a specific FLH_{int}. Low effective diameters associated with a tongue of cool waters from the south, and stretching north westwards off the coast from Cape Columbine, reveal relatively high chlorophyll-a specific FLH_{int}. This inverse trend is also seen in the small newly upwelled region near the north coast. The trend hints at a potential phytoplankton assemblage effect that might dominate chlorophyll-a specific FLH_{int} variability. Phytoplankton cells of the southwestern warm water region do not reveal this trend.

The assumptions regarding the phytoplankton light environment mentioned above simplify the assessment of ϕ_f in terms of phytoplankton physiology. Possible effects of photodamage on the

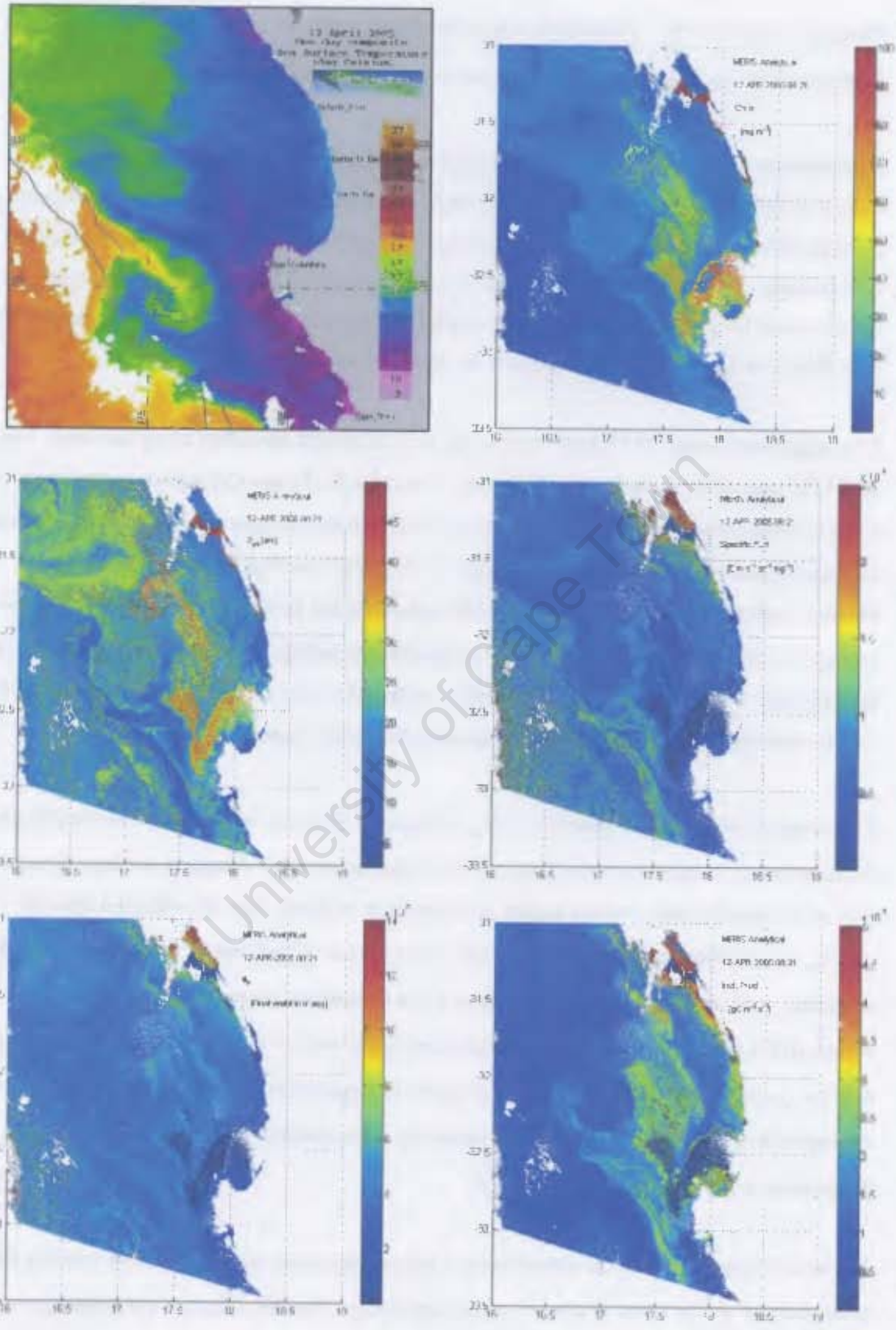

Figure 5.10: Reflectance-fluorescence products derived from MERIS data for 12 April 2005

variability of ϕ_f are assumed to be negligible. Heat dissipation of absorbed light energy is thought to contribute to ϕ_f variability of phytoplankton cells in a consistent manner throughout the region depicted in the image. If it is assumed that an assemblage consisting of similar effective diameters constitutes approximately the same phytoplankton groups, then the variability of ϕ_f occurs mainly as a result of changes in photochemistry and nutrients (see section 2.1.3).

The north coast newly upwelled region that shows similar effective diameters reveal pixels of high ϕ_f corresponding to the 12°C water of the temperature image. Maximum ϕ_f corresponds to the coolest water. This is not consistent with relatively high nutrient concentrations due to new upwelling, or with the higher photochemistry efficiency expected in such waters. The result may be due to the effect of cloud that is visible in the northern region, or it might be an artefact of algorithm analysis in the vicinity of cloud. Low ϕ_f pixels are seen near the coast that stretches between Cape Columbine and Cape Town. The newly upwelled waters and concurrent high nutrient concentrations, as well as a probable increased photochemistry efficiency of phytoplankton cells, cause ϕ_f to be relatively low.

Instantaneous primary production is high off Lamberts Bay, in the region of high $[chla]$, and also along the cool tongue of water extending from the south.

On 28 March 2006 (figure 5.11) the upwelling event is more extensive towards the north and the upwelled water is colder as compared to 12 April 2005. The newly upwelled cold water (~11°C) extends along the entire coast. Water with a temperature of 9°C occurs along the coast between Cape Columbine and Cape Town, as well as further north. Blooms are visible northwest of St. Helena Bay and offshore along the Cape Columbine to Cape Town coast. A high biomass bloom is seen in the far north, which was not analysed for fluorescence parameters. It becomes less concentrated southwards and parallel to the coast. This bloom is seen to consist almost exclusively of very high phytoplankton effective diameters. The other blooms consist of a mixture of relatively high effective diameter cells. West of the blooms and parallel to the coast, a band of relatively high effective diameters can be seen.

Chlorophyll-a specific FLH_{int} again reveals the inverse trend with effective diameter, except for phytoplankton of the warm southwest region and in the direct vicinity of the coast. The

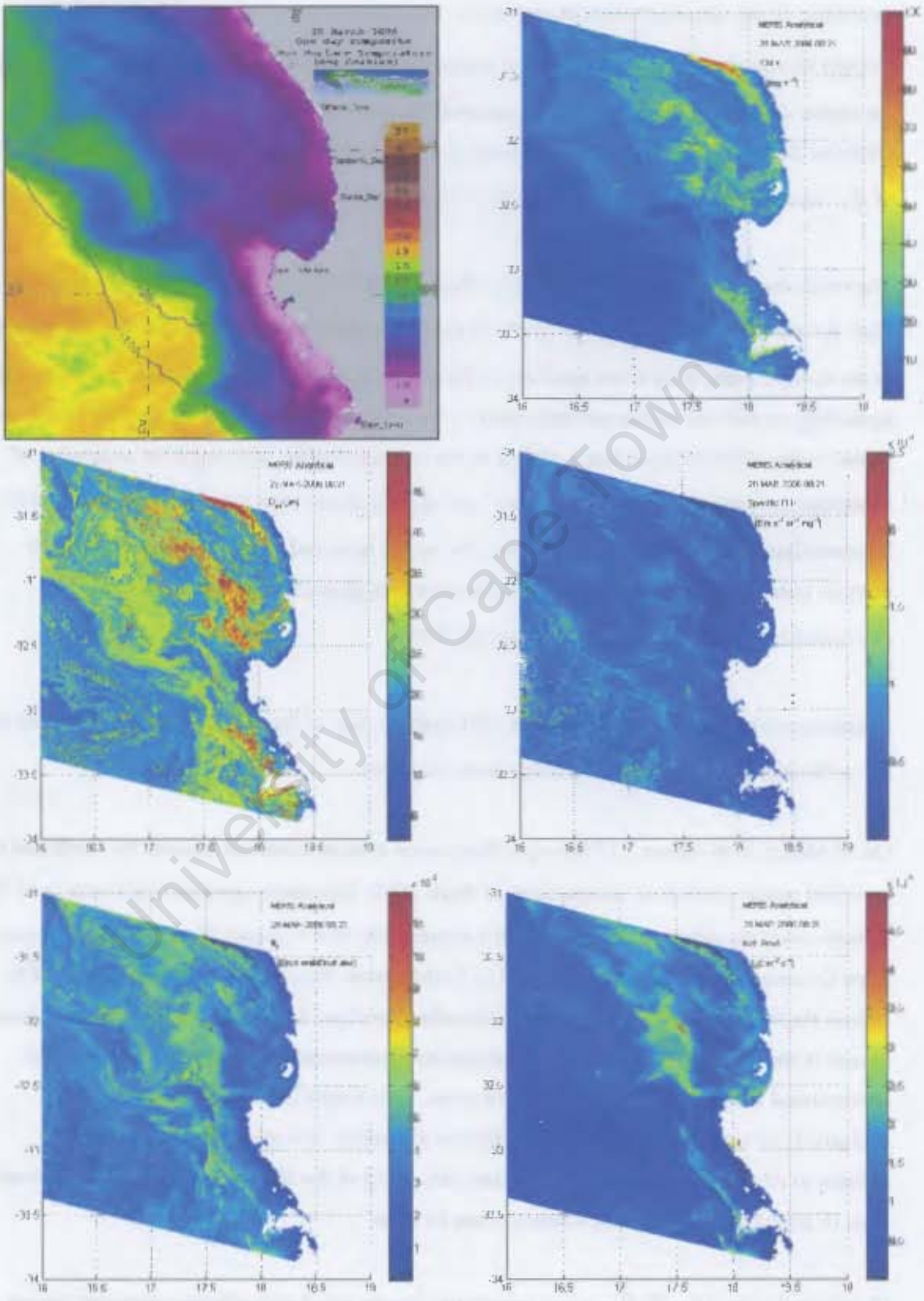

Figure 5.11: Reflectance-fluorescence products derived from MERIS data for 28 March 2006

phytoplankton bloom northwest off St. Helena Bay shows low ϕ_f in its southern section, but elevated ϕ_f in the northern part of the bloom. If the entire bloom consists of a similar assemblage, then its physiology can be described in terms of disparate nutrient availability or photochemistry efficiency. Since the northern part of the bloom extends into relatively warmer waters, it is possible that nutrient concentrations were lower there, which could explain higher ϕ_f in the north. However, the northern and southern parts of the bloom might consist of very different assemblages, which might be the reason for the differences in ϕ_f. Instantaneous primary production is high in the region west of the high biomass bloom, and low inside the bloom.

Reflectance-fluorescence algorithm parameters derived from satellite ρ_{norm} images, in combination with the temperature images, have great potential for the synoptic assessment of phytoplankton assemblage physiology and group composition in their natural environment. The interpretation difficulties caused as a result of advection past a Eulerian point, emerging in the analysis of *in situ* bio-optical assessments, are removed when the parameters are considered via an extensive synoptic image. Some simplifying assumptions are possible in the interpretation of parameter images, such that phytoplankton physiology can be assessed via images of calculated ϕ_f. Chlorophyll-a specific FLH_{int} images show that it might be possible to draw some assemblage distinctions. Interpretative abilities of parameter images can be improved by viewing time series of satellite images, such that development of blooms and the fluorescence parameter responses can be considered jointly.

5.4 Summary

The reflectance-fluorescence algorithm allows the assessment of fluorescence parameters as Eulerian, *in situ* data in combination with environmental and assemblage indicators, such as temperature, ambient light intensity, effective diameter, and biomass. Interpretative abilities of these parameters are slightly hampered by the complexity of the southern Benguela system, especially from the perspective of a Eulerian instrument in a dynamic system. Interpretation is improved through application of the reflectance-fluorescence algorithm to satellite imagery that enables certain simplifying assumption to be made with regard to phytoplankton physiology. This

application has great potential, since it allows the physiological assessment of phytoplankton from space. A substantial amount of information can be deduced from the derived imagery examined in conjunction with environmental and assemblage indicators, but it is necessary to study more images for better interpretative abilities. Instantaneous primary production estimates are viable, although they are not expected to be accurate, and might be useful when bloom development is studied. These estimates might be valuable in a qualitative sense.

Chapter 6

Conclusion

The rate of fluorescence by phytoplankton cells relates to cellular mechanisms that ensure light absorption, excitation energy transport, photochemistry, and heat dissipation. Fluorescence variability within a phytoplankton cell thus indicates physiological change. Additionally, fluorescence differences between cells might be due to species dissimilarity. The fluorescence quantum yield parameter provides a direct means for the assessment of fluorescence-related change at the phytoplankton cellular level.

Sun-induced fluorescence of phytoplankton is measured through passive techniques. This study shows the viability of using autonomous bio-optical instruments for the remote estimation of sun-induced fluorescence of phytoplankton in the natural marine environment, and the derivation of the fluorescence quantum yield. The technique is useful, since it allows the real-time investigation of phytoplankton physiology *in situ*. Moreover, phytoplankton physiology can be examined synoptically over extensive spatial scales from space. No other independent means exists for physiologically related measurements from space. Furthermore, the potential exists to make phytoplankton group distinctions remotely, as well as studying phytoplankton primary production rates qualitatively. These parameters will provide much insight into the development and decay of blooms, and towards general phytoplankton dynamics in the natural marine environment.

Physiological state of phytoplankton assemblages depends appreciably on the environmental conditions. Fluorescence emission rate, the fluorescence quantum yield, and other related physiological parameters, such as the photosynthetic quantum yield, vary with environmental factors. Various published investigations of these parameters, through both passive and active techniques, show variability with light intensity and nutrient availability. In the dynamic ocean environment the various causal factors of fluorescence variability affect assemblages in a complex way, and in relation to the particular groups constituting an assemblage. Therefore, interpretation of fluorescence variability of marine phytoplankton is complicated.

Data acquired from the field survey provided insight into the variability of fluorescence parameters with environmental variables, although the results reflected very specific ocean conditions and assemblage compositions of the southern Benguela. Assessment of the data with the purpose of obtaining a general functional physiological proxy regarding the remote interpretation of assemblages was thus not viable. Variability of fluorescence parameters as a result of assemblage differences was suggested in field data trends. The data generally resembled published evaluations of fluorescence parameter variability, and factors forcing the variability were found to contribute in a complex way.

The algorithm developed for the purpose of this study calculates viable fluorescence parameters from hyperspectral *in situ* radiometer data, and from multi-spectral satellite spectroradiometer imagery. The algorithm therefore provides a useful tool for the autonomous real-time *in situ* assessment, and the spatially extensive synoptic estimation, of sun-induced chlorophyll-a fluorescence and the fluorescence quantum yield of natural phytoplankton assemblages. It was found that the reflectance-fluorescence algorithm cannot be operated at very high phytoplankton biomass. This implies that HAB events cannot be studied directly through algorithm-derived parameters. However, calculated fluorescence parameter variability during periods of relatively low phytoplankton biomass and during the formative stages of bloom events can be assessed. Knowledge of calculated fluorescence parameter variability provides insight to phytoplankton assemblage dynamics and physiology in relation to the changing ocean environment.

The study shows that instantaneous primary production can be calculated from derived fluorescence by incorporating published empirical relationships into the reflectance-fluorescence algorithm. Application of the reflectance-fluorescence algorithm to the estimation of instantaneous primary production is preliminary, and it is intended to contribute in an experimental sense towards operational monitoring purposes. Estimations are not expected to be robust, but they might contribute to the assessment of phytoplankton dynamics in a qualitative way.

Time series of environmental variables with relation to derived fluorescence parameters afford the investigation of their concurrent temporal variability. Interpretation of the variability is complicated by the fact that *in situ* moorings are Eulerian. In the dynamic southern Benguela, advection of phytoplankton patches and water masses prohibits the study of distinct, and stable environmental and assemblage conditions. Derived satellite imagery of fluorescence parameters,

in combination with temperature imagery, and calculated effective diameter and chlorophyll-a concentrations portray useful information regarding phytoplankton dynamics. When certain acceptable simplifying assumptions are made, much can be inferred about differences in assemblage structures, and physiological responses to the environment. Daily investigations of the imagery will reveal fluorescence variability of, for example, developing or decaying assemblages, which will assist in an understanding of phytoplankton dynamics over large spatial scales in the productive upwelling system. Considering these applications the study finds that the reflectance-fluorescence algorithm is a useful tool with regard to remote observations of phytoplankton dynamics.

Future endeavours necessary to build on the present study include more extensive field research in a variety of southern Benguela ocean conditions, and close inspection of *in situ* time series and satellite imagery fluorescence products in relation to available environmental variables. A more extensive dataset would allow robust validation of the algorithm products, and would consequently permit appropriate algorithm improvements. A large dataset will provide better insight into fluorescence variability of different assemblages with relation to the environment, and might reveal operationally useful empirical relationships, or generally applicable physiological proxies. Frequent investigation of algorithm products might reveal useful patterns, and it will improve the ability to interpret these products.

References

Abbott M.R., Richerson P.J., and T.M. Powell (1982), *In situ* response of phytoplankton fluorescence to rapid variations in light, *Limnology and Oceanography*, 27, 2, 218 – 225

Abbott M.R., Brink K.H., Booth C.R., Blasco D., Swenson M.S., Davis C.O. and L.A. Codispoti (1995), Scales of variability of bio-optical properties as observed from near-surface drifters, *Journal of Geophysical Research*, 100, C7, 13345 – 13367

Aiken J. (2001), Fluorometry for biological sensing, In *Encyclopaedia of Ocean Sciences*, Steele J.H., Thorpe S.A., and K.K. Turekian (eds.), Academic Press, London, pp. 1073 – 1081

Albert A. and C.D. Mobley (2003), An analytical model for subsurface irradiance and remote sensing reflectance in deep and shallow case-2 waters, *Optics Express*, 11, 22, 2873 – 2890

Babin M. (2003), *In vivo* chlorophyll a fluorescence: Theoretical background and related applications in marine sciences, Habwatch Workshop 2003, WKHABWATCH, 11 – 21 June 2003, Villefranche-sur-Mer, France, viewed 10 July 2006, < http://www.obs-vlfr.fr/habwatch/>

Babin M., Therriault J.C., Legendre L., Nieke B., Reuter R., and A. Condal (1995), Relationship between the maximum quantum yield of carbon fixation and the minimum quantum yield of chlorophyll-a *in vivo* fluorescence in the Gulf of St. Lawrence, *Limnology and Oceanography*, 40, 5, 956 – 968

Babin M., Morel A., and B. Gentili (1996), Remote sensing of sea surface sun-induced chlorophyll fluorescence: consequences of natural variations in the optical characteristics of phytoplankton and the quantum yield of chlorophyll-a fluorescence, *International Journal of Remote Sensing*, 17, 12, 2417 – 2448

Barlow R., Sessions H, Silulwane N., Engel H., Hooker S.B., Aiken J., Fishwick J., Vicente V., Morel A., Chami M., Ras J., Bernard S., Pfaff M., Brown J.W., and A. Fawcett (2003), BENCAL Cruise Report, *NASA/TM 2003-206892*, 27, Hooker S.B. and E.R. Firestone (eds.), NASA Goddard Space Flight Center, Greenbelt, Maryland, pp. 62

Behrenfeld M.J. and P.G. Falkowski (1997), A consumer's guide to phytoplankton primary productivity models, *Limnology and Oceanography*, 42, 7, 1479 – 1491

Berges J.A. and P.G. Falkowski (1998), Physiological stress and cell death in marine phytoplankton: Induction of proteases in response to nitrogen or light limitation, *Limnology and Oceanography*, 43, 1, 129 – 135

Bernard S. (2005), The bio-optical detection of harmful algae, PhD Thesis, University of Cape Town, South Africa, pp. 232

Bernard S., Balt C., Pitcher G., Probyn T., Fawcett A., and A. du Randt (2005), The use of MERIS for harmful algal bloom monitoring in the southern Benguela, Proceedings of the MERIS (A)ATSR Workshop 2005, ESA SP-597, 26 – 30 September 2005, ESRIN, Frascati, Italy, Lacoste H. (ed.). Published on CDROM., p.26.1

Bird R.E. and C. Riordan (1986), Simple solar spectral model for direct and diffuse irradiance on horizontal and tilted planes at the earth's surface for cloudless atmospheres, *Journal of Applied Meteorology*, 25, 1, 87 – 97

Bricaud A., Babin M., Morel A., and H. Claustre (1995), Variability in the chlorophyll-specific absorption coefficient of natural phytoplankton: Analysis and parameterisation, *Journal of Geophysical Research*, 100, C7, 13321 – 13332

Chamberlin W.S., Booth C.R., Kiefer D.A., Morrow J.H., and R.C. Murphy (1990), Evidence for a simple relationship between natural fluorescence, photosynthesis and chlorophyll in the sea, *Deep-Sea Research*, 37, 6, 951 – 973

Chamberlin S and J. Marra (1992), Estimation of photosynthetic rate from measurements of natural fluorescence: analysis of the effect of light and temperature, *Deep-Sea Research*, 39, 1695 – 1706

Cleveland J.S. and M.J. Perry (1987), Quantum yield, relative specific absorption and fluorescence in nitrogen-limited *Chaetoceros gracilis*, *Marine Biology*, 94, 489 – 497

Collins D.J., Kiefer D.A., Soohoo J.B., and I.S. McDermid (1985), The role of reabsorption in the spectral distribution of phytoplankton fluorescence emission, *Deep-Sea Research*, 32, 983 – 1003

Conover, W.J. (1980), *Practical Nonparametric Statistics*, Wiley, New York, pp. 357

Critchley C. (1988), The molecular mechanisms of photoinhibition – Facts and fiction, *Australian Journal of Plant Physiology*, 15, 27 – 41

Cullen J.J., Lewis M.R., Davis C.O., and R.T. Barber (1992), Photosynthetic characteristics and estimated growth rates indicate grazing is the proximate control of primary production in the Equatorial Pacific, *Journal of Geophysical Research*, 97, C1, 639 – 654

Cullen J.J. and M.R. Lewis (1995), Biological processes and optical measurements near the sea surface: some issues relevant to remote sensing, *Journal of Geophysical Research*, 100, C7, 13255 – 13266

Cullen J.J., Ciotti A.M., Davis R.F., and M.R. Lewis (1997), Optical detection and assessment of algal blooms, *Limnology and Oceanography*, 42, 5(2), 1223 – 1239

Duysens L.M.N. (1956), The flattening effect of the absorption spectra of suspensions as compared to that of solutions, *Biochimica et Biophysica Acta*, 19, 1 – 12

Falkowski P.G. and D.A. Kiefer (1985), Chlorophyll a fluorescence in phytoplankton: relationship to photosynthesis and biomass, *Journal of Plankton Research*, 7, 5, 715 – 731

Falkowski P.G., Ziemann D., Kolber Z., and P.K. Bienfang (1991), Role of eddy pumping in enhancing primary production in the ocean, *Nature*, 352, 55 – 58

Falkowski P.G., Greene R.M., and R.J. Geider (1992), Physiological limitations on phytoplankton productivity in the ocean, *Oceanography Magazine*, 5, 84 – 91

Falkowski P.G. and Z. Kolber (1995), Variations in Chlorophyll Fluorescence Yields in Phytoplankton in the World Oceans, *Australian Journal of Plant Physiology*, 22, 341 – 355

Falkowski P.G. and J.A. Raven (1997), *Aquatic Photosynthesis*, Blackwell Publishers, Massachusetts, pp. 432

Fawcett A., Bernard S., Pitcher G.C., Probyn T.A., and A du Randt (2006), Real-time monitoring of harmful algal blooms in the southern Benguela, *African Journal of Marine Science*, 28, 2 (in press)

Fisher R.A. (1921), On the 'probable error' of a coefficient of correlation deduced from a small sample, *Metron*, 1, 1 – 32

Garcia-Mendoza E. and H. Maske (1996), The relationship of solar-stimulated natural fluorescence and primary productivity in Mexican Pacific waters, *Limnology and Oceanography*, 41, 8, 1697 – 1710

Gordon H.R. (1979), Diffuse reflectance of the ocean: The theory of its augmentation by chlorophyll a fluorescence at 685nm, *Applied Optics*, 18, 1161 – 1166

Gordon, H.R. and W.R. McLuney (1975), Estimation of the depth of sunlight penetration in the sea for remote sensing, *Applied Optics*, 14, 413 – 416

Gordon H.R., Voss K.J., and K.A. Kilpatrick (1993), Angular distribution of fluorescence from phytoplankton, *Limnology and Oceanography*, 38, 7, 1582 – 1586

Gower J.F.R., Doerffer R., and G.A. Borstad (1999), Interpretation of the 685nm peak in water-leaving radiance spectra in terms of fluorescence, absorption and scattering, and its observation by MERIS, *International Journal of Remote Sensing*, 20, 9, 1771 – 1786

Greene R.M., Kolber Z.S., Swift D.G., Tindale N.W., and P.G. Falkowski (1994), Physiological limitation of phytoplankton photosynthesis in the eastern equatorial Pacific determined from variability in the quantum yield of fluorescence, *Limnology and Oceanography*, 39, 5, 1061 – 1074

Gregg W.W. and K.L. Carder (1990), A simple spectral solar irradiance model for cloudless maritime atmospheres, *Limnology and Oceanography*, 35, 8, 1657 – 1675

Hitachi F-4000 manual, Hitachi, Ltd. Tokyo

Hoge F.E. and R. N. Swift (1983), Airborne dual laser excitation and mapping of phytoplankton photopigments in a Gulf Stream warm core ring, *Applied Optics*, 22, 2272 – 2278

Johnsen G. and E. Sakshaug (1993), Bio-optical characteristics and photoadaptive responses in the toxic and bloom-forming dinoflagellates *Gyrodinium aureolum*, *Gymnodinium galatheanum*, and two strains of *Prorocentrum minimum*, *Journal of Phycology*, 29, 627 – 642

Jeffrey S.W., Mantoura R.F.C., and S.W. Wright (eds.) (1997), *Phytoplankton pigments in oceanography: Guidelines to modern methods*, UNESCO Publishers, Paris, pp. 661

Johnsen G., Prézelin B.B., and R.V.M. Jovine (1997), Fluorescence excitation spectra and light utilisation in two red tide dinoflagellates, *Limnology and Oceanography*, 42, 5(2), 1166 – 1177

Kiefer D.A. (1973a), Fluorescence properties of natural phytoplankton populations, *Marine Biology*, 22, 263 – 269

Kiefer D.A. (1973b), Chlorophyll a fluorescence in marine centric diatoms: Responses of chloroplasts to light and nutrient stress, *Marine Biology*, 23, 39 – 46

Kiefer D.A., Chamberlin W.S., and C.R. Booth (1989), Natural fluorescence of chlorophyll a: Relationship to photosynthesis and chlorophyll concentration in the western South Pacific gyre, *Limnology and Oceanography*, 34, 5, 868 – 881

Kirk J.T.O. (1996), *Light and Photosynthesis in Aquatic Ecosystems*, Cambridge University Press, Cambridge, pp. 528

Kishino M., Takahashi M., Okami N., and S. Ichimura (1985), Estimation of the spectral absorption coefficients of phytoplankton in the sea, *Bulletin of Marine Science*, 37, 634 – 642

Kolber Z., Zehr J., and P. Falkowski (1988), Effects of growth irradiance and nitrogen limitation on photosynthetic energy conversion in photosystem II, *Plant Physiology*, 88, 923 – 929

Kolber Z., Wyman K.D., and P.G. Falkowski (1990), Natural variability in photosynthetic energy conversion efficiency: A field study in the Gulf of Maine, *Limnology and Oceanography*, 35, 1, 72 – 79

Kolber Z. and P.G. Falkowski (1993), Use of active fluorescence to estimate phytoplankton photosynthesis *in situ*, *Limnology and Oceanography*, 38, 8, 1646 – 1665

Kolber Z.S., Prášil O., and P.G. Falkowski (1998), Measurements of variable chlorophyll fluorescence using fast repetition rate techniques: defining methodology and experimental protocols, *Biochimica et Biophysica Acta*, 1367, 88 – 106

Kyewalyanga M.N., Platt T., and S. Sathyendranath (1997), Estimation of the photosynthetic action spectrum: Implication for primary production models, *Marine Ecology Progress Series*, 146, 207 – 223

Lakowicz J.R. (1983), *Principles of fluorescence spectroscopy*, London Plenum, New York, pp. 496

Laney S.R., Letelier R.M., and M.R. Abbott (2005), Parameterising the natural fluorescence kinetics of *Thalassiosira weissflogii*, *Limnology and Oceanography*, 50, 5, 1499 – 1510

Lin S., Borstad G.A., and J.F.R. Gower (1984), Remote sensing of chlorophyll in the red spectral region, In *Remote Sensing of Shelf Sea Hydrodynamics*, Nihoul J.C.J. (ed.), Elsevier, New York, pp. 317 – 386

Lippemeier S., Hintze R., Vanselow K.H., Hartig P., and F. Colijn (2001), In-line recording of PAM fluorescence of phytoplankton cultures as a new tool for studying effects of fluctuating nutrient supply on photosynthesis, *European Journal of Phycology*, 36, 89 – 100

Lizotte M.P. and J.C. Priscu (1994), Natural fluorescence and quantum yields in vertically stationary phytoplankton from perennially ice-covered lakes, *Limnology and Oceanography*, 39, 6, 1399 – 1410

Lutz V.A., Sathyendranath S., Head E.J.H., and W.K.W. Li (2001), Changes in the *in vivo* absorption and fluorescence excitation spectra with growth irradiance in three species of phytoplankton, *Journal of Plankton Research*, 23, 6, 555 – 569

Maritorena S, Morel A., and B. Gentili (2000), Determination of the fluorescence quantum yield by oceanic phytoplankton in their natural habitat, *Applied Optics*, 39, 36, 6725 – 6737

Marra J (1997), Analysis of diel variability in chlorophyll fluorescence, *Journal of Marine Research*, 55, 767 – 784

Marshall H.L., Geider R.J., and K.J. Flynn (2000), A mechanistic model of photoinhibition, *New Phytologist*, 145, 2, 347 – 359

Mobley C.D. (1994), *Light and water: Radiative Transfer in Natural Waters*, Academic Press, California, pp. 592

Montagnes D.J.S. and D.J. Franklin (2001), Effect of temperature on diatom volume, growth rate, and carbon and nitrogen content: Reconsidering some paradigms, *Limnology and Oceanography*, 46, 8, 2009 – 2018

Morel A. (1988), Optical modeling of the upper ocean in relation to its biogenous matter content (case I waters), *Journal of Geophysical Research*, 93, C9, 10749 – 10768

Morel A. (1991), Light and marine photosynthesis: a spectral model with geochemical and climatological implications, *Progress in Oceanography*, 26, 263 – 306

Morel A. (2001), Bio-optical models, In *Encyclopaedia of Ocean Sciences*, Steele J.H., Thorpe S.A., and K.K. Turekian (eds.), Academic Press, London, pp. 317 – 325

Morel A. and R.C. Smith (1974), Relation between total quanta and total energy for aquatic photosynthesis, *Limnology and Oceanography*, 19, 4, 591 – 600

Morel A. and L. Prieur (1977), Analysis of variations in ocean color, *Limnology and Oceanography*, 22, 4, 709 – 722

Morel A. and A. Bricaud (1981), Theoretical results concerning light absorption in a discrete medium, and application to specific absorption of phytoplankton, *Deep-Sea Research*, 28A, 11, 1375 – 1393

Morel A. and J.F. Berthon (1989), Surface pigments, algal biomass profiles, and potential production of the euphotic layer: Relationships reinvestigated in view of remote-sensing applications, *Limnology and Oceanography*, 34, 8, 1545 – 1562

Morrison J.R. (2003), In situ determination of the quantum yield of phytoplankton chlorophyll-a fluorescence: A simple algorithm, observations, and a model, *Limnology and Oceanography*, 48, 2, 618 – 631

Müller P., Li X.P., and K.K. Niyogi (2001), Non-photochemical quenching. A response to excess light energy, *Plant Physiology*, 125, 1558 – 1566

Neori A., Holm-Hansen O., Mitchell B.G., and D.A. Kiefer (1984), Photoadaptation in marine phytoplankton. Changes in spectral absorption and excitation of chlorophyll a fluorescence, *Plant Physiology*, 76, 518 – 524

Neville R.A. and J.F.R. Gower (1977), Passive remote sensing of phytoplankton via chlorophyll a fluorescence, *Journal of Geological Research*, 82, 3487 – 3493

Nydahl F. (1976), On the optimum conditions for the reduction of nitrate to nitrite by cadmium, *Talanta*, 23, 349 – 357

Olaizola M., Geider R.J., Harrison W.G., Graziano L.M., Ferrari G.M., and P.M. Schlittenhardt (1996), Synoptic study of variations in the fluorescence-based maximum quantum efficiency of photosynthesis across the North Atlantic ocean, *Limnology and Oceanography*, 41, 4, 755 – 765

Parsons T.R., Maita Y., and C.M. Lalli (1984), *A manual of chemical and biological methods for seawater analysis*, Pergamon Press, Oxford, pp. 173

Pitcher G.C., Boyd A.J., Horstman D.A., and B.A. Mitchell-Innes (1998), Subsurface dinoflagellate populations, frontal blooms and the formation of red tide in the southern Benguela upwelling system, *Marine Ecology Progress Series*, 172, 253 – 264

Pitcher G.C. and D. Calder (2000), Harmful algal blooms of the southern Benguela Current: A review and appraisal of monitoring from 1989 to 1997, *South African Journal of Marine Science*, 22, 255 – 271

Platt T., Gallegos C.L., and W.G. Harrison (1980), Photoinhibition of photosynthesis in natural assemblages of marine phytoplankton, *Journal of Marine Research*, 38, 687 – 701

Prézelin B.B. and A.C. Ley (1980), Photosynthesis and chlorophyll a fluorescence rhythms of marine phytoplankton, *Marine Biology*, 55, 295 – 307

Probyn T.A., Waldron H.N., and A.G. James (1990), Size-fractionated measurements of nitrogen uptake in aged upwelled waters: Implications for pelagic food webs, *Limnology and Oceanography*, 35, 1, 202 – 210

Roesler C.S. (1998), Theoretical and experimental approaches to improve the accuracy of particulate absorption coefficients derived from the quantitative filter technique, *Limnology and Oceanography*, 43, 7, 1649 – 1660

Roesler C.S. and M.J. Perry (1995), *In situ* phytoplankton absorption, fluorescence emission, and particulate backscattering spectra determined from reflectance, *Journal of Geophysical Research*, 100, C7, 13279 – 13294

Sakshaug E., Johnsen G., Andresen K., and M. Vernet (1991), Modeling of light-dependent algal photosynthesis and growth: experiments with the Barents Sea diatoms *Thalassiosira nordenskioeldii*, and *Chaetoceros furcellatus*, *Deep-Sea Research*, 38, 415 – 430

Sakshaug E., Bricaud A., Dandonneau Y., Falkowski P.G., Kiefer D.A., Legendre L., Morel A., Parslow J., and M. Takahashi (1998), Parameters of photosynthesis: definitions, theory and interpretation of results, *The Joint Global Ocean Flux Study (JGOFS)*, Report no. 27

Slovacek R.E. and P.J. Hannan (1977), *In vivo* fluorescence determinations of phytoplankton chlorophyll a, *Limnology and Oceanography*, 22, 5, 919 – 925

Sosik H.M., Chisholm S.W., and R.J. Olson (1989), Chlorophyll fluorescence from single cells: Interpretation of flow cytometric signals, *Limnology and Oceanography*, 34, 8, 1749 – 1761

Sosik H.M. and B.G. Mitchell (1991), Absorption, fluorescence, and quantum yield for growth in nitrogen-limited *Dunaliella tertiolecta*, *Limnology and Oceanography*, 36, 5, 910 – 921

Stegmann P.M., Lewis M.R., Davis C.O., and J.J. Cullen (1992), Primary production estimates from recordings of solar-stimulated fluorescence in the Equatorial Pacific at 150°W, *Journal of Geophysical Research*, 97, C1, 627 – 638

Stegmann P.M. and M.R. Lewis (1997), Shipboard measurements of phytoplankton production and solar-stimulated fluorescence rates in the northwest Atlantic, *Continental Shelf Research*, 17, 7, 743 – 760

Stramski D., Sciandra A., and H. Claustre (2002), Effects of temperature, nitrogen, and light limitation on the optical properties of the marine diatom *Thalassiosira pseudonana*, *Limnology and Oceanography*, 47, 2, 392 – 403

Turner 10-AU Manual, Turner Designs, Sunnyvale

Wood M.D. and R.L. Oliver (1995), Fluorescence transients in response to nutrient enrichment of nitrogen- and phosphorous-limited *Microcystis aeruginosa* cultures and natural phytoplankton populations: a measure of nutrient limitation, *Australian Journal of Plant Physiology*, 22, 331 – 340

Yentsch C.S. (1962), Measurement of visible light absorption by particulate matter in the ocean, *Limnology and Oceanography*, 7, 207 – 217

Yentsch C.S. and C.M. Yentsch (1979), Fluorescence spectral signatures: The characterization of phytoplankton populations by the use of excitation and emission spectra, *Journal of Marine Research*, 37, 471 – 483

Yentsch C.M., Horan P.K., Muirhead K, Dortch Q., Haugen E., Legendre L., Murphy L.S., Perry M.J., Phinney D.A., Pomponi S.A., Spinrad R.W., Wood M., Yentsch C.S.,and B.J. Zahuranec (1983), Flow cytometry and cell sorting: A technique for analysis and sorting of aquatic particles, *Limnology and Oceanography*, 28, 6, 1275 – 1280

Yentsch C.S. and D.A. Phinney (1989), A bridge between ocean optics and microbial ecology, *Limnology and Oceanography*, 34, 1694 – 1705

Appendix A

Glossary of Symbols

Symbol	Unit (As adopted in this study)	Description
$a_\phi(\lambda)$	m^{-1}	phytoplankton absorption coefficient
$a_\phi^*(\lambda)$	$m^2.(mg\ chl\text{-}a)^{-1}$	chlorophyll-a specific phytoplankton absorption coefficient
$\overline{a}_\phi^*$	$m^2.(mg\ chl\text{-}a)^{-1}$	spectrally weighted phytoplankton mean specific absorption coefficient
$a_\phi^*(685)$	$m^2.(mg\ chl\text{-}a)^{-1}$	chlorophyll-a specific phytoplankton absorption coefficient at 685nm
$a_{sol}^*(685)$	$m^2.(mg\ chl\text{-}a)^{-1}$	chlorophyll-a specific phytoplankton absorption coefficient in solution at 685nm
$a_w(685)$	m^{-1}	absorption coefficient of pure water at 685nm
α	$mg\ C.(mg\ chl\text{-}a)^{-1}.h^{-1}.(\mu Einst.m^{-2}.s^{-1})^{-1}$	initial linear slope of the P/E curve
β	$mg\ C.(mg\ chl\text{-}a)^{-1}.h^{-1}.(\mu Einst.m^{-2}.s^{-1})^{-1}$	parameter that characterises photoinhibition in the P/E curve
$c(685)$	m^{-1}	beam attenuation coefficient at 685nm
c_v	$nm.s^{-1}$	velocity of light in a vacuum
c_i	$kg.m^{-3}$	intracellular chlorophyll-a concentration
$[chla]$	$mg.m^{-3}$	chlorophyll-a concentration
d	m	sensor depth
dz	m	infinitesimally thin layer of seawater
$\Delta\phi_{sat}$	dimensionless	$F_v / F_m = \Delta\phi_{sat} / (\Delta\phi_{sat} - 1)$ from

		saturating pump flash
$\Delta\lambda$	nm	spectral width of integration
$E_d(0+,\lambda)$	$\mu W.cm^{-2}.nm^{-1}$, **or** $Einst.m^{-2}.s^{-1}.nm^{-1}$	downward vector irradiance above the ocean surface
$E_d(0,\lambda)$	$Einst.m^{-2}.s^{-1}.nm^{-1}$	downward vector irradiance just below ocean the surface
E_{dPAR}	$Einst.m^{-2}.s^{-1}$	downward vector irradiance PAR
$E_{d\,\mathrm{int}}(0+)$	$\mu W.cm^{-2}$	wavelength-integrated $E_d(0+,\lambda)$
E_k	$Einst.m^{-2}.s^{-1}$	irradiance when linear part of the P/E curve is extrapolated to P_m
$E_\circ(0,\lambda)$	$Einst.m^{-2}.s^{-1}.nm^{-1}$	scalar irradiance just below the ocean surface
$E_{\circ F}$	$Einst.m^{-2}.s^{-1}$	instantaneous rate of emitted phytoplankton chlorophyll-a fluorescence
$E_{\circ PAR}$	$Einst.m^{-2}.s^{-1}$	scalar irradiance PAR
$E_{\circ Xe}(\lambda)$	$Einst.m^{-2}.s^{-1}.nm^{-1}$	spectrofluorometer xenon lamp scalar emission
F	$Einst.m^{-3}.s^{-1}$	phytoplankton chlorophyll-a fluorescence emission rate
F^*	$Einst.mg^{-1}.s^{-1}$	phytoplankton chlorophyll-a specific fluorescence emission rate
FLH_{int}	$Einst.m^{-2}.s^{-1}.sr^{-1}$	spectrally integrated fluorescence line height
$F_\circ$	relative units	active minimum fluorescence yield (dark adapted)
F_m	relative units	active maximal fluorescence yield (dark adapted)
F_v	relative units	active variable fluorescence (dark adapted)
F_v / F_m	dimensionless	active maximum change in the quantum yield of fluorescence (dark adapted)
$F_{corr}(\lambda)$	$Einst.m^{-2}.s^{-1}.nm^{-1}$	spectrofluorometer xenon lamp-corrected sample fluorescence emission
$F_{instr}(\lambda)$	counts	spectrofluorometer sample fluorescence

		emission
h	joules.s^{-1}	Planck's constant
I	Einst.m^{-2}.s^{-1}	tungsten light intensity
k_{cf}	Einst.m^{-2}.s^{-1}	irradiance when $(\phi_c / \phi_f)_{max}$ is equal to half of its maximum value
K_{PAR}	m^{-1}	vertical diffuse attenuation coefficient for PAR
K_t	m^{-1}	total diffuse attenuation coefficient for PAR
K_f	m^{-1}	total diffuse attenuation coefficient for fluorescence at 685nm radiance
L_F	Einst.m^{-2}.s^{-1}.sr^{-1}	upward radiance signal detected due to emitted fluorescence
$L_u(d,\lambda)$	μW.cm^{-2}.nm^{-1}.sr^{-1}, **or** Einst.m^{-2}.s^{-1}.nm^{-1}.sr^{-1}	upward radiance at the sensor depth d
$L_w(0+,\xi)$	W.m^{-2}.nm^{-1}.sr^{-1}	water-leaving radiance
λ	nm	wavelength in a vacuum
N	hrs	hours of incubation
ξ	sr, nm	direction of light at specified wavelength detected by satellite
P	gramsC.m^{-2}.s^{-1}, **or** molC.m^{-2}.s^{-1}	phytoplankton photosynthetic rate, **or** instantaneous rate of carbon fixation
P^*	gramsC.m.(mg chl-a)$^{-1}$.s^{-1}	chlorophyll-a specific phytoplankton photosynthetic rate, or chlorophyll-a specific instantaneous primary production
$P(d)$	molC.m^{-2}.s^{-1}	vertically depth-integrated instantaneous rate of carbon fixation within the column of fluorescing cells to below sensor depth
P'	mg C.m^{-3}.h^{-1}	instantaneous rate of phytoplankton photosynthesis from P/E experiment

P_B	mg C.(mg chl-a)$^{-1}$.h^{-1}	chlorophyll-a normalised instantaneous photosynthesis rate from P/E experiment
P_S	mg C.(mg chl-a)$^{-1}$.h^{-1}	maximum rate of photosynthesis in the absence of photoinhibition from P/E experiment
P_m	mg C.(mg chl-a)$^{-1}$.h^{-1}	maximum rate of photosynthesis from P/E experiment
P_{680}	unitless	protein-complexed chlorophyll-a molecule; primary electron donor
PQH_2	unitless	plastoquinol
ρ_{norm}	counts	normalised water-leaving reflectance
Q_a	unitless	quinone; primary electron acceptor
Q_b	unitless	plastoquinone; secondary electron acceptor
$Q_a^*(685)$	dimensionless	fluorescence reabsorption factor at 685nm
R	dpm	total activity scintillation count
R_b	dpm	time zero scintillation count
R_s	dpm	sample scintillation count
$R_{fil}(\lambda)$	counts	filter pad reflectance
R_{rs}	sr^{-1}	remote sensing reflectance
T_0	unitless	time zero
T_A	unitless	total activity
σ_{PSII}	Å^2	relative functional absorption cross-section for PSII
ϕ_f	Einst emitted.(Einst absorbed)$^{-1}$	phytoplankton fluorescence quantum yield
ϕ_c	molC.(Einst)$^{-1}$	phytoplankton photosynthetic quantum yield
ϕ_c / ϕ_f	molC.(Einst)$^{-1}$	phytoplankton quantum yield ratio
ϕ_m	molC.(Einst)$^{-1}$	maximum phytoplankton photosynthetic quantum yield
$(\phi_c / \phi_f)_{max}$	Catoms.(photon)$^{-1}$	maximum value of the quantum yield ratio

W	mg $C.m^{-3}$	weight of total carbon dioxide
Z_e	m	euphotic depth
z	m	depth
$0+$	unitless	above the ocean surface
0	unitless	just below the ocean surface

W	mg C.m^{-3}	weight of total carbon dioxide
Z_e	m	euphotic depth
z	m	depth
$0+$	unitless	above the ocean surface
0	unitless	just below the ocean surface

Appendix B

Acronyms

BOB	Benguela Optical Buoy
DCMU	3-(3,4-dichlorophenyl)-1,1-dimethylurea
ESA	European Space Agency
FLH	Fluorescence Line Height
FRRF	Fast Repetition Rate Fluorometry
HAB	Harmful Algal Bloom
HPLC	High Performance Liquid Chromatography
HyperTSRB	Tethered Hyperspectral Radiometer Buoy
MERIS	Medium Resolution Imaging Spectrometer
PAM	Pulse Amplitude Modulation
PAR	Photosynthetically Available Radiation
P&P	Pump and Probe
P/E	Photosynthesis-Irradiance
PNF	Profiling Natural Fluorometer
PSI	Photosystem I
PSII	Photosystem II
PSU	Photosynthetic Unit